

Higher Order Corrections to Multi Jet Final States at Colliders

Zur Erlangung des akademischen Grades eines
DOKTORS DER NATURWISSENSCHAFTEN
von der Fakultät für Physik des
Karlsruher Instituts für Technologie (KIT)

genehmigte

DISSERTATION

von

Dipl.-Phys. Johannes Bellm
aus Rheinfelden (Baden)

Tag der mündlichen Prüfung: 20. November 2015

Referent: PD Dr. Stefan Gieseke

Korreferent: Prof. Dr. Dieter Zeppenfeld

Abstract

General-purpose Monte Carlo event generators, like Herwig++, are essential tools for the comparisons between theory and experiment at particle colliders like the Large Hadron Collider at CERN. The combination of parton shower approximations with multiple leading order (LO) matrix element corrections and the inclusion of single next-to-leading order (NLO) corrections was extensively investigated in the past. Recent developments aim to include higher order corrections in the showering process to gain higher precision. In this work an algorithm was developed to consistently merge multiple NLO corrections, without reducing the accuracy of the shower approximation or the NLO calculation. Corrections above and below a technical required merging scale are included. The algorithm was implemented in the event generator Herwig++. The effects of the NLO corrections are studied and direct comparisons to data measured at the LEP and LHC experiments are discussed. Improvements above and below the merging scale are observed. The consistent inclusion of expected higher order effects are tested.

Zusammenfassung

Universell einsetzbare Generatoren zur Ereignissimulation, wie das Programm Herwig++, sind essentielle Bestandteile in der Verbindung zwischen experimentellen Beobachtungen und der theoretischen Vorhersage von Teilchenbeschleunigern wie dem LHC am CERN. Die Kombination von Partonschauer-Simulationen mit Korrekturen, die durch Matrixelemente führender Ordnung erhalten werden, und die Hinzunahme von nächst-führender Ordnung (engl. NLO) zum Produktionsprozess wurden in der Vergangenheit häufig untersucht. Um höhere Präzision der Vorhersage zu erhalten, werden neuerdings immer mehr Schleifen und mehrere NLO-Korrekturen mit der Partonschauer-Simulation verbunden. In dieser Arbeit wurde ein Algorithmus entwickelt, um konsistent mehrere NLO-Korrekturen miteinander zu verbinden. Dabei wird weder die Präzision der Partonschauer-Simulation noch die der Korrektur beeinträchtigt. Die NLO-Korrekturen werden ober- und unterhalb einer technisch notwendigen Übergangsskala eingefügt. Der Algorithmus wurde in das Programm Herwig++ integriert. Effekte, die durch die Korrekturen entstehen, werden in dieser Arbeit untersucht. Der direkte Vergleich mit Daten, die an Experimenten der Beschleuniger LEP und LHC gemessen wurden, wird diskutiert. Verbesserungen werden ober- und unterhalb der Übergangsskala beobachtet. Des Weiteren wird die konsistente Hinzunahme von bekannten Termen getestet, die durch höhere Ordnungen erzeugt werden.

Contents

1. Introduction	1
2. Theoretical Basics	3
2.1. The Standard Model	3
2.2. Cross Section	9
2.3. Perturbation Theory	10
2.3.1. Divergences and Regularization	11
2.3.2. Renormalization and Asymptotic Freedom	13
2.3.3. Additional Unresolved Emissions and DGLAP Evolution	16
2.4. NLO Cross Sections	17
2.5. Catani-Seymour Formalism	19
2.6. Matching Fixed Order to Resummed Results	23
3. Theoretical Framework	27
3.1. Fixed Order Problems	27
3.2. Parton Shower	28
3.3. Parton Shower with CS-Dipoles	33
3.4. Initial State Parton Showers and DGLAP Equation	34
3.5. Matching Fixed Order NLO Corrections to a Parton Shower	36
4. Merging Matrix Elements and Parton Showers	41
4.1. Change of Notation	41
4.2. LO Matrix Element Merging	43
4.3. Changes of Inclusive Observables and Restoring Unitarity	49
4.4. Review 1	52
4.5. Dipole Shower Clustering	52
4.6. Unordered Histories	55
4.7. Remarks on Merging Smoothness and Accuracy	56
4.8. Notation of Merged Cross Sections	57

5. Merging Matrix Elements and Parton Showers with NLO Corrections	59
5.1. Merging with NLO Corrections to the First LO	59
5.1.1. Review 2	63
5.2. NLO Merging with Two NLO Corrections	65
5.2.1. Review 3	74
5.3. Extending the NLO Merging to Multiple NLO Corrections	76
5.4. Scale Choice and Variation	77
6. Implementation and Validation	81
6.1. Sudakov Form Factor Reweighting	81
6.2. α_s -Expansion of Shower Related Weights	83
6.3. Phase Space Boundaries and Definitions	84
6.4. Smearing	85
6.5. External Matrix Element Provider	85
7. Phenomenological Results and Improvements	87
7.1. Parton Production in $e^+ e^-$ Annihilation	87
7.1.1. Discussion of the α_s Value and Improving the Behaviour	90
7.2. Comparison to LEP Data	93
7.3. LHC Results	97
7.3.1. Z Boson Production at LHC	97
7.3.2. W Boson Production at LHC	100
7.3.3. Higgs Boson Production at LHC	103
7.3.4. Jet Production at LHC	105
8. Summary and Outlook	107
Bibliography	109
A. Clustering the real emissions kinematics	109
B. Algorithm to produce NLO corrections	111
C. Phase Space Boundaries and Variable Definitions	113
D. Simulation Results	115
Acknowledgment	125

CHAPTER 1

Introduction

In July 2012 the experiments ATLAS [1] and CMS [2] simultaneously announced a resonance in the mass spectra measured at the Large Hadron Collider (LHC). The combination of the decay channels of a neutral particle showed a significant excess at an invariant mass of $126.0 \pm 0.4(\text{stat.}) \pm 0.4(\text{syst.})$ GeV at ATLAS and $125.3 \pm 0.4(\text{stat.}) \pm 0.5(\text{syst.})$ GeV at CMS. While at this time the physicists at CERN, where the LHC is located, were cautious by calling the new particle a Higgs-like particle, nowadays, after measuring the properties it is common to call it "the Higgs boson", or at least "one of the Higgs bosons". The properties are described by the Standard Model (SM) of particle physics which describes three of the four fundamental forces of nature. The discovery of the Higgs boson confirmed the mechanism that gives mass to the SM particles. For a long time particle physicists explored the fundamental principles which the SM is based on.

On the experimental side, large electron-positron-colliders (e.g. LEP), proton-proton-colliders (LHC) or proton-antiproton colliders (Tevaton), were build to accelerate and scatter charged particles. In these collisions new particles can be created from the energy provided by the initial state particles. Hereby fundamental laws of nature are respected. On the theory side these laws are formulated and need to make predictions. The formulation of the SM and the resultant predictions have been tested extensively and an overall good agreement is found between theory and experiment. At the LHC higher and higher energies are produced in order to test the SM and find deviations and confirmations. The collision of these high energetic particles produces very rarely configurations, which can be interpreted as Higgs bosons candidates. And even if such an event is measured, many other particles are created at the same time. These particles are created similar to Bremsstrahlung, when electric charges are accelerated. The constituents of the proton, called partons (gluons and quarks), radiate coloured particles, which then again radiate gluons or create quark-antiquark-pairs ($q\bar{q}$ -pairs). Coloured particles are strongly bound and cannot be observed as isolated particles. Instead they form hadrons, like mesons and baryons. Bundles of these hadrons are then called jets. These jets are measured in the detectors.

Event generators like Herwig++ [3], Pythia [4] or Sherpa [5] describe the events at a collider. The event generators factorize the different parts of the simulation. The hard process is described by perturbation theory. The radiations of additional particles from initial and final states are described by parton shower algorithms which are derived from basic properties of the perturbation theory in the approximation of soft and collinear emissions. The hadronization of partons into hadrons is modelled with assumptions derived from the properties of quantum chromo dynamics (QCD) and parameters measured at experiments. Additional secondary emissions are modelled with distributions gained from perturbative and non-perturbative effects. Event generators build the link between experiments and the theory of hard process calculations. Improving this link is a key to get to more precision and reliable results.

The factorization of the different steps in the event simulation is described by scales. Starting from a hard scale the parton shower evolves a state with more and more resolvable softer emissions to a scale where the hadronization model is needed. Next-to-leading order (NLO) calculations in QCD include, along with the virtual correction to a process also processes with an additional unresolved parton emission. The naive factorization between parton shower and hard process calculation leads to double counting of the approximations from the parton shower emissions and the real emission described in NLO calculations. By matching parton showers to NLO calculations in the MC@NLO approach [6–10] the problem is solved. Variants of the matching algorithms like the POWHEG [9, 11–14] approach have been developed over the last 15 years and are widely used in experimental collaborations to compare to the data measured at experiments. Another approach to improve the approximations made in parton showers is to merge multiple leading-order (LO) matrix elements, by replacing and reweighting simulated events like in [15–22]. In more recent years the combination of these methods of matching and merging of single [23] and multiple NLO corrections have been developed [24–30]. Efforts have been made to extend to next-to-next-to-leading order (NNLO) matching [31–36] to reach higher and higher precision on the theory side of elementary particle physics.

In this work the merging of multiple NLO corrections is developed from basic concepts. In Ch. 2 fundamental basics of the SM, perturbative calculations and corrections are introduced. Renormalization and scale dependence is explained and an overview of the Catani-Seymour (CS) subtraction formalism is given. An introduction to parton showers is given in Ch. 3. Comments on the difference between DGLAP Equation and CS dipole showers are provided and the matching of fixed order calculations to parton shower in the conventional way is explained and discussed.

The approximations made by the LO merging descriptions are reviewed and parts are replaced in order to restore inclusive observables at the same order as the corrections included in the following. The inclusion of multiple NLO corrections is described in Ch. 5 and the single expressions and their properties are explained in detail. The implementation and validation of these expressions described in Ch. 6, leads to numerical results which are shown and discussed in Ch. 7. Further improvements are included without changing the accuracy of the fixed order calculation nor the shower approximation. Comparisons to measured LEP and LHC data are provided. The inclusion of higher order corrections to multi jet final states provides a theoretical improvement compared to LO and NLO matched parton shower description of the fundamental processes in nature.

CHAPTER 2

Theoretical Basics

The SM successfully describes the fundamental particles and three of the four fundamental forces discovered in nature. In Sec. 2.1 an introduction to the SM is given. Followed by a brief discussion of the cross section , as one of the key observables measured at colliders in Sec. 2.2. In Sec. 2.3 concepts and problems of perturbation theory are explained. Here the appearance of divergences, which are treated on the one hand with the concepts of regularization and renormalization and on the other hand with the inclusion of all contributions at the same order in perturbation theory, are discussed. Renormalized NLO calculations are significantly simplified by the construction of the Catani-Seymour dipole formalism, see Sec. 2.5. The chapter is closed in Sec. 2.6 with an example of matching resummed expressions to fixed order expressions, which will be the starting point of many discussions in this work.

2.1. The Standard Model

As a relativistic quantum field theory (QFT) the particles and forces are described in the SM as representations of the Poincare group. Extrinsic degrees of freedom like spin and mass, but also intrinsic like colour and charge, give by their quantization the particle character of the objects they describe. The SM sorts the particles into representations of a $SU(3)_C \times SU(2)_L \times U(1)_Y$ gauge group. The intrinsic properties of the particles like colour and charge are the ones which makes the SM so applicable. In the following a brief introduction of this gauge group is given. Starting with the particle classification we present the electroweak sector – $SU(2)_L \times U(1)_Y$ – and then move to the strong interactions described by $SU(3)_C$.

The particles are divided into fermions and bosons. In the SM fermions carry the spin 1/2 and bosons are characterized as Spin 0 or 1 particles. The fermions further separate into quarks and leptons, where quarks are affected by all three group interactions and leptons are colour singlets and therefore not affected by the strong interaction. The Spin 1 bosons of the SM are responsible for the forces between the fermions. The special and only, recently discovered [1, 2] spin 0 particle is called the Higgs boson [37]. The interactions of the particles with the Higgs field are responsible for the generation of the masses. The mass is an invariant under Poincare

	1. Gen.	2. Gen.	3. Gen.	T	T^3	Y	Q	
Electroweak Sector	$\begin{pmatrix} u \\ d \end{pmatrix}_L$	$\begin{pmatrix} c \\ s \end{pmatrix}_L$	$\begin{pmatrix} t \\ b \end{pmatrix}_L$	$\frac{1}{2}$	$+\frac{1}{2}$	$+\frac{1}{6}$	$+\frac{2}{3}$	
	u_R	c_R	t_R	$\frac{1}{2}$	$-\frac{1}{2}$	$+\frac{1}{6}$	$-\frac{1}{3}$	
	d_R	s_R	b_R	0	0	$+\frac{2}{3}$	$+\frac{2}{3}$	
				0	0	$-\frac{1}{3}$	$-\frac{1}{3}$	
								Strong Sec.
leptons	$\begin{pmatrix} \nu_e \\ e^- \end{pmatrix}_L$	$\begin{pmatrix} \nu_\mu \\ \mu^- \end{pmatrix}_L$	$\begin{pmatrix} \nu_\tau \\ \tau^- \end{pmatrix}_L$	$\frac{1}{2}$	$+\frac{1}{2}$	$-\frac{1}{2}$	0	
				$\frac{1}{2}$	$-\frac{1}{2}$	$-\frac{1}{2}$	-1	
				0	0	-1	-1	

Table 2.1.: Fermions (quarks and leptons) of the SM with their electroweak quantum numbers: weak isospin T with eigenvalues T_3 , hypercharge Y , and electric charge $Q = T^3 + Y$. The quarks are further triplets in colour space. The quantum numbers of antiparticles are the negative values of the particles.

transformations and must be included in a theory to describe the particles observed in nature. How to include the mass within the Higgs mechanism and briefly explain properties of the SM fermions, which are listed in Tab. (2.1), are part of the next sections.

Electroweak Sector

The electroweak sector of the SM is described by the Glashow-Weinberg-Salam theory that uses the $SU(2)_L \times U(1)_Y$ group to describe interactions. Left-handed fermion spinors Ψ_L are collected into isospin doublets ($T = 1/2$) and transform under $SU(2)_L$ rotations. Right-handed fermion spinors Ψ_R are isospin singlets ($T = 0$) and are unaffected by these rotations. The field $\Psi_{L/R}$ with weak isospin T and hypercharge Y transforms as [38]^{*}

$$\Psi_{L/R} \rightarrow \Psi'_{L/R} = \left[e^{-iT_k\omega_k(x)-iY\mathbb{1}\alpha(x)} \right] \Psi_{L/R} = \mathcal{T} \Psi_{L/R}, \quad (2.1)$$

where T_k are the generators of the $SU(2)_L$ group. For singlets $T_k = 0$ and for doublets $T_k = \frac{1}{2}\tau_k$, with the usual Pauli-matrices τ_k satisfying

$$\left[\frac{\tau_a}{2}, \frac{\tau_b}{2} \right] = i\epsilon^{abc} \frac{\tau_c}{2} \text{ and the Levi - Civita symbol denoted by } \epsilon^{abc}. \quad (2.2)$$

Repeated indices are summed if not stated otherwise. $U(1)_Y$ rotations change the phase of the field but are diagonal with respect to the $SU(2)_L$ subspace, which is denoted by $\mathbb{1}$. Here $\mathbb{1}$ is with respect to the dimensionality of the field, so two for doublets and one for singlets. The unitary[†] transformation \mathcal{T} is described by $\omega_k(x)$ and $\alpha(x)$ which are the 'angles' of rotations in the $SU(2)_L \times U(1)_Y$ group space. For the doublet Ψ_L , the components are rotated by \mathcal{T} . If the transformation described by \mathcal{T} is global (independent of local variations: $\omega_k(x) = \omega_k$ and $\alpha(x) = \alpha$) the Lagrangian [39]

$$\mathcal{L} = \bar{\Psi}_L(i\partial) \Psi_L + \bar{\Psi}_R(i\partial) \Psi_R = \bar{\Psi}(i\partial) \Psi \quad (2.3)$$

^{*}Note that the hypercharge here is half of the convention used in [38].

[†]Unitary operators fulfil $\mathcal{T}^\dagger \mathcal{T} = \mathbb{1}$.

with $\not{d} = \gamma_\mu \partial^\mu$, is invariant under $SU(2)_L \times U(1)_Y$ group and Lorentz transformations. The combination Ψ of the left and right handed spinors $\Psi_{L/R}$ is manifest in the chiral representation of the Dirac matrices γ_μ , where the Lorentz transformation is block diagonal for the left and right handed components [39]. For these Lorentz transformations, it is necessary to define $\bar{\Psi} = \Psi^\dagger \gamma^0$. The transformation \mathcal{T} acts on $\bar{\Psi}_{L/R}$ as

$$\bar{\Psi}_{L/R} \rightarrow \bar{\Psi}'_{L/R} = \bar{\Psi}_{L/R} \mathcal{T}^\dagger = \bar{\Psi}_{L/R} \mathcal{T}^{-1}. \quad (2.4)$$

Hence, the massless Lagrangian \mathcal{L} is independent under global $SU(2)_L \times U(1)_Y$ group transformations. Eq. (2.3) leads to the equation of motions for massless spinor-fields Ψ , namely the Dirac equation. The derivative between the fields breaks this independence for local rotations represented by $\omega_k(x)$ and $\alpha(x)$. In order to get a theory in which group transformations can be local but the Lagrangian remain invariant under these (gauge-)transformations[‡], the derivative of the field $\partial^\mu \Psi_{L/R}$ is replaced by $D^\mu \Psi_{L/R}$. One requires that the (gauge-)covariant derivative D^μ of $\Psi_{L/R}$ transforms as the field $\Psi_{L/R}$ [38]

$$D^\mu \Psi_{L/R} \rightarrow (D^\mu \Psi_{L/R})' = D^{\mu'} \Psi'_{L/R} = \mathcal{T} D^\mu \Psi_{L/R}. \quad (2.5)$$

To achieve this property, the derivative must be modified by so-called gauge fields as

$$D^\mu = \partial^\mu \mathbb{1} - ig T_k W_k^\mu(x) - ig' Y \mathbb{1} B^\mu(x). \quad (2.6)$$

$W_k^\mu(x)$ and $B^\mu(x)$ compensate for the additional terms originating from the derivative acting on the transformation. The constants g and g' are introduced as coupling constants since, with the inclusion of D_μ into the Lagrangian, new terms with two fermions and one gauge-field appear that are needed to describe the interaction of the fermions to the gauge-fields. Eq. (2.5) implies the gauge fields transform as [38]

$$\tau_k W_k^\mu(x) \rightarrow \tau_k W_k^\mu(x)' = \mathcal{T}(\tau_k W_k^\mu(x)) \mathcal{T}^{-1} - \frac{i}{g T} [\partial_\mu \mathcal{T}] \mathcal{T}^{-1}, \quad (2.7)$$

and respectively for B^μ with $\{g, T_k\} \rightarrow \{g', Y \mathbb{1}\}$. For the Abelian group $U(1)_Y$, the only addition is proportional to $[\partial_\mu \mathcal{T}] \mathcal{T}^{-1} \sim \partial_\mu \alpha(x)$. Such transformations acting on electrodynamic potentials, which respect $U(1)_{em}$ symmetry, leave physical quantities like the electric and magnetic fields unchanged and are known as gauge transformations. With Eq. (2.6), the gauge fields transform under Lorentz transformations like ∂^μ , as vector fields (Spin 1), and describe gauge-bosons.

For infinitesimal transformations $\omega_k(x) \ll 1$, one finds that the gauge fields $W_k^\mu(x)$ transform as [38]

$$W_k^\mu(x)' = W_k^\mu(x) + \epsilon_{kij} \omega_i(x) W_j^\mu(x) - \frac{1}{g} \partial^\mu \omega_k(x). \quad (2.8)$$

This implies that the gauge fields of the non-Abelian $SU(2)_L$ group transform as a triplet (the adjoint) representation, meaning that the gauge fields carry an isospin charge.

[‡]The reason for naming the transformation gauge-transformations will be clear shortly.

For W_k^μ , the Lorentz and $SU(2)_L \times U(1)_Y$ group invariant kinetic terms

$$-\frac{1}{4}W_{k,\mu\nu}W_k^{\mu\nu}, \quad \text{with} \quad W_k^{\mu\nu} = \partial^\mu W_k^\nu - \partial^\nu W_k^\mu - g\epsilon_{kbc}W_b^\mu W_c^\nu, \quad (2.9)$$

are added to the Lagrangian. The Lagrangian now takes the form

$$\mathcal{L}_{\mathcal{EW}} = \bar{\Psi}(iD)\Psi - \frac{1}{4}W_{k,\mu\nu}W_k^{\mu\nu} - \frac{1}{4}B_{\mu\nu}B^{\mu\nu}. \quad (2.10)$$

The last term is the kinetic for B^μ only containing bilinear terms of B^μ , since $\mathcal{T}\mathbb{1}\mathcal{T}^{-1} = \mathbb{1}$.

In order to describe nature, mass terms for the Bosons of the form

$$\frac{1}{2}m_V^2 V_\mu V^\mu, \quad V \in \{W_k, B\} \quad (2.11)$$

should be possible in the theory. But simply adding those terms to the Lagrangian explicitly breaks the gauge invariance.

A way to keep the local invariance and consistently introduce masses in the formalism, is known as the Brout-Englert-Higgs mechanism. The discovery of a SM-like Higgs boson in 2012 at the LHC [1, 2] was recognised by the Physics Nobel Prize in 2013. The idea is to add a field which transforms under the gauge symmetries of the $SU(2)_L \times U(1)_Y$ group and has a non-vanishing vacuum expectation value. The solution is a complex, isospin doublet scalar field, with hypercharge $Y = 1/2$:

$$\Phi = \begin{pmatrix} \phi_+ \\ \phi_0 \end{pmatrix}. \quad (2.12)$$

Note that only the upper component receives a phase under the gauge transformation

$$\Phi = e^{-i(\frac{1}{2}\tau_3 + \frac{1}{2}\mathbb{1})\beta(x)} \begin{pmatrix} \phi_+ \\ \phi_0 \end{pmatrix} = \begin{pmatrix} e^{-i\beta(x)} & 0 \\ 0 & 1 \end{pmatrix} \begin{pmatrix} \phi_+ \\ \phi_0 \end{pmatrix}. \quad (2.13)$$

The lower component is invariant. The combination of W_3^μ and B^μ , which compensated for this gauge transformation in the Lagrangian, is identified as the photon field of quantum electrodynamics (QED). The subscript at the components of Φ denote their charge $Q = T_3 + Y$ with respect to the $U(1)_{em}$. For the other particles of the SM, the charges are related by $Q = T_3 + Y$, see Tab. 2.1.

In a next step, the doublet field Φ is re-parametrized with a general $SU(2)$ gauge transformation as

$$\Phi = e^{-i\tau_k\varphi_k(x)} \frac{1}{\sqrt{2}} \begin{pmatrix} 0 \\ v + h(x) \end{pmatrix}. \quad (2.14)$$

Here, the real-valued lower component is the vacuum expectation value v and the field $h(x)$. The field $h(x)$ is now the excitation along the axis of the vacuum and the other degrees

of freedom enter as rotations in the $SU(2)$ space. This parametrization is motivated by introducing the potential for the field Φ as

$$\mathcal{L}_{Higgs, Pot} = \mu^2 \Phi^\dagger \Phi - \lambda (\Phi^\dagger \Phi)^2 , \quad (2.15)$$

with positive, real-valued parameters μ^2 and λ . This potential is invariant under $SU(2)_L \times U(1)_Y$ group transformations and has one minimum at $\sqrt{2}\phi_0 = v = \frac{\mu}{\sqrt{\lambda}}$. This minimum is not unique, since the rotation with the $SU(2)$ group only changes the field but not the potential. The vacuum can be fixed at each point in space-time to be exactly in the lower, uncharged component of Φ with the freedom of the $SU(2)_L \times U(1)_Y$ gauge group. This choice does not change the original symmetry of the theory, but still breaks the symmetry by choosing the direction of the vacuum. This is called spontaneous symmetry breaking and the field $h(x)$ describes an uncharged, scalar (spin 0) particle called the Higgs boson. The 'vanishing' degrees of freedom of the $SU(2)$ rotation of the field Φ enter as longitudinal polarizations of the now massive gauge bosons.

To see the mass terms of the gauge fields, the kinetic term for the field Φ needs to be constructed. The kinetic term

$$\mathcal{L}_{Higgs, Kin} = (D_\mu \Phi)^\dagger (D^\mu \Phi) \quad (2.16)$$

is invariant under the $SU(2)_L \times U(1)_Y$ group transformations as well as Lorentz transformations. With $h(x) = 0$, the additional terms in the Lagrangian are therefore [39]

$$\mathcal{L}_{Higgs, Kin} [h(x) = 0] = \frac{1}{2} \begin{pmatrix} 0 & v \end{pmatrix} \left(g \frac{1}{2} W_{k,\mu} \tau_k + g' \frac{1}{2} B_\mu \right) \left(g \frac{1}{2} W_{k,\mu} \tau_k + g' \frac{1}{2} B_\mu \right) \begin{pmatrix} 0 \\ v \end{pmatrix} \quad (2.17)$$

Parametrize the linear combinations of W_μ^a and B_μ as

$$W_\mu^\pm = \frac{1}{\sqrt{2}} (W_\mu^1 \mp iW_\mu^2) , \quad (2.18)$$

$$\text{and } Z_\mu = \frac{1}{\sqrt{g^2 + g'^2}} (gW_\mu^3 - g'B_\mu) \quad (2.19)$$

$$(2.20)$$

the new fields W_μ^\pm and Z_μ receive mass terms proportional to the expectation value v of the Higgs field

$$M_W = \frac{gv}{2} \quad \text{and} \quad M_Z = \sqrt{g^2 + g'^2} \frac{v}{2} . \quad (2.21)$$

The photon field which compensates for the rotations that are not changing the lower component of Φ , see Eq. (2.13), remains massless and is given by the linear combination

$$A_\mu = \frac{1}{\sqrt{g^2 + g'^2}} (g'W_\mu^3 + gB_\mu) . \quad (2.22)$$

The massive bosons are named W^\pm and Z boson and couple to the Higgs boson directly.

As a consequence of the reparametrization one can derive the Higgs mass $M_h \sim v$ and the self interaction $hhh \sim v\lambda$. The discovery of the Higgs/a Higgs-like boson in 2012 is one of the great achievements of particle physics. Still a measurement of the self-interaction and the exact determination of the quantum numbers will help to understand the mechanism of spontaneous symmetry breaking and mass generation.

In addition to the massive gauge boson, the fermions and quarks are observed as massive particles. To include mass terms for the electron to the Lagrangian like the expression

$$-m_e(\bar{e}_L e_R + \bar{e}_R e_L) \quad (2.23)$$

with the left and right handed components components of the electron field would explicitly break $SU(2)_L \times U(1)_Y$ invariance. The field Φ can be used to introduce mass terms for the fermions while keeping the invariance. This is given by

$$\mathcal{L}_{Yukawa} = -\lambda_e \bar{e}_L \Phi e_R + h.c. = -\frac{\lambda_e}{\sqrt{2}} (\bar{\nu}_e \quad \bar{e}_L) \begin{pmatrix} 0 \\ v + h(x) \end{pmatrix} e_R + H.c. , \quad (2.24)$$

with the coupling strength λ_e . The *H.c.* is the Hermitian conjugate of the first expression. The mass of the electron is then given by $m_e = \lambda_e v / \sqrt{2}$. Similar expressions are added for the muon and tau flavours.

The general addition to the Lagrangian, for quarks masses in the SM, is [38]

$$\mathcal{L}_{Yukawa} = -\lambda_d^{ij} \bar{Q}_L^i \Phi d_R^j - \lambda_u^{ij} \bar{Q}_L^i \tilde{\Phi} u_R^j + H.c. , \quad (2.25)$$

where the λ 's are general, complex mixing matrices between the quark generations Q_L^i , d_R^i and u^i that is used to parametrize the difference between mass and interaction eigenstates. The isospin doublet $\tilde{\Phi} = i\tau_2 \Phi^*$ is included with hypercharge -1/2 to respect $SU(2)_L \times U(1)_Y$ invariance.

Strong Sector

Interactions between the particles of the SM are given by their gauge group definition, the quantum numbers and the coupling constants. Since the coupling constant defines the strength of the interaction and the relatively large coupling constant g_s of the $SU(3)_C$, compared to the couplings of the electroweak sector, the sector described by $SU(3)_C$ is called the *strong sector*. The gauge group of strong interactions is $SU(3)_C$, where the C denotes the quantum number called colour. The theory describing the strong sector and its colour charges is called Quantum Chromo Dynamics (QCD). Fermions influenced by the the strong interaction are called quarks and the gauge bosons gluons.

While the unbroken $U(1)_{em}$ of the SM which leads to interactions of charged fields with photons is an Abelian group, the non-Abelian nature of the $SU(3)$ leads to self interactions of the gluons. The kinematic part of the gauge field is similar to the one for the W^a s of the electroweak interaction in Eq. (2.9) given by

$$-\frac{1}{4} G_{\mu\nu}^a G^{a,\mu\nu}, \quad \text{with} \quad G_{\mu\nu}^a = \partial_\mu G_\nu^a - \partial_\nu G_\mu^a - g_s f^{abc} G_\mu^b G_\nu^c, \quad \text{and} \quad i f^{abc} t^c = [t^a, t^b]. \quad (2.26)$$

While the fundamental doublet representation of the $SU(2)$ is transformed with the generators $T_k = \frac{1}{2}\tau_k$, the 8 generators t^a for fundamental triplets of the $SU(3)$ are produced with the Gell-Mann-matrices $\lambda^a = 2t^a$.

A similar treatment of local gauge invariance as in the electroweak part of the SM and some modifications (as described below) lead to the Lagrangian of QCD [40]

$$\mathcal{L}_{QCD,free} = \bar{\Psi}(i\cancel{d} - m)\mathbb{1}\Psi - \frac{1}{4}(\partial_\mu G_\nu^a - \partial_\nu G_\mu^a)^2 - \frac{1}{2\xi}(\partial_\mu G^{a,\mu})^2 + \partial_\mu \bar{\eta}^a \partial^\mu \eta^a \quad (2.27)$$

$$\mathcal{L}_{QCD,int.} = -g_s \bar{\Psi} t^a \not{G}^a \Psi + g_s f^{abc} G^{b,\mu} G^{c,\nu} \partial_\mu G_\nu^a - \frac{g_s^2}{4} \left(f^{abc} G^{b,\mu} G^{c,\nu} \right)^2 + g_s f^{abc} \partial^\mu \bar{\eta}^c G_\mu^b \eta^a \quad (2.28)$$

The quark multiplets Ψ here are 3 dimensional and the index a of G^a is summed over the 8 linear independent, traceless and hermitian matrices in three dimensions. Since the $SU(3)_C$ does not distinguish between left- and right-handed fields the mass term does not break the $SU(3)_C$ symmetry.

In the quantization within the path integral formalism the functional integral is not well defined since the integration is performed over all possible gauge transformations. To cure this divergent behaviour Faddeev and Popov introduced – also in the electroweak part – a gauge fixing term $\frac{1}{2\xi}(\partial_\mu G^{a,\mu})^2$ to the path integral formalism in a way that the divergent part is separated and removed from correlator functions, see [39]. Within the Faddeev-Popov formalism it is found that non-Abelian gauge theories like QCD need an extra term in the Lagrangian. The term is needed for the transformation properties of the gauge field itself and the self interaction of the gauge field. The extra parts in the Lagrangian containing η (called ghosts) are included to correct for the unphysical timelike and longitudinal degrees of freedom of the gauge bosons [39].

2.2. Cross Section

After the introduction of particles, basics of SM and field theory an introduction to one of the central observables in high energy physics is given. Close to the notation of [41] the cross section for the process $h_1 h_2 \rightarrow X$ is defined as

$$\sigma(p, \bar{p})_X = \sum_{a,b} \int_0^1 dx_1 f_a^{h_1}(x_1, \mu_F^2) \int_0^1 dx_2 f_b^{h_2}(x_2, \mu_F^2) \sigma_{ab}(x_1 p, x_2 \bar{p}, \mu_F^2)_X , \quad (2.29)$$

The cross section is proportional to the rate of observing the final state X in collisions of incoming particles h_1 and h_2 with momenta p and \bar{p} . Here, the incoming particles can be composed particles like protons. In the parton picture the constituents (called partons) of the composed particles interact. To get the cross section/rate one needs to sum and integrate all possibilities to arrive at the final state X . The sum in (2.73) therefore contains all constituents. These constituents are extracted with a momentum fraction $x_{1/2}$ from the initial particles. The *parton density functions* $f_{a/b}^{h_i}(x_{1/2}, \mu_F^2)$ [§] (PDFs) parametrize the probability for the extraction

[§]In the following the superscript h_i are suppressed.

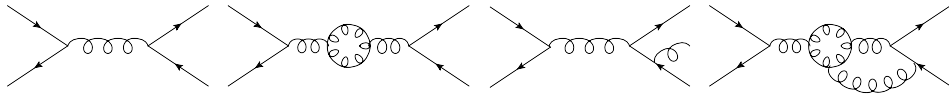


Figure 2.1.: Example feynman diagrams for $q\bar{q} \rightarrow q\bar{q} + X$ at tree level, 1 loop, real emission and 2 loop level.

of a parton of type (flavour) a/b from the composed particle h_i at the scale μ_F . Since the total momentum must be conserved, the momentum sum rule

$$\sum_a \int_0^1 dx \, x \, f_a(x, \mu_F^2) = 1 . \quad (2.30)$$

must be fulfilled[¶]. The factorization scale μ_F is introduced in the renormalization of collinear divergences, see Sec. 2.3.3. In Eq. 2.29, σ_{ab} is the partonic cross section of the partons a/b to produce the final state X and arbitrary other particles, see in Sec. 3.4. The method to calculate the partonic cross section will be briefly discussed in the following section, for more details standard textbooks on QFT should be considered [39, 40, 42].

2.3. Perturbation Theory

The nature of a field theory dictates that the probability to observe a final state $\langle f |$ from an initial state $|i\rangle$ all possible field configurations leading from $i \rightarrow f$ are possible and need to be taken into account. The overlap between the in and out states is related to the unitary operator called the S -matrix [39]. The interesting part of this matrix is the T -matrix, where the interactions are isolated as $S = \mathbf{1} + iT$. R. Feynman developed a formalism to calculate the matrix elements of the T -Matrix and physical quantities in a diagrammatic way. Starting from a path integral – the mathematical way of summing the configurations – with an action depending on the Lagrangian, Feynman rules are extracted. The derivation of these can be found in standard textbooks on QFT like [39].

For example in QCD the Feynman rules for a propagating gluon and the vertex of a gluon with a quark line are

$$\begin{array}{ccc}
 \text{propagator: } & & \text{vertex: } \\
 a, \mu \text{ } \overbrace{\text{---}}^p \text{---} b, \nu & \left[-g_{\mu\nu} + (1 - \xi) \frac{p_\mu p_\nu}{p^2 + i0} \right] \frac{i}{p^2 + i0} & \begin{array}{c} j, \sigma \\ \nearrow \\ a, \mu \end{array} \text{---} \begin{array}{c} i, \rho \\ \searrow \\ -ig_s(t^a)_{ij} \gamma^\mu \end{array}
 \end{array}$$

where the Latin indices are the colour indices of the attached fields and the Greek indices are the Lorentz indices of the spinors or polarization vectors components. The $i0$ is added to the propagators to ensure causality. Rules for other vertices and propagators as well as the integration of internal loop momenta are not written out. With these rules it is possible to derive matrix elements \mathcal{M} of the T -matrix. The vertices, as the $q\bar{q}g$ -vertex, are proportional to the coupling constants g_s or g_s^2 for the four gluon vertex.

[¶]This holds at LO and later in the $\overline{\text{MS}}$ scheme.

Since the previously mentioned sum over all field configurations has infinitely many terms the calculation of physical observables is usually treated in a perturbative approximation. The matrix elements of the T -matrix are then expressed as an expansion in the coupling constant g_s . Here, a precise final state configuration is required and one speaks of a physical process as

$$h_1 h_2 \rightarrow N_l \text{Leptons} + N_b \text{Bosons} + N_j \text{Partons} , \quad (2.31)$$

which can be produced with the minimal number of vertices. This process is then called the leading order (LO) process. Physical observables like the cross section are proportional to the squared matrix elements. For the most processes the Feynman diagrams at LO are of a tree like structure (see lhs. of Fig. 2.1), therefore LO and tree level is often used synonymously. The LO of Higgs production via gluon fusion on the other hand is an example where the LO already contains a loop of massive particles.^{||}

The first correction to the LO process contains also diagrams that have two orders higher in the coupling constant g_s . The particle excitation needs to be produced and destroyed at a vertex. Squaring the matrix elements leads to interference between the LO diagrams and the loop diagrams which are then proportional to g_s^2 . In Sec. 2.3.3 it is explained that also processes with more external particles need to be taken into account. Including all processes with the same number of couplings is then called the next-to-leading order (NLO) correction.

2.3.1. Divergences and Regularization

At NLO one obtains that the summation/integration over all configurations leads to problems. In the following a brief introduction should be given. Additional field excitations are included within the Feynman diagrams at NLO (see second diagram in Fig. 2.1). These so called virtual particles can form loops with the other particles in the diagram. Not only external particles underlie the energy-momentum conservation, also at each vertex in the diagrams $\sum p_{in} = \sum p_{out}$ is fulfilled. The closed loop opens the possibility to have any momentum running within the loop. All possible configurations must be summed/integrated. However, the integration of the loop momentum, e.g. k is not restricted and leads to mathematically divergent expressions.

Loop integrals with n legs attached to the loop are of the form

$$(-ig)^2 \int \frac{d^4 k}{(2\pi)^4} \frac{k^{\mu_1} \dots k^{\mu_m}}{D_0 \dots D_{n-1}} \quad \text{with} \quad D_i = \left(k + \sum_{j=1}^i p_j \right)^2 - m_i^2 + i0 . \quad (2.32)$$

Where usually $m < n$ and D_i describes the i 'th propagator in the loop diagram with mass m_i . p_j are the momenta of the external legs entering the loop diagram. The factor $(-ig)^2$ arises since two additional vertices are needed to close the loop. Different types of divergences can appear in the calculation.

^{||}Since the Higgs doublet is colourless there is no direct coupling to gluons.

UV-Divergences

Large loop momenta $|\mathbf{k}| \rightarrow \infty$, corresponding to short wavelength, can lead to a divergent behavior for $n < 4$ propagators in the loop diagram, which is then called *ultra violet* (UV) divergent. To handle the mathematical expressions in the first step, these divergences must be parametrized. A nowadays popular method to regularize the divergences is to change the dimension of space-time in the integration from $4 \rightarrow d = 4 - 2\epsilon$.

The integration measure in (2.32) changes to

$$(-ig^B)^2 \frac{d^4 k}{(2\pi)^4} \rightarrow (-iZ_g g^R \mu_R^\epsilon)^2 \frac{d^{4-2\epsilon} k}{(2\pi)^{4-2\epsilon}}. \quad (2.33)$$

Changing the dimensionality, but keeping the mass dimension of the action $[S] = 0$ fixed**, leads to a mass dimension of the coupling constant $[g_s^B] = \epsilon$ [43]. The mass dimension is absorbed into an arbitrary mass parameter μ_R^ϵ ^{††} in order to have a dimensionless coupling g_s^R . This is done since the expansion of the perturbative series should be performed in a dimensionless parameter.

Reducing the integration measure regularizes the UV divergences and leads to single poles in $1/\epsilon$ at NLO. In calculations these poles usually appear in combination with $S_\epsilon = (4\pi)^\epsilon / \Gamma(1-\epsilon)$ as

$$\frac{S_\epsilon}{\epsilon} = \frac{1}{\epsilon} + \log(4\pi) - \gamma_E + \mathcal{O}(\epsilon) \quad (2.34)$$

with the Euler-Gamma-function and the Euler constant γ_E . The factor Z_g , and the indices B and R in Eq. (2.33) will be explained in Sec. 2.3.2.

IR and Collinear Divergences

While the UV divergences arise from short wavelength, other types of divergences are present in the loop calculation if the propagators attached to external legs are massless. These so called *mass singularities* [44] appear, if either

- the exchanged, massless particle between two onshell, external legs has vanishing loop momentum (*soft* or *infrared*(IR) singularity), or
- the loop momentum of two massless propagators, which are attached with an on shell, massless external leg, becomes collinear to the momentum of the external leg. These regions lead to so called *collinear* (C) singularities.

The region where both conditions are fulfilled, so *soft* and *collinear*, is already included in the soft limit.

As the UV also the soft and collinear divergences can be regularized by changing the dimension of space-time. Soft poles appear as $1/\epsilon^2$ and $1/\epsilon$, while the collinear poles produce $1/\epsilon$ contributions.

**since it appears in the exponent of the path integral formulation [43].

^{††}Here one can introduce a so called 't Hooft mass μ , which is different from the later interpreted renormalization scale. This introduces additional logarithms of the ratio μ/μ_R to the counter terms. For this brief discussion it is not needed and it is set $\mu = \mu_R$.

2.3.2. Renormalization and Asymptotic Freedom

After regularizing the divergent integrals within the *dimensional regularization* the expressions are well defined in $d = 4 - 2\epsilon$ dimensions. In the limit $\epsilon \rightarrow 0$ the expressions are still divergent. In order to predict finite physical quantities the parameters of the theory must be reinterpreted.

UV renormalization

The divergences originating from short wave lengths, leading to UV poles $1/\epsilon$ are absorbed into the parameters and fields of the Lagrangian. Multiplicative renormalization as it is described in many textbooks on QFT, e.g. [40, 45], treats this divergences by rewriting the parameters and fields of the Lagrangian as

$$\Psi^B = Z_\Psi^{1/2} \Psi^R, \quad G_\mu^B = Z_G^{1/2} G_\mu^R, \quad g_s^B = \frac{Z_1}{Z_\Psi Z_G^{1/2}} \mu_R^\epsilon g_s^R = Z_g \mu_R^\epsilon g_s^R, \quad m_q^B = Z_m m_q^R. \text{ ‡‡} \quad (2.35)$$

The classical fields and couplings in the Lagrangian are interpreted as *bare* parameters and operators (upper index B). Mathematical divergences are factorized into the prefactors of the *renormalized*, now physical quantities labelled with the upper index R . The renormalization constants Z_i are written as $Z_i = 1 + \delta_i$. Rewriting the Lagrangian induces 'new' §§ contributions to two point functions (propagators) and interaction vertices. The scale μ_R is introduced in Eq. (2.33).

The renormalized Lagrangian is written in the form

$$\mathcal{L} = \mathcal{L}_{QCD,free}^R + \mathcal{L}_{QCD,int.}^R(\mu_R^\epsilon) + \mathcal{L}_{QCD,c.t.}^R(\delta_i, \mu_R^\epsilon), \quad (2.36)$$

where the bare quantities have been replaced by the renormalized ones. $\mathcal{L}_{QCD,free}^R$ containing only the renormalized fields, $\mathcal{L}_{QCD,int.}^R(\mu_R^\epsilon)$ depends on the introduced scale to fix the mass dimension of the coupling and the *counter term* Lagrangian $\mathcal{L}_{QCD,c.t.}^R(\delta_i, \mu_R^\epsilon)$ contains the δ_i s, included to absorb the UV singularities.

After rewriting the Lagrangian the δ_i s must be determined. Therefore *renormalization conditions* need to be formulated in order to fix the finite terms of the constants δ_i . In QCD the constants are determined by calculating the divergent self energy diagrams to determine the field renormalization and mass insertions constants. Furthermore, one vertex correction is used to determine the divergent structure, which must be absorbed into the redefinition of the coupling constant.

The divergence structure is proportional to Eq. (2.34). In the *minimal subtraction* scheme (MS-scheme) the counter term expressions are fixed by subtracting exactly the pole structure of the UV divergent virtual expressions. As given in Eq. (2.34) the poles in the calculations are in practice dressed with functions originating from d -dimensional angular integration which depends on the dimensional regulator ϵ . In the *modified minimal subtraction* MS-scheme the counter terms absorb also the $\mathcal{O}(\epsilon^0)$ expansion of these terms. This is done, because it is

‡‡ Additional factors are needed for ghosts and gaugefixing parameter. The term renormalization may be more intuitive by writing $\Psi^R = \frac{1}{\sqrt{Z_\Psi}} \Psi^B$.

§§ At this point it is just a redefinition of the parameters.

expected that the higher order calculation will produce expressions that are proportional to the LO expressions. So absorbing known/expected finite expressions into the LO expression reduces the NLO corrections [45].

The expression for Z_i and deeper discussion on the interpretation of renormalization, can be found e.g. in [40]. In the $\overline{\text{MS}}$ -scheme Z_g is given by [40]

$$g_s^B = g_s^R \mu_R^\epsilon \left[1 - \underbrace{\frac{(g_s^R)^2}{8\pi^2} \frac{S_\epsilon}{2\epsilon}}_{\frac{\alpha_s}{2\pi}} \underbrace{\left(\frac{11}{6} C_A - \frac{2}{3} T_R N_F \right)}_{\beta_0} + \mathcal{O}(\alpha_s^2) \right]. \quad (2.37)$$

Here $\alpha_s = g_s^2/4\pi$ is introduced in analogy to the fine structure constant in QED. N_F is the number of massless quark flavours. Note that the expansion is, like the perturbative expansion, in the dimensionless renormalized coupling g_S^R .

Colour Factors

C_A is the Casimir constant which arises in the summation over the adjoint representation of the $SU(N)$ gauge group. T_R comes from the normalization of the colour matrices and β_0 is the first term of the so called β -function of QCD, which will be part of the next section. C_A and T_R are also called *colour factors* which arise in many QCD calculations due to the summation of the colour structure of the amplitudes. C_A usually also appears in matrix elements with $g \rightarrow gg$ splittings^{¶¶}, T_R comes with $g \rightarrow q\bar{q}$ splittings and the colour factor, not present in the β_0 coefficient, C_F describes $q \rightarrow qg$ splittings. In QCD these factors are $C_A = N = 3$, $T_R = 1/2$ and $C_F = (N^2 - 1)/2N = 4/3$.

Running Coupling and Asymptotic Freedom

Eq. (2.37) depends on the scale μ_R introduced to get a dimensionless expansion parameter g_S^R . The theory itself must not depend on the arbitrary scale μ_R – the bare fields and couplings are independent – but the truncation of the perturbative series at a fixed order of the coupling constant requires to introduce a scale to separate the UV degrees of freedom, which should not affect the low energy behaviour of the theory. The prediction of observables then also depends on the scale μ_R used to fix the values of the parameters of the truncated series. More precisely, they depend on the renormalization prescription [40]. So the values of the parameters are fixed in comparison to measurements for a given scale μ_R used in the calculation.

In a next step, after fixing the parameters of the renormalized theory at scale μ_R , observables, other than the ones used to fix the parameters, can be predicted for the scale μ_R by calculating the fixed order up to the renormalized order in α_s . The calculation of the other observables now again contains loop integrations, which have to be performed in d dimensions. If the loop integral I_4 in Eq. (2.32) has mass dimension $[I_4] = A$, other than zero, the change to d dimensions and the introduction of the scale as in Eq. (2.33) changes the mass dimension of the integral – without the scale μ_R – to $[I_d/\mu_R^{2\epsilon}] = A - 2\epsilon$. The solution must be proportional to $X \cdot s^{-2\epsilon}$ with $[X] = A$ and $[s] = -\epsilon$. After integration of the loop momentum the only scales remaining, to form s , are combinations of the external momenta p_i or the masses of particles that appear in the loops. This leads when contracted to the UV poles to logarithms of the form $\log(\mu_R/s)$. If the ratio is large, also the correction due to the NLO correction can become large. These changes from higher order corrections to the Born prediction would be

^{¶¶} $g \rightarrow gg$ is gluon \rightarrow gluon gluon, $g \rightarrow q\bar{q}$ is gluon \rightarrow quark antiquark, $q \rightarrow qg$ is (anti-)quark \rightarrow (anti-)quark gluon.

small if the parameters would have been fixed/renormalized near to the scale s in the first place. The LO prediction can be improved with the following discussion.

Since the left hand side of Eq. (2.37) is independent of the scale μ_R it is found that in dimensional regularization the renormalized coupling 'constant' must be a scale dependent function. The derivative of Eq. (2.37) with respect to the scale gives [40]

$$0 = \frac{d}{d \log \mu_R} g_s^B(\mu_R, g_s^R(\mu_R), \epsilon) = \frac{\partial g_s^B}{\partial \log \mu_R} + \frac{\partial g_s^B}{\partial g_s^R} \frac{d}{d \log \mu_R} g_s^R(\mu) . \quad (2.38)$$

Using the more convenient expression for $\alpha_s(\mu_R)$ the differential Equation

$$\frac{d\alpha_s(\mu_R)/4\pi}{d \log \mu_R} = 2\beta(\alpha_s(\mu_R)/4\pi) \quad (2.39)$$

is found for the renormalized and now scale dependent $\alpha_s(\mu_R)$ at $\epsilon = 0$ [40]. This Equation is the *renormalization group Equation* (RGE) for α_s . The β -function depends on the structure of the gauge group and is at the one loop level for QCD given by

$$\beta(\alpha_s(\mu_R)/4\pi) = -\left(\frac{\alpha_s}{4\pi}\right)^2 2\beta_0 + \mathcal{O}(\alpha_s^3) . \quad (2.40)$$

Solving the RGE with the one loop β -function leads to

$$\alpha_s(Q) = \frac{\alpha_s(Q_0)}{1 + \frac{\alpha_s(Q_0)}{2\pi} \beta_0 \log \frac{Q^2}{Q_0^2}} . \quad (2.41)$$

with the integration constant $\alpha_s(Q_0)$, so that $\alpha_s(Q)|_{Q=Q_0} = \alpha_s(Q_0)$. This is the leading behaviour of the *running* coupling $\alpha_s(Q)$.

With the RGE we can translate the renormalized – fixed at some scale μ_R – α_s to an other scale μ'_R . This is used to improve predictions when a 'typical' scale of the physical process is known. The physical observable is calculated with the running coupling evolved from the measured value. At the same time the scale in the integrals is set to the typical scale. In [40] this is described as a change of the renormalization scheme. For $\overline{\text{MS}}$ -renormalized coupling constant the change of the renormalization scale can be expressed at NLO by multiplying $(\mu_R^2/\mu'^2_R)^\epsilon$ to the pole structure of the counter term, see [46] after expansion.

In QCD with $N_F < 16$ the coupling decreases for growing scales and vanishes for $Q \rightarrow \infty$, so that QCD is an *asymptotically free* theory. On the other hand the coupling is increasing with for decreasing scales and even diverges if the denominator vanishes. This defines the scale

$$\Lambda_{QCD} = \mu_R \exp\left(\frac{-4\pi}{\beta_0 \alpha_s(\mu_R)}\right) \longrightarrow \alpha_s(\mu_R) = \frac{1}{(b_0 \log(\mu_R^2/\Lambda_{QCD}^2))} , \quad (2.42)$$

with $b_0 = \beta_0/2\pi$. The perturbative series breaks down if the expansion parameter is diverging. The large coupling between strongly interacting partons makes the confinement of partonic states into colourless hadrons plausible [45].

In this work the approximate, explicit form of the two loop running coupling is utilized as it is implemented in **Matchbox** and given by [45]

$$\begin{aligned}\alpha_s(Q) &= \frac{1}{(b_0 \log(Q^2/\Lambda_{QCD}^2))} \left(1 - \frac{b_1}{b_0^2} \frac{\log(\log(Q^2/\Lambda_{QCD}^2))}{\log(Q^2/\Lambda_{QCD}^2)} \right. \\ &\quad \left. + \frac{b_1^2}{b_0^4 \log^2(Q^2/\Lambda_{QCD}^2)} \left[(\log(\log(Q^2/\Lambda_{QCD}^2)) - \frac{1}{2})^2 - \frac{5}{4} \right] \right). \end{aligned}\quad (2.43)$$

with $b_1 = (153 - 19N_F)/24\pi^2$ ^{***}.

2.3.3. Additional Unresolved Emissions and DGLAP Evolution

After renormalization is applied to the parameters and fields of the theory, the UV divergences are removed (with the same counter terms) from the calculation of any process up to the given order in perturbation theory. Still, the description of massless particles leads to IR and C divergences. This is solved by a redefinition of the process itself. The KLN theorem [44, 49] states that the total cross section and observables not resolving additional emissions, are finite for the sum of virtual emissions and real unresolved emissions. So only the sum of the process itself, containing IR and C divergences, and the *real emission process* with an additional unresolved emission gives physical results.

Thus measurement and calculation of an observable depend on the definition of a resolution parameter for which the additional emission is defined as unresolved. Defining a process as the process with the minimal number of particles to be expected and arbitrary hard additional real emissions is then called inclusive.

Inclusive observables cannot resolve additional soft or collinear emissions. In the calculation beyond leading order additional collinear divergences arise due to composite external states. Composite initial states, e.g. the protons at the LHC, but also identified final state momenta of partons with transition probabilities to produce composite final state hadrons resolve collinear emissions. The weight coming from the e.g. PDFs for initial states is different if the emission is real or virtual, since the initial state changes its momentum fraction for real emission. This leads to remaining divergences in the sum of real emission process and virtual contributions. It is handled by renormalization of the PDFs. As in the case of UV renormalization the classical probability functions to extract a parton from a composite hadron is redefined (in $\overline{\text{MS}}$ -scheme) as [41]

$$f_a^B(x) = f_a^R(x, \mu_F) - \frac{\alpha_s}{2\pi} S_\epsilon \sum_b \int_0^1 \frac{dz}{z} \left[-\frac{1}{\epsilon} \left(\frac{\mu^2}{\mu_F^2} \right)^\epsilon P_{ab}^r(z) f_b^R(x/z, \mu_F) \right] + \mathcal{O}(\alpha_s^2). \quad (2.44)$$

Here $P_{ab}^r(z)$ are the regularized Altarelli-Parisi (AP) splitting functions [50]

$$\begin{aligned}P_{qg}^r(z) &= C_F \frac{1 + (1-z)^2}{z}, \quad P_{gg}^r(z) = T_R [z^2 + (1-z)^2], \quad P_{qq}^r(z) = C_F \left(\frac{1+z^2}{1-z} \right)_+, \\ P_{gg}^r(z) &= 2C_A \left[\left(\frac{1}{1-z} \right)_+ + \frac{1-z}{z} - 1 + z(1-z) \right] + \delta(1-z) \left(\frac{11}{6}C_A - \frac{2}{3}N_f T_R \right).\end{aligned}$$

^{***}The expression defined in [45] differs from [47, 48] in $\mathcal{O}(\alpha_s^3)$.

The $(\dots)_+$ is the $+$ -distribution defined as

$$\int_0^1 dz [f(z)]_+ g(z) = \int_0^1 dz \left[\overbrace{f(z)g(z)}^{'}_{real'} - \overbrace{f(z)g(1)}^{'}_{virtual'} \right]. \quad (2.45)$$

where the first part matches the singularity in the real contribution and the second is needed to subtract the remaining divergence in the virtual contribution. The possibility of having a different factorization scale than the scale of the loop integrals is already included via the factor $(\mu^2/\mu_F^2)^\epsilon$.

AP splitting functions describe the emissions in the collinear limit. Only gluon emission leads to collinear divergent behaviour at $z = 1$, so that only the flavour diagonal P_{qq} and gg receive the $+$ -distribution. The expressions describing the splittings without regularization will also be needed and are given by

$$P_{qg}(z) = C_F \frac{1 + (1-z)^2}{z}, \quad P_{gq}(z) = T_R [z^2 + (1-z)^2], \quad P_{qq}(z) = C_F \frac{1+z^2}{1-z}, \quad (2.46)$$

$$P_{gg}(z) = 2C_A \left[\frac{z}{1-z} + \frac{1-z}{z} + z(1-z) \right]. \quad (2.47)$$

The appearance of the term proportional to $\delta(1-z)$ in $P_{gg}^r(z)$ is due to conditions required by PDFs which is the overall momentum conservation of the composite particle and charge conservation.

As in the UV renormalization of the coupling constant, the PDF becomes scale dependent by this and, similar to the RGE for α_s , the PDFs must fulfil a differential equation. This is now, due to the integration over the momentum fraction z and the possibility to change flavour, a coupled set of integro-differential equations.

$$\frac{\partial f_a^R(x, \mu_F)}{\partial \log \mu_F^2} = \frac{\alpha_s}{2\pi} \sum_b \int_0^1 \frac{dz}{z} P_{ab}^r(z) f_b^R(x/z, \mu_F) + \mathcal{O}(\alpha_s^2). \quad (2.48)$$

This coupled set of DGLAP Equations describe the *factorization scale* μ_F evolution of the PDFs used to fix a renormalization point. The renormalization of the PDFs requires, similarly to the α_s -renormalization, a new measurement of NLO PDFs in order to predict new observables, other than the observable used to measure the PDFs.

2.4. NLO Cross Sections

After including all processes up to the same order in α_s (real emission) and construction of counter terms for the UV and PDF renormalization, the cross section can be calculated as a finite and physical quantity. The NLO cross section is written as in Eq. (2.29) with

$$\sigma_{ab}(x_1 p, x_2 \bar{p}) = \sigma_{ab}^{LO}(x_1 p, x_2 \bar{p}) + \sigma_{ab}^{VRC}(x_1 p, x_2 \bar{p}; \mu_F^2) + \mathcal{O}(\alpha_s^2). \quad (2.49)$$

Here the differential LO cross section is integrated over the full m -particle phase space ϕ_m for all final state combinations $\{m\}$ contributing to the process as

$$\sigma_{a,b}^{LO}(x_1 p, x_2 \bar{p}) = \int_m d\sigma_{ab}^B(x_1 p, x_2 \bar{p}), \quad (2.50)$$

$$= \mathcal{N}_{in} \frac{1}{n_s(a)n_c(a)n_s(b)n_c(b)} \sum_{\{m\}} \int d\phi_m(p_1, \dots, p_m; x_1 p + x_2 \bar{p} + Q) \frac{1}{S_{\{m\}}} \\ \cdot |\mathcal{M}_{m,a,b}(p_1, \dots, p_m; x_1 p, x_2 \bar{p})|^2 F_J^{(m)}(p_1, \dots, p_m; x_1 p, x_2 \bar{p}). \quad (2.51)$$

\mathcal{N}_{in} contains all non QCD related symmetry factors and the flux factor. The n_c and n_s are factors to average the initial state colours and helicities and the symmetry factor $S_{\{m\}}$ is needed to account for identical, indistinguishable final state particles. Expressions for the squared matrix element are obtained by applying the Feynman rules, as described in textbooks, e.g. [39]. $F_J^{(m)}(p_1, \dots, p_m; x_1 p, x_2 \bar{p})$ serves as a measurement function^{†††} that can be used to define cuts on the final state to receive fiducial cross sections and to define the process properly. It can define also differential cross sections via δ -functions on integration variables of the $\phi_{\{m\}}$ phase space.

All $\mathcal{O}(\alpha_s)$ corrections are then collected into

$$\sigma_{ab}^{VRC}(x_1 p, x_2 \bar{p}; \mu_F^2) = \int_m d\sigma_{ab}^V(x_1 p, x_2 \eta \bar{p}) + \int_{m+1} d\sigma_{ab}^R(x_1 p, x_2 \bar{p}) + \int_m d\sigma_{ab}^C(x_1 p, x_2 \bar{p}; \mu_F^2). \quad (2.52)$$

The first term contains all renormalized, virtual contributions with the same factors and measurement function as the Born contributions. The real emission contains one additional final state and needs to be integrated over the $\phi_{\{m+1\}}$ phase space. The symmetry and averaging factors are also modified to match the processes with the additional emission. For the measurement function the condition must be fulfilled that collinear and/or soft emissions are not resolved, so

$$F_J^{(m+1)}(p_1, \dots, p_{m+1}; x_1 p, x_2 \bar{p}) \rightarrow F_J^{(m)}(p_1, \dots, p_m; x_1 p, x_2 \bar{p}) . \quad (2.53)$$

The last term in Eq. (2.52) contains the collinear counter term for initial state emissions (and/or identified final state partons, see [41]). In [41] it is given for one initial state as

$$d\sigma_a^C(xp; \mu_F) = \frac{\alpha_s}{2\pi} S_\epsilon \sum_b \int_0^1 dz \left[\frac{1}{\epsilon} \left(\frac{\mu^2}{\mu_F^2} \right)^\epsilon P_{ab}(z) \right] d\sigma_b^B(xzp) \quad (2.54)$$

which can be produced by a variable transformation from Eq. (2.44) in order to have the same PDF weights. The measurement function is now $F_J^{(m)}(p_1, \dots, p_m; xzp)$ and is also affected by the $+$ -distribution of $P_{ab}^r(z)$.

^{†††}In [41] it is called a jet defining function.

^{‡‡‡}See [41] for deeper discussion. Especially the beginning of Ch. 7 in [41].

2.5. Catani-Seymour Formalism

Although the sum of all $\mathcal{O}(\alpha_s)$ contributions to the cross section is finite, the full calculation of NLO corrections need to be performed in d dimensions. The measurement function and the phase space integration of the real emission must be translated. Together with the fact that the PDFs are measured functions, which must be evolved to new scales, the prediction of (differential) NLO corrections could not be performed with Monte Carlo integration techniques.

The method, which was generalized to arbitrary NLO calculations in QCD for massless [41, 51] and then extended to massive coloured partons – including SUSY partners – in [52] solves this issue. Here, as in other approaches like FKS- [53] or antenna-subtraction [54, 55], the idea is to use the factorising properties of IR and C divergences. A fully differential auxiliary cross sections is constructed that can be subtracted from the real emission and added in an integrated form to the virtual contribution.

The method proposed in [41] is based on colour dipoles. So each splitting of an emitter i emitting an emission j is described by the sum over contributions of all colour correlated spectators k of the emitter. A spectator is introduced to preserve momentum conservation

$$p_i^\mu + p_j^\mu + p_k^\mu = \tilde{p}_{ij}^\mu + \tilde{p}_k^\mu . \quad (2.55)$$

\tilde{p}_{ij}^μ and \tilde{p}_k^μ are the momenta of the Born emitter $i j$ and the spectator k after clustering the three momenta. The tilde kinematics, on the right hand side of Eq. 2.55, for all dipole configurations are given in [41] and Tab. (C.1).

The idea is to find expressions which exactly mimic the IR and/or C behaviour of the real emission contribution in 4 dimensions but can be expressed as Born amplitudes and dipole functions depending on the emitter-emission-spectator configuration. An important point of the procedure is, that the measurement function of the subtracted contribution only depends on the tilde kinematics of Eq. (2.55).

In a second step the phase space describing the real emission is factorized in d -dimensions into a one particle reduced phase space and a one particle phase space expressed in the variables used to mimic the real emission. The Integration of the one particle phase space is then performed once and can be used for arbitrary processes. It is not needed to integrate the real emission process in d -dimensions since the difference of the real emission and the Dipole expressions is constructed to be finite. Due to the KLN theorem also the ϵ -poles of the integrated dipoles must cancel.

To construct those terms in the limit where $p_i p_j \rightarrow 0$ the matrix element should therefore be described by

$${}_{m+1} < 1, \dots, m+1 | 1, \dots, m+1 >_{m+1} = \sum_{k \neq i,j} \mathcal{D}_{ij,k}(p_1, \dots, p_{m+1}) + \text{not singular} \quad (2.56)$$

Here the left hand side is the squared Amplitude for $m+1$ coloured final states, without initial state partons. The dipole terms $\mathcal{D}_{ij,k}(p_1, \dots, p_{m+1})$ can then be written as

$$\begin{aligned} \mathcal{D}_{ij,k}(p_1, \dots, p_{m+1}) &= -\frac{1}{2p_i \cdot p_j} \\ &\cdot {}_m<1, \dots, \tilde{i}\tilde{j}, \dots, \tilde{k}, \dots, m+1| \frac{\mathbf{T}_k \cdot \mathbf{T}_{ij}}{\mathbf{T}_{ij}^2} \mathbf{V}_{ij,k} |1, \dots, \tilde{i}\tilde{j}, \dots, \tilde{k}, \dots, m+1>_m . \end{aligned} \quad (2.57)$$

where the \mathbf{T} s are the colour charges of the indexed particle as defined in [41], $\mathbf{V}_{ij,k}$ are matrices in the helicity space of the Born emitter $\tilde{i}\tilde{j}$. Born emitter denotes the parton which is produced by clustering of partons i and j . The bra/ket is the m particle amplitude of the underlying Born process where partons i and j were clustered. This amplitude has open colour and helicity/spinor indices of the Born emitter $\tilde{i}\tilde{j}$ and Born spectator \tilde{k} .

As an example dipole, the splitting of a gluon into a gluon pair within the Catani Seymour formalism should be briefly discussed. The helicity dependent dipole part in d dimensions is

$$\begin{aligned} \langle \mu | \mathbf{V}_{g_i g_j, k}(z; y) | \nu \rangle &= 16\pi\mu^{2\epsilon}\alpha_s C_A \left[-g^{\mu\nu} \left(\frac{1}{1-z(1-y)} \right. \right. \\ &+ \left. \left. \frac{1}{1-(1-z)(1-y)} - 2 \right) + (1-\epsilon) \frac{1}{p_i p_j} (zp_i^\mu - (1-z)p_j^\mu) (zp_i^\nu - (1-z)p_j^\nu) \right] . \end{aligned} \quad (2.58)$$

where μ, ν are the Lorentz indices of the Born emitter gluon polarisation vector. z and y are given by

$$z = \frac{p_i p_k}{p_j p_k + p_i p_k} = \frac{p_i \tilde{p}_k}{\tilde{p}_{ij} \tilde{p}_k}, \quad y = \frac{p_i p_j}{p_i p_j + p_j p_k + p_k p_i}, \quad (2.59)$$

respectively.

The dipoles are used to mimic the singular behaviour of an arbitrary real emission matrix element. In order to preserve the cross section and not to change infrared safe observables it is required that the dipoles subtracting the real emission are added in an integrated form. For this the average over the helicity states is taken. The spin-averaged dipole-kernel from above is given by

$$\frac{< \mathbf{V}_{gg,k}(z; y) >}{8\pi\alpha_s\mu^{2\epsilon}} = 2C_A \left[\frac{1}{1-z(1-y)} + \frac{1}{1-(1-z)(1-y)} - 2 + z(1-z) \right]. \quad (2.60)$$

The difference between the averaged dipole function and the corresponding AP splitting function is given by the absence of $(1-y)$ expressions in the denominators. In the collinear limit where the AP splitting function is calculated y vanishes. In order to subtract the exact divergent behaviour of the real emission contribution these factors are needed without neglecting phase space effects. As a result the addition of all possible dipole configurations coherently subtract the divergences.

The AP splitting functions instead subtract too much in the $z \rightarrow 0$ region, which would introduce another singularity. If a parton shower, which will be subject of the next chapter,

is based on AP splitting functions/kernels this non-coherent property is solved by requiring angular ordering [56].

(z, y) -parametrization of the factorized one particle phase space and performing angular integration, leads to a point where the terms of Eq. (2.60) or other dipole terms need to be integrated like

$$\mathcal{V}_{ij}(\epsilon) = \int_0^1 d\tilde{z} (\tilde{z}_i(1-\tilde{z}))^{-\epsilon} \int_0^1 \frac{dy}{y} (1-y)^{1-2\epsilon} y^{-\epsilon} \frac{\langle \mathbf{V}_{ij,k}(\tilde{z}; y) \rangle}{8\pi\alpha_s\mu^{2\epsilon}} . \quad (2.61)$$

While the origin of the $1/y$ is basically the $1/p_i p_j$ prefactor in Eq. (2.57), the factor $(1-y)$ can be traced back to the change of phase space measure originating of the local recoil [57].

The integration of Eq. (2.61) leads to

$$\mathcal{V}_{qg}(\epsilon) = C_F \left[\frac{1}{\epsilon^2} + \frac{3}{2\epsilon} + 5 - \frac{\pi^2}{2} + \mathcal{O}(\epsilon) \right] , \quad (2.62)$$

$$\mathcal{V}_{q\bar{q}}(\epsilon) = T_R \left[-\frac{2}{3\epsilon} - \frac{16}{9} + \mathcal{O}(\epsilon) \right] , \quad (2.63)$$

$$\mathcal{V}_{gg}(\epsilon) = 2C_A \left[\frac{1}{\epsilon^2} + \frac{11}{6\epsilon} + \frac{50}{9} - \frac{\pi^2}{2} + \mathcal{O}(\epsilon) \right] . \quad (2.64)$$

for the various splittings. Note that we can add an arbitrary function of the form

$$f(y, z) = y \cdot g(z, y), \quad (2.65)$$

with $g(z, y)$ being a polynomial in z and y to Eq. (2.60), which would not change the pole structure, but only the finite parts.

The integrated dipoles only depend on the colour and flavour structure of the underlying Born process and can now be accumulated into so-called insertion operators. The first insertion operator I is given by

$$I(\{p\}; \epsilon) = -\frac{\alpha_s}{2\pi} \frac{1}{\Gamma(1-\epsilon)} \sum_i \frac{1}{\mathbf{T}_i^2} \mathcal{V}_i(\epsilon) \sum_{k \neq i} \mathbf{T}_i \cdot \mathbf{T}_k \left(\frac{4\pi\mu^2}{|2p_i \cdot p_k|} \right)^\epsilon . \quad (2.66)$$

This form is kept for processes with coloured initial states and contains the full divergent structure to cancel the IR and C divergences of the virtual contributions. The indices i and k sum all (also initial states) external Born partons. And

$$\mathcal{V}_i(\epsilon) = \mathbf{T}_i^2 \left(\frac{1}{\epsilon^2} - \frac{\pi^2}{3} \right) + \gamma_i \frac{1}{\epsilon} + \gamma_i + K_i + \mathcal{O}(\epsilon) , \quad (2.67)$$

is obtained after counting the symmetry factors of the various real emission and Born combinations. \mathbf{T}_i^2 is C_F for particle i being a quark or antiquark and C_A for gluons.

The universal factors

$$\gamma_q = \gamma_{\bar{q}} = \frac{3}{2} C_F, \quad \gamma_g = \frac{11}{6} C_A - \frac{2}{3} T_R N_f = \beta_0, \quad (2.68)$$

and

$$K_q = K_{\bar{q}} = \left(\frac{7}{2} - \frac{\pi^2}{6} \right) C_F, \quad K_g = \left(\frac{67}{18} - \frac{\pi^2}{6} \right) C_A - \frac{10}{9} T_R N_f, \quad (2.69)$$

appear in various calculations and especially K_g will be discussed in Sec. 7.1.1.

For processes with partons in the initial state the dipoles are again constructed to capture all divergences of the real emission. Due to the mismatch which leads to PDF renormalization only the sum of integrated dipoles and collinear counter terms provides the pole structure of the virtual contribution. The poles are fully included in the insertion operator I . The additional finite insertion operators P and K are introduced to collect the remaining expressions^{§§§}. P depends on the factorization scale and is proportional to the regularized AP-kernels. P mainly compensates the factorization scale running of the Born process to $\mathcal{O}(\alpha_s^2)$. The Operator K collects the remaining parts.

A strong test for the correct implementation of the dipole subtraction is to demand cuts on the variables of the dipole phase space. The calculation was performed in [58]. One requires that e.g. for the final-final dipoles in Eq. (2.57) $y \in [0, 1]$ is smaller than a fixed α . As a consequence logarithms of this cutoff parameter α appear in the I and K operators. For example, if only final-final dipoles are needed the only difference is to add

$$- \mathbf{T}_i^2 \log^2 \alpha + \gamma_i (\alpha - 1 - \log \alpha), \quad (2.70)$$

to the squared brackets in Eqs. (2.62)-(2.64). Note that for $\alpha = 1$ no restriction is made on the phase space of the Dipoles and the expression in Eq. 2.70 vanishes. As a validation for the Matchbox framework, the cutoff parameter α was implemented and can be used in the next version of Herwig++.

Symmetry Factors

In [41] the combinations and relations between symmetry factors of real and Born processes are evaluated. Also with respect to parton showers, see Sec. 3.2, an important result of the discussion is, that there is a difference between final state and initial state gluon splitting. While the final state gluon splitting produces two indistinguishable gluons, in initial state splitting one of the gluons is determined by remaining an initial state. In the summation of the integrated dipole configurations this produces a factor of 1/2 for final state dipole contributions, see Eq. (7.19) in [41] for final states and e.g. Eq. (8.18) for initial states in [41].

P and K Operator

With the formulas given in [41] the integral of the P and K operator can be written as

$$\begin{aligned} \sigma(p)_{PK} = & \sum_a \int_0^1 d\eta \sum_b \int_0^1 dx \int d\Phi^{(m)}(x\eta p) f_a(\eta, \mu_F^2) F_J^{(m)}(p_1, \dots, p_m; x\eta p) \\ & \cdot {}_{m,b} < 1, \dots, m; x\eta p | \left(\mathbf{K}^{a,b}(x) + \mathbf{P}^{a,b}(x\eta p, x; \mu_F^2) \right) | 1, \dots, m; x\eta p >_{m,b} . \end{aligned} \quad (2.71)$$

^{§§§}For identified final states an additional operator H is defined, which is not discussed here.

where it is convenient to perform the variable transformation^{¶¶¶}

$$\eta' = x \cdot \eta \quad , z = x \rightarrow dx d\eta = \frac{1}{z} d\eta' dz \quad (2.72)$$

to get

$$\begin{aligned} \sigma(p)_{PK} = & \sum_a \int_0^1 d\eta' \sum_b \int_{\eta'}^1 \frac{dz}{z} \int d\Phi^{(m)}(\eta' p) f_a\left(\frac{\eta'}{z}, \mu_F^2\right) F_J^{(m)}(p_1, \dots, p_m; \eta' p) \\ & \cdot {}_{m,b<1,\dots,m;\eta' p|} \left(\mathbf{K}^{a,b}(z) + \mathbf{P}^{a,b}(\eta' p, z; \mu_F^2) \right) |{}_{1,\dots,m;\eta' p>m,b} . \end{aligned} \quad (2.73)$$

This transformation has the advantage that the matrix element, as well as the measurement function is independent of z , so that it can be integrated together with the Born and virtual parts of the calculation without recalculation of the matrix elements. The z -integral can then be treated as a Monte Carlo integral with one additional dimension.

2.6. Matching Fixed Order to Resummed Results

After applying the renormalization prescription physical observables become finite. However these predicted quantities are now related to other observables measured at the renormalization scale μ_R . The relation manifests itself for example in a scale dependent coupling constant. As described above the $\mathcal{O}(\alpha_s)$ dependence can be related via the RGE to result in an all order expression for α_s . The leading logarithmic dependence is resummed as

$$\alpha_s(Q) = \alpha_s(\mu_R) \sum_{n=0}^{\infty} (-1)^n \left[\frac{\alpha_s(\mu_R)}{2\pi} \beta_0 \ln\left(\frac{Q^2}{\mu_R^2}\right) \right]^n = \frac{\alpha_s(\mu_R)}{1 + \frac{\alpha_s(\mu_R)}{2\pi} \beta_0 \ln\left(\frac{Q^2}{\mu_R^2}\right)}. \quad (2.74)$$

In order to explain the physical importance and to introduce the first matched expression we think of two observables \mathcal{A} and \mathcal{B} . Both should be α_s dependent and have a perturbative expansion as

$$\mathcal{A} = \mathcal{A}_0(\mu_R) + \mathcal{A}_1(\mu_R) + \mathcal{O}(\alpha_s^{N+2}) = \alpha_s(\mu_R)^N A_0 + \alpha_s(\mu_R)^{N+1} A_1(\mu_R) + \mathcal{O}(\alpha_s^{N+2}), \quad (2.75)$$

where $\mathcal{A}_0(\mu_R)$ is the LO approximation and $\mathcal{A}_1(\mu_R)$ the $\mathcal{O}(\alpha_s)$ contribution to the NLO correction. While the scale dependence of the LO approximation $\mathcal{A}_0(\mu_R)$ is purely¹⁷ in the argument of $\alpha_s(\mu_R)$, the NLO is evaluated for a given renormalization scale μ_R .

The LO calculation of the observable $\mathcal{A}_0(\mu_R)$ is scale dependent due to the truncation of the perturbative series. The scale μ_R can be chosen freely with the RGE of the running coupling. The problem can have many scales $\{q_i\}$, but we should use a 'reasonable' scale μ_R ¹⁸

^{¶¶¶}This variable transformation is the inverse of the transformation which is used to receive the P and K operator from the collinear counter term produced with the Eq. (2.44).

¹⁷We concentrate on the RGE evolution of α_s and ignore other scale dependent parameters or the renormalized PDFs.

¹⁸As an example one can think of dijet production at a hadron collider. The transverse momentum of the hardest jets, but also the scalar sum of all transverse jet momenta H_T seems reasonable.

in order to induce no large logarithms in the higher order corrections, see Sec. 2.3.2. Now the measurement of the observable \mathcal{A} by comparison to $\mathcal{A}_0(\mu_R)$ fixes the value of $\alpha_s(\mu_R)$ at this scale μ_R .

Since α_s is fixed, we can now predict observable \mathcal{B} with a LO calculation at a scale μ_R or q with the value of $\alpha_s(\mu_R)$ or $\alpha_s(q)$, evolved with the RGE. Both predictions are then accurate at LO since the dependence on the scale is one order higher in the perturbative expansion. By using the $\alpha_s(q)$ calculated via the expression above we try to catch the leading logarithmic behaviour by guessing the scale q , again to keep the logarithms of the NLO corrections moderate. We can therefore speak of a resummed prediction for observable $\mathcal{B}_{res} = \mathcal{B}(q)$ when using the value $\alpha_s(q)$.

Expanding the LO expression for $\mathcal{B}(q)$ up to $\mathcal{O}(\alpha_s^{n+1})$ leads to

$$\begin{aligned}\mathcal{B}_0(q) &= \alpha_s(q)^N B(\{q_i\}) = \mathcal{B}(\mu_R) + \alpha_s \partial_{\alpha_s}^1 \mathcal{B}_{res} + \alpha_s^2 \partial_{\alpha_s}^2 \mathcal{B}_{res} + \mathcal{O}(\alpha_s^{N+3}) \\ &= \alpha_s(\mu_R)^N B(\{q_i\}) \\ &\quad - N \alpha_s(\mu_R)^N \left[\frac{\alpha_s(\mu_R)}{2\pi} \beta_0 \ln\left(\frac{q^2}{\mu_R^2}\right) \right] B(\{q_i\}) + \mathcal{O}(\alpha_s^{N+2}).\end{aligned}\tag{2.76}$$

Here the first line defines the 'operators' $\alpha_s^n \partial_{\alpha_s}^n$, which should be seen as expansion operators. They extract the n -th term in a Taylor expansion in α_s . The $\mathcal{O}(\alpha_s)$ part of the inclusive, renormalized NLO correction to the observable \mathcal{B} takes the following form

$$\begin{aligned}\mathcal{B}_1(q) &= \alpha_s^{N+1} B_1(\{q_i\}, q) + \mathcal{O}(\alpha_s^{N+2}) \\ &= \alpha_s^{N+1} B_1(\{q_i\}, \mu_R) \\ &\quad + N \alpha_s^N \left[\frac{\alpha_s}{2\pi} \beta_0 \ln\left(\frac{q^2}{\mu_R^2}\right) \right] B_0(\{q_i\}) + \mathcal{O}(\alpha_s^{N+2})\end{aligned}\tag{2.77}$$

$$\begin{aligned}&= \mathcal{B}_1(\mu_R) \\ &\quad - \alpha_s \partial_{\alpha_s}^1 \mathcal{B}_{res} + \mathcal{O}(\alpha_s^{N+2}).\end{aligned}\tag{2.78}$$

The scale choice of α_s is already $\mathcal{O}(\alpha_s^{N+2})$. By adding the α_s correction to the LO we can see two properties.

On the one hand the scale q drops out at order $\mathcal{O}(\alpha_s^{N+1})$. This is known as scale compensation of higher order corrections. In $B_1(q)$ the scale q is related to the scales of the process which comes out of process dependent NLO calculations. The scale variation decreases by including higher orders. It can still happen that for real physical processes the scale variation increases if the NLO contributions are large, e.g. by newly opened channels.

On the other hand one can get to another interpretation. The first line in Eq. (2.76) is the 'resummed' result $\mathcal{B}_0(q)$. The third line of Eq. (2.76) is then the subtracted $\mathcal{O}(\alpha_s)$ expansion of $\mathcal{B}(q)$. This gives us the first matched expression. To achieve the NLO corrected observable we need to subtract the $\mathcal{O}(\alpha_s)$ expansion from the resummed expression and then add the NLO corrections at the starting scale

$$\mathcal{B}_{NLO} = \mathcal{B}_{matched} = \mathcal{B}_{0,res}(q) - \alpha_s \partial_{\alpha_s}^1 \mathcal{B}_{0,res} + \mathcal{B}_1(\mu_R) = \mathcal{B}_0(q) + \mathcal{B}_1(q) + \mathcal{O}(\alpha_s^2).\tag{2.79}$$

This brief and constructed glance to resummation and matching, already gives the idea of matching

$$d\sigma^{\text{matched}} = d\sigma^{\text{resummed}} - d\sigma^{\text{res., expanded}} + d\sigma^{\text{fixed order correction}}. \quad (2.80)$$

It is not conventional to introduce matching in this context, especially since this work is about parton showers where matching is usually used in the context of resumming soft/collinear logarithms, but we see the same properties.

The next chapter will introduce the theoretical framework of this work by starting with the idea of parton showers and the summation of logarithms expected in all orders for exclusive observables. The chapter again ends with the description of matching LO and NLO calculations in the presence of a parton shower.

CHAPTER 3

Theoretical Framework

In this chapter a deeper introduction into the framework of this work is given. Calculations of fixed order cross sections are limited by the definition of inclusive observables and the perturbative expansion itself. In order to compare theory with experimental results it is often necessary to also predict fully differential observables and estimate the effects of higher orders to exclusive expressions. After pointing out some of the problems of fixed order calculations and giving examples for exclusive observables, an introduction to parton showers is given. Followed by the discussion of parton showers based on the ideas and subtraction properties of the Catani Seymour formalism, see Sec. 2.5, some remarks on initial state parton showers are provided. The chapter is closed by the discussion on matching fixed order calculation at NLO to parton shower algorithms.

3.1. Fixed Order Problems

In the perturbative expansion, it is important to define a process in an IR safe way. Since fixed multiplicity processes suffer from IR divergences, it is necessary to define IR safe observables and to calculate all contributions up to the same order in the perturbative expansion. Additional processes with extra emissions need to be considered in the calculations, since IR safe observables cannot resolve soft and/or collinear emissions. For the calculation of the fixed order it is also important to define the observables properly. This leads to the concept of inclusive and exclusive observables: Inclusive observables, like total cross sections or decay rates do not resolve additional emissions. Exclusive observables are defined by a resolution parameter that is used to resolve additional QCD activity*. If one, for example, wants to know from fixed order calculations the two jet rate in $e^+e^- \rightarrow \text{jets}$ with jets/partons that can have additional emissions with the resolution parameter $y_{ij} = 2p_i p_j / Q^2 < y_{max}$, one needs to calculate the $N^n\text{LO}$ with cuts on the additional emission phase spaces. This was performed to NNLO [59]. The exclusive $N^3\text{LO}$ to this process has been performed in [60].

*In general also additional QED and W/Z emissions, but this work concentrates on QCD emissions.

Prominent examples of exclusive observables are:

- jet rates with resolution parameters defined with jet algorithms as defined by[61–64] (also at hadron colliders),
- transverse momenta of electroweak bosons at hadron colliders, produced by recoiling against QCD radiation (momentum conservation),
- and the angle between weak bosons and/or jets.

The fixed order calculations of these quantities will produce logarithms of the resolution parameter. The leading structure of these logarithms is already given in Eq. (2.70), where the cut on the dipoles phase space, and therefore the non cancellation of the leading behavior of the real emission, lead to logarithms in the cutting parameter. These logarithms can become large and need to be controlled/resummed in order to describe exclusive observables. The result of [59] show that to second order in α_s these logarithms build the first elements in an exponential series for the quark form factor, which was suggested in [65].

The cuts on the dipole phase space are not process dependent and appear at each multiplicity. The same holds for factorization of an arbitrary process in the soft/collinear limit. The process with an additional soft and/or collinear emission can be factorized into a sum of universal splitting functions and the process with one leg less. The consequences of this process independence lead to the development of parton showers.

3.2. Parton Shower

Parton showers make use of the approximation of the real emission process in the quasi-collinear limit to a Born process B_0 : $ab \rightarrow X + f$. In terms of the Born contribution times splitting functions

$$d\sigma_{ab \rightarrow X + \{f \rightarrow f'e\}}^R \approx \frac{\alpha_s}{2\pi} \frac{dq^2}{q^2} dz \frac{d\phi}{2\pi} P_{ff'}(z) d\sigma_{ab \rightarrow X + f}^{LO} \quad (3.1)$$

if the partons f' and e are getting collinear in the final state, and

$$d\sigma_{\{a' \rightarrow a\}b \rightarrow X + f\{+e\}}^R(f_{a'}(x/z)) \approx \frac{f_{a'}(x/z)}{f_a(x)} \frac{dq^2}{q^2} \frac{dz}{z} \frac{d\phi}{2\pi} P_{a'a}(z) d\sigma_{ab \rightarrow X + f}^{LO}(f_a(x)) . \quad (3.2)$$

if the parton e is emitted collinear to the incoming parton a' in the initial state. The variable q captures the collinear behaviour of the propagator structure of the propagator the emission is produced from in the collinear limit. The real emission contains a changed PDF weight, compared to the Born PDF weight, due to the changed incoming momentum fraction x/z .

Here the spin averaged AP splitting functions of Eq. (2.46) and

$$P_{gg}(z) = \frac{2}{1 + \delta_{\text{final}}} C_A \left[\frac{z}{1 - z} + \frac{1 - z}{z} - z(1 - z) \right] \quad (3.3)$$

are used to approximate the matrix elements with an additional emission. δ_{final} is 0 for initial state gluon splitting and 1 for final state gluon splitting and compensates for the fact that the gluons in the final state splitting are indistinguishable, see Sec. 2.5.

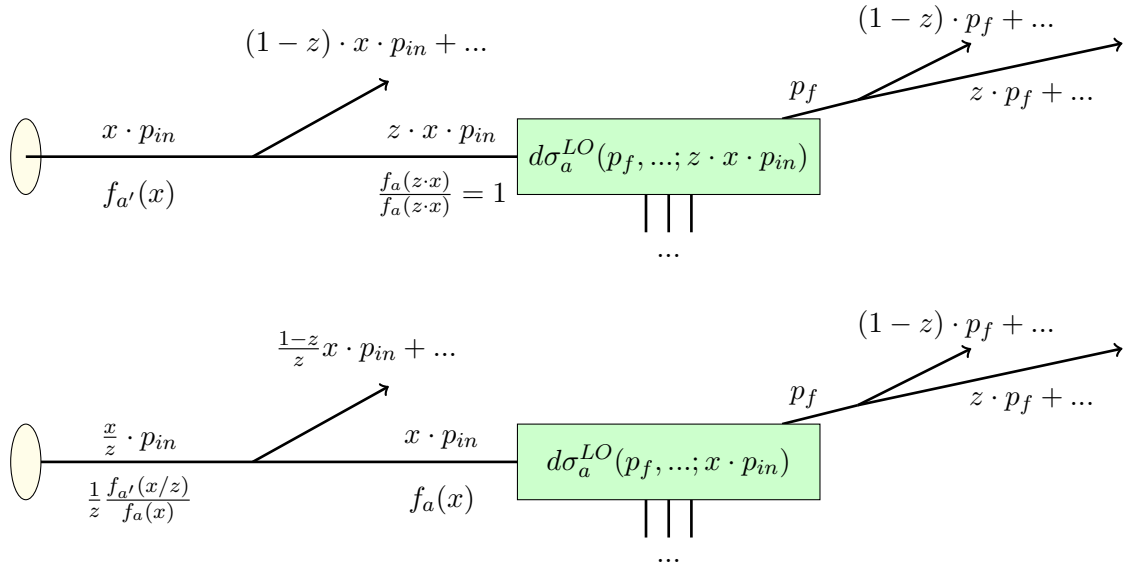


Figure 3.1.: The emissions in the upper picture show the time-like evolution of incoming (and outgoing) partons, which enter – after possible emissions – the hard process. Final state parton shower algorithms are constructed with probabilistic emissions. The momentum fraction of the incoming parton entering the hard process is not ‘known’ before the shower reaches the hard scale/virtuality. For initial state emissions the lower, backward evolution is favourable since the sampling of the hard process depends on the incoming momenta [66]. The difference is formally higher order but also depends on the measurement of the PDFs.

If coloured initial state particles exist one needs to take into account the change of the PDF weight when a parton is evolved from the Born state to the real emission with raised initial state momentum fraction [66]. The change is illustrated in Fig. 3.1 [†].

In Eq. (3.2), the factor $1/z$ appears for the same reason as in Eq. (2.72). The Born contribution $d\sigma_{ab \rightarrow X+f}^{LO}$ is calculated with momentum fraction x of the initial state hadron and is therefore multiplied by the PDF weight $f_a(x)$ of the flavour a . The change of flavours can lead to large PDF ratios, e.g., $\{a, a'\} = \{q, g\}$ in the low x region but also $\{a, a'\} = \{g, q_V\}$ in the large x region (q_V is a valence quark flavour of the hadron). In this sense the real emission, and later the shower, resolves the structure of the initial state hadrons.

The ordering in some variable q_i is then important if we want to describe the leading behavior also beyond the $n+1$ process. In this case, we get the large contributions only if the subsequent emissions are ordered in the variable q , which can be related to an angle, virtuality, transverse momentum, or any ordering variable that behaves like the propagator structure in the soft/collinear limit. If the shower is based on AP splitting kernels, which were derived to describe the branching probability in the PDFs, one has to take care that the singularity of the splitting functions at $z \rightarrow 0$ is not double counted. This enhancement of wide angle emissions is described by coherent emissions off multiple legs, where interference effects result

[†] In principle it would also be possible to start with a time-like evolution starting from small scales and evolve to larger scales. With every emission produced by the showering process. The initial state momentum fraction would change so that the weight evaluated for resonant Born processes would be very inefficient and time consuming.

in an destructive interference for wide angle emissions. The coherent treatment of emissions off different legs can be described as an angular ordering [56]. Only emissions with decreasing angles compared to the previous emissions are allowed by the shower.

The KLN theorem states that the IR divergences cancel between the virtual contributions and the real emission contributions for unresolvable kinematics. The virtual correction can be approximated by subtracting the real emission contributions, added as real emissions contributions above the resolution parameter, below the resolution parameter. Neglecting the change of inclusive observables due to NLO corrections, the parton shower describes exclusive observables in the leading logarithmic approximation. Including more than one emission leads to a change of the weight of the real emission since double emissions must again be subtracted from the single emission contributions. They need to subtract from the 'no emission'/Born contribution. Different ordering variables can lead to different results. But for multiple emissions ordered in q^2 , the phase space integration leads to nested integrals of the form

$$\int_{\mu^2}^{q_0^2} dq_1^2 f(q_1^2) \int_{\mu^2}^{q_1^2} dq_2^2 f(q_2^2) \dots \int_{\mu^2}^{q_{n-1}^2} dq_n^2 f(q_n^2) = \frac{1}{n!} \left(\int_{\mu^2}^{q_0^2} dq^2 f(q^2) \right)^n \quad (3.4)$$

which leads to an exponentiation of the leading behavior of a single emission as a weight for the "no emission" contribution. Ordering the emissions is a necessary condition for the exponentiation. The μ in Eq. (3.4) is from now on called the shower cutoff, which prevents the integrals from diverging as $q^2 \rightarrow 0$.

The physical picture of this shower cutoff is given by the factorization of collinear emissions into PDF/fragmentation at the factorization scale μ_F in the hard, perturbative process. The shower can be seen as a mechanism to evolve the states, factorized at scale q_0 to lower scales. This will be discussed for PDFs in Sec (3.4). Perturbation theory breaks down due to the growing coupling constant evaluated at lower and lower q . Non-perturbative effects and the confinement of partons into hadronic states must be handled by a model of hadronization [3, 67]. However, observables insensitive to either IR/C emissions or particle multiplicities, i.e. inclusive observables, are less affected by the choice of μ . The shower cutoff can be seen as a parameter of the hadronization model and must be tuned together with the parameters of the model.

In the evolution picture, each leg of the Born process is evolved from an hard scale q_0 to the shower cutoff μ with the exponential factors, called Sudakov form factors. The expectation value of an exclusive observable $\mathcal{O}(\{p_i\})$ that can resolve emissions, is described by

$$\langle \mathcal{O}(\{p_i\}) \rangle = \int d\{p'_i\} \rho(\{p'_i\}) \delta(\mathcal{O}(\{p_i\}) - \mathcal{O}(\{p'_i\})) , \quad (3.5)$$

where $\{p'_i\}$ is the set of all possible parton multiplicities that are integrated over their usual phase spaces including momentum conservation. The density $\rho(\{p'_i\})$ is now approximated with the formula

$$\rho(\{p'_i\}) = \sum_{sub} \int_{\phi_0} d\sigma_{B_0}^{sub}(\phi_0, q_0) \mathcal{PS}_{q_0 \rightarrow \mu} [X_0(\phi_0, q_0)] , \quad (3.6)$$

in which we define the parton shower 'operator' $\mathcal{PS}_{q_0 \rightarrow \mu} [.]$ [‡] as an operator that acts on the $\{\{p_i\}(\phi_0), \{f\}, \{i\}\}$ -configuration $X_0(\phi_0, q_0)$ characterized by the momenta and flavour structure of the Born phase space point.

The summation in front of the integral contains the subprocesses of the Born process with the same number of partons. This operator is able to produce new partons in an iterative manner and acts on the Born configuration $X_0(\phi_0, q_0)$ like

$$\begin{aligned} \mathcal{PS}_{q_0 \rightarrow \mu} [X_0(\phi_0, q_0)] &= \prod_{f,i} \Delta_f(q_0 \rightarrow \mu) \Pi_i(q_0 \rightarrow \mu) X_0(\phi_0, \mu) \\ &+ \int_{\mu^2}^{q_0^2} \frac{dq_1^2}{q_1^2} \int_{z_-}^{z_+} dz \frac{\alpha_s(q_1)}{2\pi} \sum_{f,f'} \left[\prod_{f,i} \Delta_f(q_0 \rightarrow q_1) \Pi_i(q_0 \rightarrow q_1) \right] \\ &\cdot P_{ff'}(z) \mathcal{PS}_{q_1 \rightarrow \mu} [X_1(\phi_1, q_1)] \\ &+ \int_{\mu^2}^{q_0^2} \frac{dq_1^2}{q_1^2} \int_{z_-}^{z_+} \frac{dz}{z} \frac{\alpha_s(q_1)}{2\pi} \sum_{i,i'} \left[\prod_{f,i} \Delta_f(q_0 \rightarrow q_1) \Pi_i(q_0 \rightarrow q_1) \right] \\ &\cdot \frac{f_{i'}(x_i/z, q_1)}{f_i(x_i, q_1)} P_{i'i}(z) \mathcal{PS}_{q_1 \rightarrow \mu} [X_1(\phi_1, q_1)] . \end{aligned} \quad (3.7)$$

The first line keeps the Born configuration with no emissions and is weighted by a Sudakov factor for each final state external leg, exponentiating the integral of the second and third line

$$\Delta_f(q_0 \rightarrow \mu) = \exp \left(- \sum_{f'} \int_{\mu^2}^{q_0^2} \frac{dq_1^2}{q_1^2} \int_{z_-}^{z_+} dz \frac{\alpha_s(q_1)}{2\pi} P_{ff'}(z) \right) . \quad (3.8)$$

The factor

$$\Pi_i(q_0 \rightarrow \mu; x_i) = \exp \left(- \sum_{i'} \int_{\mu^2}^{q_0^2} \frac{dq_1^2}{q_1^2} \int_{x_i}^{z_+} \frac{dz}{z} \frac{\alpha_s(q_1)}{2\pi} \frac{f_{i'}(x_i/z, q_1)}{f_i(x_i, q_1)} P_{i'i}(z) \right) . \quad (3.9)$$

is the Sudakov factor for initial states containing the PDF ratio and the functions of the fourth and fifth line. The squared brackets in the second and fourth line have their origin in the ordering and incorporate the fact that no harder emission took place before the splitting at scale q_1 . The boundaries on the z -integration are needed to regulate the soft singularity at $z = 1$, but can also be used to implement angular ordering [56].

[‡] No vector space was defined properly, so the word 'operator' should be treated more in a pictorial way, not a strictly mathematical. In the following we drop the quotation marks.

In principle and to break it down to the basics, the parton shower makes iterative use of the identity

$$1 = e^{-\int_a^b dx f(x)} + \int_a^b dx f(x) e^{-\int_x^b f(x') dx'} \quad (3.10)$$

with $f(x)$ being the sum in Eqs. (3.1) and (3.2).

After the parton shower splits the external legs to arrive at state $X_1(\phi_1, t_1)$, this is now again able to evolve from q_1 to lower scales of the ordering parameter, again described by the parton shower. A new '1' is inserted into Eq. (3.10). Note that $\mathcal{PS}_{q_0 \rightarrow \mu}[X_0(\phi_0, q_0)] \neq \mathcal{PS}_{q_0 \rightarrow \mu}[X_1(\phi_1, q_0)]$ since the second operator acts on a state with an additional parton in the final state and a potentially changed initial state.

Even if the leading logarithms can be resummed by this description, next-to-leading logarithms play an important role in the description of nature and exclusive observables. Eq. (2.70) shows the structure of logarithms if we make a cut in the real emission phase space as

$$\frac{\alpha_s}{2\pi} (T_i^2 \log^2 \alpha + \gamma_i \log \alpha),$$

with the γ_i as defined in Eq. (2.68). The leading logarithm (LL) $- \alpha_s \log^2$ – from this expression is proportional to the Casimir of the splitting, and the next-to-leading logarithm (NLL) $- \alpha_s \log$ – is proportional to γ_i , which are closely related to quark number conservation and momentum conservation in the z integration [50].

In Addition to the two logarithms coming from the integration of the splitting functions, we can construct two more logarithms that come from the scale choice of the argument of α_s and the PDFs. Since α_s is a resummed expression in schemes like $\overline{\text{MS}}$, if the argument of α_s is chosen to be the ordering variable, one gets $\mathcal{O}(\alpha_s^2 L^3)$ from the expansion of $\alpha_s(q_1)$. This is the same level of logarithm as the interference of the T_i^2 and the γ_i term in the expansion of the exponential, so too at NLL. The same holds for the PDF ratio from DGLAP evolution. In this construction, the approximate 'real' emission contributions are subtracted and in the parton shower then exponentiated to build the LL-approximations.

NLO corrections in scale dependent schemes, will shift the scale dependence one order higher in perturbation theory. The NLO calculation itself relates the scale used to calculate the Born contribution and which is then used as a renormalization scale of the virtual contributions to scales which are relevant for the process, see discussion in Sec (2.3.2). As described in [3] higher orders can be resummed by choosing the argument of α_s close to the scale of the splitting. If the scale used to calculate the LO contribution is not related to the scales of the process, large corrections from the NLO corrections are expected.

Various parton shower approximations differ mostly in the choice of the splitting functions and in the choice of the ordering variable. Based on subtraction formalisms like CS dipole subtraction or antenna subtraction, new terms were introduced more with the intention of simplifying NLO calculations. New dipole-like parton shower terms were introduced. The advantage of having kernels that intrinsically damp large angle emissions, respect momentum conservation, and are at the same time used for NLO-matching will be explained in the next section.

3.3. Parton Shower with CS-Dipoles

The interference effects that lead to angular ordering [56, 68] are present in all kinds of real emission amplitudes with gluons involved. A general NLO subtraction formalism for real emission contributions like the CS dipole formalism needs to respect these effects in order to subtract the soft gluon emissions properly. In [41] it was proven that the construction of the dipoles approaches the real emission amplitudes in all IR regions. Momentum conservation and the phase space measure of single dipoles are crucial to achieve the subtractive properties. Double counting of the region $z \rightarrow 0$ in AP showers is not present since the dipole subtractions damp this region in a way that the sum of multiple dipoles leads to the correct behavior. The interference effects, which led to the coherence effects, are covered by the dipoles. No angular ordering is needed.

For the construction of, e.g. Eq. (2.57), the spin-colour-correlated matrix elements for Born processes involving gluons, or at least the colour-correlated-matrix elements of the Born amplitudes, are needed to perform the subtraction. This is not handy for large multiplicity amplitudes. One falls back to the large N_C treatment of the amplitudes in the shower algorithm. Spin averaged splitting functions are also provided in [41]. So in order to construct the parton shower, one needs to invert the tilde kinematics, e.g. Eq. (2.55), and define an ordering variable. Since angular ordering is not required with the dipole functions the choice of ordering parameter is the p_T of the individual dipole, see discussion in [69]. Also in the argument of α_s the p_T of the individual splitting is used [57, 69].

In [69] and [57], inversion and modified-inverted tilde kinematics were constructed. The question of phase space boundaries in order to exponentiate logarithms present in analytic calculations was addressed in [57]. In the dipole shower of Herwig++ based on [57], additional terms were added in order to render the kernels positive. In the subtraction formalism [41] the positiveness of the kernels is not needed but additional powercorrections can be added in order to interpret the splittings as probabilities. In the Sherpa shower [5] based on [69], these are set to zero. Both treatments are beyond NLL accuracy.

In showers that do not respect momentum conservation for each emission, the momenta are reshuffled when the showering process is finished in order to preserve the overall momentum conservation. The choice of variables that are fixed in the reconstruction are ambiguous. The tilde kinematics of [41] shuffle the momenta of the involved dipole only, with the exception of initial-initial (II) dipoles. If no II-dipole is present in the process, like in DIS[§] or LEP-like beam configurations, the momenta of non-coloured objects will not be changed by the showering process.

Radiation of II-dipoles will perform a boost on the full electroweak system, in order to keep the initial states on the beam axis like in CS subtraction. Drell-Yan-like processes with pure initial state $q\bar{q}$ pairs that radiate a final state gluon, have no large N_C connection between the initial states after the emission. Additional gluon emissions will not change the electroweak system. This is important for low p_T observables. In [69], the scale of the initial state splittings was chosen to be $p_T/2$, which leads to an enhancement of the initial state radiation and therefore a shift of the Sudakov peak[¶].

[§]Deep inelastic scattering (DIS) describes the collision of electrons and hadrons.

[¶]The enhancement of emissions for small splitting scales is compensated by the no emission probability (Sudakov form factor). This leads to maxima in various distributions like the transverse momentum of the electroweak systems. This behaviour is called the Sudakov peak.

Using the CS dipole shower for the purpose to match with higher order corrections has the advantage that the shower and the subtraction are closely related, see Ch. 3.5. For the merging of multiple LO and NLO calculations the fact that the tilde kinematics preserve momentum conservation is valuable since the clustering of states with additional emissions can be performed with the same kinematic constraints the shower also produces. This will help in the construction of the merging algorithm.

3.4. Initial State Parton Showers and DGLAP Equation

The evolution Equation for the initial state shower can also be obtained by solving the DGLAP Equations as [42]

$$\frac{f_i(x, q_0)}{\Delta_i(q_0 \rightarrow \mu)} = f_i(x, \mu) + \int_{\mu^2}^{q_0^2} \frac{dq^2}{q^2} \frac{\alpha_s}{2\pi} \frac{1}{\Delta_i(q \rightarrow \mu)} \sum_j \int_x^1 \frac{dz}{z} P_{ij}(z) f_j(x/z, q),$$

where Δ_i are time-like Sudakov form factors and $P(z)$ are the un-regularized AP splitting functions. The Equation above is modified to

$$1 = \underbrace{\frac{f_i(x, \mu) \Delta_i(q_0 \rightarrow \mu)}{f_i(x, q_0) \Delta_i(\mu \rightarrow \mu)}}_{\Pi_i(q_0 \rightarrow \mu)} + \int_{\mu^2}^{q_0^2} \frac{dq^2}{q^2} \frac{\alpha_s}{2\pi} \sum_j \int_x^1 \frac{dz}{z} P_{ij}(z) \frac{f_j(x/z, q)}{f_i(x, q)} \underbrace{\frac{f_i(x, q) \Delta_i(q_0 \rightarrow \mu)}{f_i(x, q_0) \Delta_i(q \rightarrow \mu)}}_{\Pi_i(q_0 \rightarrow q)}. \quad (3.11)$$

Using an exponential ansatz like in Eq. (3.10) and ignoring phase space constrains which regulate the soft singularity at $z = 1$, this leads to the solution of Eq. (3.9), which corresponds to the idea that a parton shower evolves PDFs.

CS based showers respect momentum conservation and the splitting kernels are not the AP kernels. Additionally final state emissions can induce changes of initial state momentum fraction, which is the case for FI dipoles. So too for final state splittings do PDF ratios appear, which then are evaluated at the scale of the final state splitting [69].

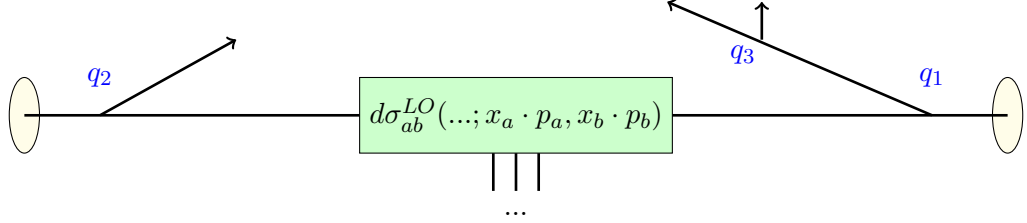
Thus a shower based on CS dipoles does not reproduce the exact DGLAP Equations used to perform the running of the PDFs. In the merging of matrix elements, where we will expand the expressions coming from the shower and from PDF ratios, we will take care that we do not mix shower expansion and DGLAP running.

Another comment is about the interplay between final and initial state Sudakov form factors. Therefore we inspect an example event and review which weights the shower adds to the event. We take a look at the event of Fig. 3.2 and the corresponding shower weights. Notice that for $1 \rightarrow 2$ showers no PDF ratio is applied for the scale q_3 since q_3 is the scale of the final state splitting. Additionally the combination of backward Sudakov and PDF ratio can be written as, e.g.

$$\Pi(q_0 \rightarrow q_2) \frac{f_q(x/z, q_2)}{f_q(x, q_2)} \approx \Delta(q_0 \rightarrow q_2) \frac{f_q(x/z, q_2)}{f_q(x, q_0)}. \quad (3.12)$$

This replacement is illustrated in the lower diagram of Fig. 3.2.

An exclusive event with three additional emissions:

 Ordered scales of emissions $q_0 > q_1 > q_2 > q_3$:


Shower weights for exclusive 3 emissions (in backward evolution):

$$\begin{array}{ccc}
 \Delta(q_2 \rightarrow \mu) & & \Delta(q_3 \rightarrow \mu) \quad \Delta(q_3 \rightarrow \mu) \\
 \alpha_s(q_2) & & \alpha_s(q_3) \quad P_f(z_3) \quad \alpha_s(q_1) \\
 \text{---} & & \text{---} \\
 \text{---} & & \text{---} \\
 \Pi_a(q_0 \rightarrow q_2; x_a) & d\sigma_{ab}^{LO}(\dots; x_a \cdot p_a, x_b \cdot p_b) & \Pi_b(q_0 \rightarrow q_1; x_b) \\
 \text{---} & | | | & \text{---} \\
 \text{---} & \dots & \text{---} \\
 P_{ca}(z_2) \frac{f_c(x_a/z_2, q_2)}{z_2 f_a(x_a, q_2)} & & P_{db}(z_1) \frac{f_d(x_b/z_1, q_1)}{z_1 f_{a'}(x_b, q_1)} \\
 \Pi_c(q_2 \rightarrow \mu; x_a/z_2) & & \Pi_d(q_1 \rightarrow \mu; x_b/z_1)
 \end{array}$$

Written as time-like shower:

$$\begin{array}{ccc}
 \Delta(q_2 \rightarrow \mu) & & \Delta(q_3 \rightarrow \mu) \quad \Delta(q_3 \rightarrow \mu) \\
 \alpha_s(q_2) & & \alpha_s(q_3) \quad P_f(z_3) \quad \alpha_s(q_1) \\
 \text{---} & & \text{---} \\
 \text{---} & & \text{---} \\
 \frac{\Delta_a(q_0 \rightarrow q_2)}{f_a(x_a, q_0)} & d\sigma_{ab}^{LO}(\dots; x_a \cdot p_a, x_b \cdot p_b) & \frac{\Delta_b(q_0 \rightarrow q_1)}{f_{a'}(x_b, q_0)} \\
 \text{---} & | | | & \text{---} \\
 \text{---} & \dots & \text{---} \\
 \frac{1}{z_2} P_{ca}(z_2) & & \frac{1}{z_1} P_{db}(z_1) \\
 f_c(x_a/z_2, \mu) \Delta_c(q_2 \rightarrow \mu) & & f_d(x_b/z_1, \mu) \Delta_d(q_1 \rightarrow \mu)
 \end{array}$$

Figure 3.2.: As an example for the weights produced by the shower algorithm, the exclusive emission of three additional partons is illustrated. The shower emissions are produced at the scales q_i . Intermediate Sudakov form factors Π_i and Δ_i describe the no emission probability between two scales. The splitting is described by the AP splitting functions, which depend on the flavour configuration and the momentum fraction z_i . The scales q_i are ordered and for initial state emissions the incoming momentum fractions change. The PDF weights, how the parton was extracted from the hadron leads to ratios for each splitting, evaluated at the scale of the splitting. Time-like (or forward evolution) does not contain the PDF ratios, but the parton is extracted at the cutoff scale μ .

Neglecting phase space boundaries, the initial line can be seen as reweighted with a time-like Sudakov form factor. This only holds, if the parton shower does reproduce a DGLAP running, which is used to evolve the PDFs, at the order of accuracy that is demanded. The effect of the mismatch can be neglected for LO merging but needs to be taken into account for NLO merging. Also, the fact that we do not expect a PDF ratio for the third splitting scale q_3 needs to be taken into account, see discussion after Eq. (4.9).

3.5. Matching Fixed Order NLO Corrections to a Parton Shower

In this section the matching of a fixed order calculation to a parton shower is described. We start with the problem of double counting of real emission contributions and approximated real emissions by the shower and see how methods like MC@NLO [6] and POWHEG [11] overcome these problems. Parton showers are based on the assumption that IR and C divergences factorize from the amplitudes, and that it is possible to exponentiate the leading – and next to leading – logarithmic dependencies. The parton shower expanded up to $\mathcal{O}(\alpha_s)$ therefore describes the leading behavior of the cross sections with one additional jet above the IR cutoff. By unitarity of the parton shower and with the KLN theorem, the Sudakov form factor expanded up to $\mathcal{O}(\alpha_s)$ contains the leading behavior of the sum of virtual amplitudes and real emissions integrated to the resolution parameter. If one naively would add NLO corrections to the parton shower the leading behavior of the real emission as well as the α_s expansion of the Sudakov would be double counted. In order to cure this issue one can use the matching Eq. (2.80)

$$d\sigma^{\text{matched}} = d\sigma^{\text{resummed}} - d\sigma^{\text{res, expanded}} + d\sigma^{\text{fixed order correction}}.$$

The resummed expression is given by the parton shower acting on the Born states and the fixed order corrections is the NLO cross section without the Born contribution. Using Eq. (2.80), the NLO cross section matched to parton shower can be written in a fully differential way and for an arbitrary shower as [70]

$$d\sigma^{\text{matched}} = \mathcal{PS}[d\sigma_B u_0] \quad (3.13)$$

$$+ d\sigma^{VIPK} u_0 + \sum_i (P_i d\sigma_B \theta_{PS} - D_i d\sigma_B) \theta(q_i - \mu) \tilde{u}_{0,i} \quad (3.14)$$

$$+ \left(d\sigma_R - \sum_i P_i d\sigma_B \theta(q_i - \mu) - \sum_i D_i d\sigma_B \theta(\mu - q_i) \frac{u_{1||0}}{u_1} \right) \theta_{PS} u_1 \quad (3.15)$$

$$+ d\sigma_R \prod_j \theta(q_j - \mu) \theta_{PS} u_1. \quad (3.16)$$

In Eq. (3.13), the parton shower acts on a phase space configuration u_0 with the weight $d\sigma_B$ in a differential Monte Carlo interpretation. The phase space configuration u_k is a general objects that contains all information of the current state of the process. The information on scales and momenta as well as flavour structure and phase space cuts are used to define observables and to regularize the IR/C singularities of the Born process. So u_k contains the measurement (jet defining) functions of Sec. 2.5. The index k describes the number of additional particles with respect to the Born process. When the parton shower acts on these configuration, they can be transformed to describe more additional particles. The tilde on $\tilde{u}_{0,i}$ denotes that the dipole i receives its configuration with no additional emission from clustering

to the tilde kinematic, see Sec. 2.5. The ambiguity of $u_{1||0}$, whether the contribution contains an emission or not is addressed below. $d\sigma^{VIPK}$ in Eq. (3.14) contains the virtual correction, the integrated dipoles and the collinear remainders in the sense of Eq. (2.73). The second term in Eq. (3.14) is the difference between the dipoles – or other constructions to perform subtraction of the real emission^{||} – and the expressions the shower is build on. We will call this the shower approximation. Note that the θ_{PS} is used to restrict the shower phase space to the region accessible for the first shower emission. The θ -function is used to keep all shower contributions above the shower cutoff μ . It should be also reminded that if the shower is based on the AP-kernels, angular ordering must be imposed to get the correct singular limit (see Sec. 2.5). It is important that the θ_{PS} exactly reflects this behaviour. While Eqs. (3.13) and (3.14) have Born-like kinematic, the phase space configurations/measurement functions u_1 of Eq. (3.15) contain one additional parton. Here, the real emission is subtracted by the shower approximation [70] if the phase space point is reachable by the shower and above the shower cutoff. If the scale of the splitting is below the shower cutoff, the exact dipole is subtracted. Outside the shower phase space θ_{PS} , the real emission is added without subtraction Eq. (3.16).

If the emission of a parton is below the parton shower cutoff, which is labelled as unresolved by the shower, there is no counter part coming from the shower. The fixed order calculation contains the dipole contributions, which is subtracted from the real emission. There is an ambiguity in the event interpretation of this part. This ‘bridge cross section’ can contribute to the Born-like kinematics u_0 or the real emission phase space configuration u_1 , so $u_{1||0}$. Since the subtraction formalism needs to be IR safe this contribution can only be a power correction. The ambiguity is labelled as the ratio of phase space configurations $u_{1||0}/u_1$ in Eq. (3.15). The ratio, describing the ambiguity must also be applied to the real emission contribution if the real emission phase space point shows configurations below the shower cutoff, which is suppressed in favour of readability**.

The MC@NLO and POWHEG approach are different from Eqs. (3.13)-(3.16). The difference is basically that the shower acts on $d\sigma^{\text{matched}}$ a second time. Since $\mathcal{PS}[\mathcal{PS}[\cdot]] = \mathcal{PS}[\cdot]^{\dagger\dagger}$ this does not change Eq. (3.13) but will change the other contributions. The change is formally $\mathcal{O}(\alpha_s^2 L^2)$ if the shower claims to be NLL and $\mathcal{O}(\alpha_s^2 L^3)$ if the shower reproduces the LL approximation, hence the procedure will not change the accuracy of the shower process. Due to the unitarity of the showering process, inclusive observables will not be changed, so that the accuracy of the fixed order correction is not modified.

It is known that the ratio between NLO and LO

$$K = \frac{\sigma_{NLO}}{\sigma_{LO}} \quad (3.17)$$

called the K -factor^{††} can be large. The size of the K -factor can have different reasons, which are not necessarily scheme independent. In [71] or [72] it is stated that the bulk of the

^{||}We will call the subtraction formalism dipoles in the following, but formally we are not restricted to this as long as the IR limit is properly reached.

^{**}In principal one can add arbitrary contributions to the dipoles and the corresponding counterparts in the integrated forms of the I , P and K operator that do not destroy the subtraction properties. In order to have a cancellation between dipoles and their corresponding counterparts, the choice should be u_0 .

^{††}After the shower operator was applied to some configuration, the scales are evolved to the shower cutoff. So multiple operations will not change the contributions.

^{‡‡}We will use K -factor synonymously for inclusive and differential definitions of observables.

large cross section of Drell-Yan processes and especially Higgs-Boson production is due to the π^2 terms originating from analytic continuation of logarithms with negative argument $\log(-s_{ij}^2/Q^2) = \log(s_{ij}^2/Q^2) - i\pi$ in combination with newly opening channels in the real emission. The shape distortion due to newly opening channels like ug initiated Z production is partly captured by the shower, even if the value of the cross section is not changed, the shape of the Sudakov peak depends on the PDF ratios in backward evolution. On the other hand, π^2 contributions will not be covered by showering and it is not clear that those terms are exponentiated since other power corrections can become important at higher order in the perturbative expansion, which then reduce or enlarge the cross section. Such large corrections are either part of the hard function of an analytic resummation or exponentiate. In both cases it is clear that they should not be stored at the Born kinematic but also be contributing to the emission phase space. Showering the virtual and real contributions will give a shower shape in the IR region but will still correct the 'hard' region, where only real emission contribute without shower subtraction. Both MC@NLO and POWHEG shower the ' π^2 '-terms, but lead to different results.

The difference between MC@NLO and POWHEG^{§§} can be summarized in the choice of which parts of Eqs. (3.13)-(3.16) should be set to zero, or at least be suppressed. For MC@NLO, the shower is chosen close to the subtraction formalism. In this respect the second term in Eq. (3.14) vanishes if one neglects the phase space restrictions and large N_C colour structure of the shower. For POWHEG, the parton shower is modified for the hardest emission^{¶¶}, so $\sum_i P_i d\sigma_B$ is chosen to be $d\sigma_R$. This will remove the first term in Eq. (3.15). If the phase space of the shower is not restricted and one uses the u_0 option in Eq. (3.16), then all contributions are projected to Born-like kinematics. The advantage of choosing the real emission as the shower approximation is that the events are mainly positive, where the name POsitiv-Weight Hardest Emission Generator (POWHEG) originates. The disadvantage is that the ratio of real emission and Born contribution needs to be exponentiated. Interference effects and, e.g. final state weak boson emissions, are part of the POWHEG-Sudakov factor.

The difference between POWHEG and MC@NLO in regions of phase space that are not accessible by the LO process and which are filled by either the shower or, in the case of fixed order calculations, by the real emission contributions, can become large, although they are formally of the same logarithmic accuracy. The LO accurate description of the observables testing these regions in NLO calculations is modified by the NLO corrections of the underlying process as well, especially Regions that are not accessible by the shower due to different restrictions on the shower phase space between POWHEG and MC@NLO. Since the POWHEG Sudakov for the first emission must reproduce the real emission contribution, the phase space of the emissions cannot be restricted for hard emissions. Here the LO and extra NLO contributions are then distributed over the full real emission phase space. In the case of MC@NLO, the pieces of the matched cross section, which are generated with LO like kinematics, receive the showering of the underlying Born process, which is restricted.

^{§§}Here the expressions MC@NLO and POWHEG refer to the nowadays commonly used terms of combining parton showers with NLO calculations. In the meantime also other POWHEG-like and MC@NLO-like have been constructed that take into account phase space boundaries for POWHEG, e.g [70]. Originally MC@NLO is the general matching and POWHEG is a form of MC@NLO.

^{¶¶}It is not always given that the hardest emission is the first. Especially for angular ordered showers like Herwig. Here it is necessary to inject softer but wide angled emissions with the help of an truncated showering algorithm, see e.g. [73, 74].

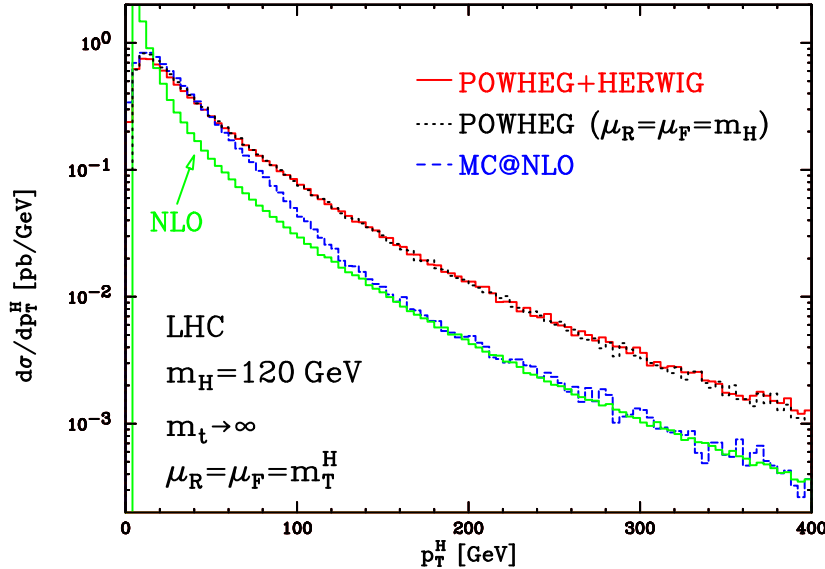


Figure 3.3.: Plot taken from [75]. The comparison between MC@NLO and POWHEG shows for Higgs production large differences in the tail of the distributions. While the MC@NLO approach restricts the emissions from Born-like configuration to the shower phase space, the POWHEG (without damping factor, see [75]) allows emissions from the Born-like configuration into the full real emission phase space. The 'NLO' distribution describing the transverse momentum of the Higgs p_T^H contains pure real emission contributions. The MC@NLO distribution shows the same behaviour as the real emission/LO H+j above the hard scale of the shower M_H (for Born-like configurations).

This behaviour can be seen in Fig. 3.3. In [75], the comparison is made between MC@NLO and POWHEG. The large K -factor of Higgs production via gluon fusion leads to large differences between MC@NLO and POWHEG. This difference between the two matching schemes happens for well-separated emissions and scales between partonic states. These regions can also be described by LO and NLO calculations, which then predict the observables with same or higher accuracy. This motivates the combination of multiple NLO corrections. How this can be achieved in a consistent way is part of the following chapters.

CHAPTER 4

Merging Matrix Elements and Parton Showers

This chapter is dedicated to the theoretical framework of merging multiple LO matrix elements with parton shower simulations. In Sec. 4.1 we introduce a shorter notation to keep the following formulas readable. In Sec. 4.2 we describe and review the formalism of merging fixed order matrix elements to a resummed parton shower calculation. Overlapping parton shower phase spaces and the consequences are shown. Changes to inclusive observables at $\mathcal{O}(\alpha_s)$ are investigated in Sec. 4.6. The effort of controlling these differences leads to an unitarization prescription. A clustering algorithm based on the CS-dipoles is given in Sec. 4.5. Discussions on unordered histories, the smoothness and accuracy of merging are studied in Sec. 4.6 and Sec. 4.7.

4.1. Change of Notation

In the previous chapters the notation was introduced in a way that is common in high energy particle physics. In the following chapters the formulas will be extended. Therefore this section is used to introduce a shorter but still precise notation. We start with the inclusive cross section of Eq. (2.29)

$$\sigma(p, \bar{p})_X = \sum_{a,b} \int_0^1 d\eta f_a(\eta, \mu_F^2) \int_0^1 d\bar{\eta} \bar{f}_b(\bar{\eta}, \mu_F^2) \sigma_{ab}(\eta p, \bar{\eta} \bar{p}, \mu_F^2)_X ,$$

which we rewrite in the perturbative expansion as

$$\sigma(p, \bar{p})_X = B_0(\mu_{F,R}) u_0 + \sum_{i=0} V_i(\mu_{F,R}) u_i + \sum_{i=1} B_i(\mu_{F,R}) u_i + \sum_{i=0} C_i(\mu_{F,R}) u_i + \sum_{i=0} \mathcal{O}(\alpha_s^{i+2}) .$$

$B_i(\mu_{F,R})$ in this notation corresponds to the Born-like phase space weights, including real emission contributions as Born-like structures. $V_i(\mu_{F,R})$ contains renormalized one loop corrections and $C_i(\mu_{F,R})$ carries the weight of the collinear counter terms needed for composite

initial states. The expressions in $\mathcal{O}(\alpha_s^{i+2})$ contains higher than one loop corrections. All weights including the PDF and α_s weights are included in B_i , V_i and C_i . The integral and sum over the full phase space and flavour combinations are carried out implicitly. B_i and V_i contain at least the final state X and i additional parton emissions. u_i is introduced in Sec. 3.5 as the phase space configuration containing the information on the current state of the process. This configuration can change by applying the shower algorithm. The information is used to define observables containing jets, as is done in [41] with the jet defining functions. For IR/C safe observables the results obtained by the information of u_{i+1} and u_i are equal, when the additional emission becomes soft/collinear.

The u_0 and u_i can, as in Sec. 3.5, be used to introduce cuts in the phase space. In this case the cross section measured is not the inclusive cross section. The combination

$$\sigma(p, \bar{p})_{X+i} = B_i(\mu_{F,R})u_i + V_i(\mu_{F,R})u_i + B_{i+1}(\mu_{F,R})u_{i+1} + C_i(\mu_{F,R})u_i , \quad (4.1)$$

defines the NLO cross section to the process with i additional emissions from the process X . Without cuts defined, the expression is divergent. For i additional separated partons Eq. 4.1 is finite and written as

$$\sigma_i^{NLO} = [B_i + \bar{V}_i(\mu_R, \mu_F) + IPK_i] u_i + \sum_j D_j \tilde{u}_i^j + B_{i+1} u_{i+1} .$$

Here, \bar{V}_i contains the UV renormalized virtual amplitude for i additional separated partons. IPK_i contain the insertion operators from the CS formalism for the process with i additional emissions. B_{i+1} is the real emission and D_i are the CS dipoles.

Now the notation for the parton shower is reduced to the essentials. The formula for the iterative parton shower Eq. (3.7)

$$\begin{aligned} \mathcal{PS}_{Q_0 \rightarrow \mu} [X_0(\phi_0, Q_0)] &= \prod_{f,i} \Delta_f(Q_0 \rightarrow \mu) \Pi_i(Q_0 \rightarrow \mu) X_0(\phi_0, \mu) \\ &+ \int_{\mu^2}^{Q_0^2} \frac{dq_1^2}{q_1^2} \int_{z_-}^{z_+} dz \frac{\alpha_s(q_1)}{2\pi} \sum_{f,f'} \left[\prod_{f,i} \Delta_f(Q_0 \rightarrow q_1) \Pi_i(Q_0 \rightarrow q_1) \right] \\ &\cdot P_{ff'}(z) \mathcal{PS}_{q_1 \rightarrow \mu} [X_1(\phi_1, q_1)] \\ &+ \int_{\mu^2}^{Q_0^2} \frac{dq_1^2}{q_1^2} \int_{z_-}^{z_+} \frac{dz}{z} \frac{\alpha_s(q_1)}{2\pi} \sum_{i,i'} \left[\prod_{f,i} \Delta_f(t_0 \rightarrow q_1) \Pi_i(Q_0 \rightarrow q_1) \right] \\ &\cdot \frac{f_{i'}(x_i/z, q_1)}{f_i(x_i, q_1)} P_{i \leftarrow i'}(z) \mathcal{PS}_{q_1 \rightarrow \mu} [X_1(\phi_1, q_1)] . \end{aligned}$$

is reduced to

$$\mathcal{PS}_0[u_0] = u_0 \Delta_\mu^{Q_0} + \alpha_s(q_1) \frac{f_1(q_1)}{f_0(q_1)} \Delta_{q_1}^{Q_0} P_1(z) \mathcal{PS}_1[u_1]. \quad (4.2)$$

In this short notation Δ_b^a contains the full Sudakov form factor for initial and final state radiation from a hard scale a (upper index) to a softer scale b (lower index). The phase space integration is taken implicit as a property of $P(z)$, which now also contains $1/2\pi$. $f_0(q_1)$ is the PDF weight of the flavour and momentum fraction x before the splitting evaluated at the scale of the splitting. $f_1(q_1)$ is the new PDF after the backward splitting. For final state emissions of $1 \rightarrow 2$ showers this ratio is one since no flavour change and x variation is induced. For dipole-like showers with momentum conservation at each emission the initial state spectator parton can change its momentum fraction. The ratio is still one if the emission is produced by pure final-final-dipoles, so if the emission is not changing the x -values of any of the initial states, the PDF ratio is one.

Iterating Eq. (4.2) multiple times, describing multiple emissions, we can write infinite emissions as

$$\mathcal{PS}_0[u_0] = \Delta_\mu^{Q_0} u_0 \quad (4.3)$$

$$+ \alpha_s(q_1) \frac{f_1(q_1)}{f_0(q_1)} \Delta_{q_1}^{Q_0} P_1(z) \Delta_\mu^{q_1} u_1 \quad (4.4)$$

$$+ \alpha_s(q_2) \frac{f_2(q_2)}{f_1(q_2)} P_2(z) \Delta_{q_2}^{q_1} \alpha_s(q_1) \frac{f_1(q_1)}{f_0(q_1)} P_1(z) \Delta_{q_1}^{Q_0} \mathcal{PS}_2[u_2] \quad (4.5)$$

$$= \sum_{i=0}^{\infty} \left[\prod_{j=1}^i \alpha_s(q_j) \frac{f_j(q_j)}{f_{j-1}(q_j)} \Delta_{q_j}^{q_{j-1}} P_j(z) \right] \Delta_\mu^{q_i} u_i. \quad (4.6)$$

where the first line describes no resolvable emission from the u_0 configuration. This is suppressed by the Sudakov form factors ($\Delta_\mu^{Q_0}$). The second line contains one exclusive emission at scale q_1 . No emissions are produced with a harder scales ($\Delta_{q_1}^{Q_0}$) or between the scale q_1 and the shower cutoff μ ($\Delta_\mu^{q_1}$). The emission can change the flavour of the initial state, which introduces the PDF ratio and the scale of the α_s weight is the one used in the showering process*. The procedure of no-emission/emission/no-emission... continues and can be summed as in Eq. (4.6).

4.2. LO Matrix Element Merging

In the following LO Matrix element merging is described with the notation of the last section. We can write the weights of the process with an additional emission in the IR/C limit as

$$\sum B_1(q_0) \approx \sum B_0(q_0) \alpha_s(q_0) \frac{f_1(q_0)}{f_0(q_0)} P_1(z).^\dagger \quad (4.7)$$

*The ordering variable and the argument of α_s are in general different, we write $\alpha_s(q_1)$ for simplicity.

[†]Note that B_0 contains $f_0(q_0)$ which is removed by the PDF ratio.

In this expression we write once the \sum , which takes into account that B_1 is defined as the fully differential weight of a phase space point calculated for a given flavour and momentum configuration. The sum which is implicitly performed in $P_1(z)$ has more than this explicit configuration. Also to approximate B_1 one needs more than just one B_0 . The sum on both sides needs to be taken. In the following this sum is taken implicit.

Multiple ordered emissions can be approximated as

$$B_N(q_0) \approx B_0(q_0) \prod_{j=1}^N \alpha_s(q_0) \frac{f_j(q_0)}{f_{j-1}(q_0)} P_j(z). \quad (4.8)$$

Only the first PDF of B_0 in the denominator and the last PDF weight survives since all $f_{i < N}$ are divided in the next factor. Dividing the α_s and PDF factors of Eq. (4.8) and multiplying those of Eq. (4.6) in order to produce a exclusive u_N state leads to

$$\Delta_\mu^{q_N} \frac{f_N(q_N^{ls})}{f_N(q_0)} \prod_{j=0}^{N-1} \frac{\alpha_s(q_{j+1})}{\alpha_s(q_0)} \frac{f_j(q_j)}{f_j(q_{j+1})} \Delta_{q_{j+1}}^{q_j} B_N(q_0) \approx B_0(q_0) \Delta_\mu^{q_N} \prod_{j=1}^N \alpha_s(q_j) \frac{f_j(q_j)}{f_{j-1}(q_j)} \Delta_{q_j}^{q_j-1} P_i(z). \quad (4.9)$$

Here an index shift is used to get

$$\frac{f_0(q_0)}{f_N(q_0)} \prod_{j=1}^N \frac{f_j(q_j)}{f_{j-1}(q_j)} = \frac{f_N(q_N)}{f_N(q_0)} \prod_{j=1}^N \frac{f_{j-1}(q_{j-1})}{f_{j-1}(q_j)} = \frac{f_N(q_N^{ls})}{f_N(q_0)} \prod_{j=0}^{N-1} \frac{f_j(q_j)}{f_j(q_{j+1})}. \quad (4.10)$$

If the emission is not associated with the initial state, the PDF ratio is one, since $q_j = q_{j+1}$ in the PDF ratios of the shower. Only if the splitting is changing the initial state momentum fraction the PDF ratio has to be taken into account. q_N^{ls} in the PDF ratio on the *lhs* is the scale of the last splitting associated with a change of the initial state momentum. This is indicated by the *ls*.

On the right hand side of Eq. (4.9) we constructed the expression for the N 'th component of the parton shower after the showering process. No further emissions will take place above the infrared cutoff μ . The left hand side is therefore the expression of an exclusive N -additional-emission state. By inserting this expression we arrive at a LO merging formula

$$\mathcal{PS}_0 \left[\sigma^{merged} u_0 \right] = \sum_{i=0}^{\infty} \left[\frac{f_i(q_i^{ls})}{f_i(q_0)} \prod_{j=0}^{i-1} \frac{\alpha_s(q_{j+1})}{\alpha_s(q_0)} \frac{f_j(q_j)}{f_j(q_{j+1})} \Delta_{q_{j+1}}^{q_j} B_i(q_0) \right] \Delta_\mu^{q_i} u_i. \quad (4.11)$$

This expression was formulated with different notations and techniques in several approaches. The first for e^+e^- -collision defined merging is named CKKW standing for the names of the inventors Catani, Krauss, Kuhn and Webber [15]. The 'events' produced by fixed order calculations for several multiplicities need to be interpreted with a *shower history*, meaning the path the shower would have most probably produced the event. This can be done by a jet algorithm that subsequently *clusters* the partonic states. Scales, corresponding to the ordering

variable of the shower, are assigned to the clusterings (backward splittings). For these scales the weights of Eq. (4.11) have to be calculated. In [15] the Sudakov factors were calculated in an analytical form that can become larger than one. Since it should be still interpreted as an probability they set the factor to one if the NLL-expression of the Sudakov form factor is larger than one.

The reweighting of the *shower history* is performed with a different approach in [16], named CKKW-L[‡]. In this approach the Sudakov suppression is found from trial showers. One constructs the processes which are seen by the cluster algorithm, then applies the appropriate scales and if the shower acting on this states, produces emissions above the next scale the event is discarded. In this manner one produces the no emission probability the shower would have produced, up to ambiguities in the clustering choice. The problem with Sudakov factors larger than one does not apply for this. It is possible that the weights of the events in singular regions of the phase space are either zero or very large for weighted events or many of the produced events are discarded for unweighted events.

In Fig. 4.1 the Sudakov suppression expected from the CS dipole shower is plotted against the NLL Sudakov expression used in [15]. While for small scales the dipole shower is close to the NLL expression the dipole shower does not exceed one due to the positive definite kernels in the physical phase space. The dipole shower expression was implemented in Mathematica to validate the implementation of the merging algorithm.

In the version of the CKKW algorithm for initial state hadrons [76] only time-like Sudakov factors are used, it is found that PDF ratios are not needed. This can easily be understood in the combination of Eq. (4.11) and Eq. (3.12). The backward evolution Sudakov form factors in Eq. (4.11) (Δ_{j+1}^j contains $\Pi(q_j \rightarrow q_{j+1})$) can be rewritten with Eq. (3.12) into a time-like Sudakov factor and a PDF ratio. The PDF ratio is the inverse of the ratios of Eq. (4.11). In this case the PDF need to be evaluated at the merging scale.

Since we are not using AP kernels for the merging, we keep in mind that the PDF ratio is needed. On the other hand, we want to keep the notation compact and define

$$\Delta_i^0 := \frac{f_i(q_i^{ls})}{f_i(q_0)} \prod_{j=0}^{i-1} \frac{\alpha_s(q_{j+1})}{\alpha_s(q_0)} \frac{f_j(q_j)}{f_j(q_{j+1})} \Delta_{q_{j+1}}^{q_j} \quad \text{and} \quad \Delta_\mu^i := \Delta_\mu^{q_i}, \quad (4.12)$$

so that we can write merging like

$$\mathcal{PS}_0 \left[\sigma^{merged} u_0 \right] = \sum_{i=0}^{\infty} \Delta_i^0 \Delta_\mu^i B_i(q_0) u_i. \quad (4.13)$$

While the Sudakov factor[§] Δ_i^0 contains all weights, which describes the shower history to get to the state $B_i(q_0)$, the second Sudakov form factor Δ_μ^i makes the state exclusive to the scale μ . In the following the lower indices μ or ρ define the second Sudakov form factor.

[‡] Lönnblad

[§] Δ_i^0 includes α_s and PDF ratios, so the name Sudakov factor is understood in a generalized way.

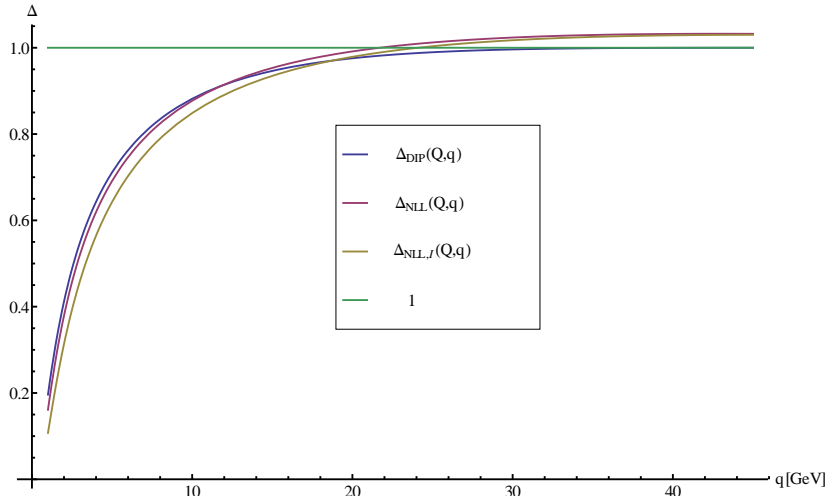


Figure 4.1.: Mathematica implementation of a Sudakov form factor for a $q\bar{q}$ pair with $Q_0=91.2$ GeV. Comparing the CS dipole expression (blue) with the NLL (purple) expression. The NNL,I (brown) corresponds to the 'improved' NLL Sudakov factor given in appendix A of [77]. While the NLL expression and the Dipole shower expression are close in the region of small q , the NLL Sudakov factor is larger than one in the hard region. The exponent of the dipole Sudakov factor is negative definite and has the property that the Sudakov factor is smoothly approaching unity at the upper phase space boundary.

Practical Implementation

The sum up to infinite number of emissions is in practice not possible, since the evaluation of matrix elements with many (infinite) legs and phase space integration of those is not possible. One therefore stops at a given finite number N of final state emissions and starts the shower evolution of these states

$$\mathcal{PS}_0 \left[\sigma^{merged} u_0 \right] = \sum_{i=0}^{N-1} \Delta_i^0 \Delta_\mu^i B_i(q_0) u_i + \mathcal{PS}_N \left[\Delta_N^0 B_N(q_0) u_N \right]. \quad (4.14)$$

The last term has no Sudakov factor Δ_μ^N . This factor represents the probability to get no emissions from the B_N state. B_N in the last term is an inclusive state. By acting with the parton shower one reproduces the same Sudakov suppression and additional emissions.

Another problem arises for low values of μ . Even though the Sudakov form factors regularize the individual parts of the sum the matrix elements get divergent as well. This can lead to numerical instabilities due to the evaluation/estimation of the Sudakov factors. To achieve numerical stability and efficiency a scale is introduced which separates the matrix-element-from the shower-region (ME/PS-region). This scale is called the merging scale ρ . The definition of such a scale is in principal not trivial since usually there is a mismatch between choosing such a scale from final state kinematics and the evolution variable of the shower.

All clustering scales, of the clustering algorithm[¶], for the first clustering need to be above the merging scale. This introduces a product of θ functions in Eq. (4.14) on all possible

[¶]like the jet algorithm in CKKW.

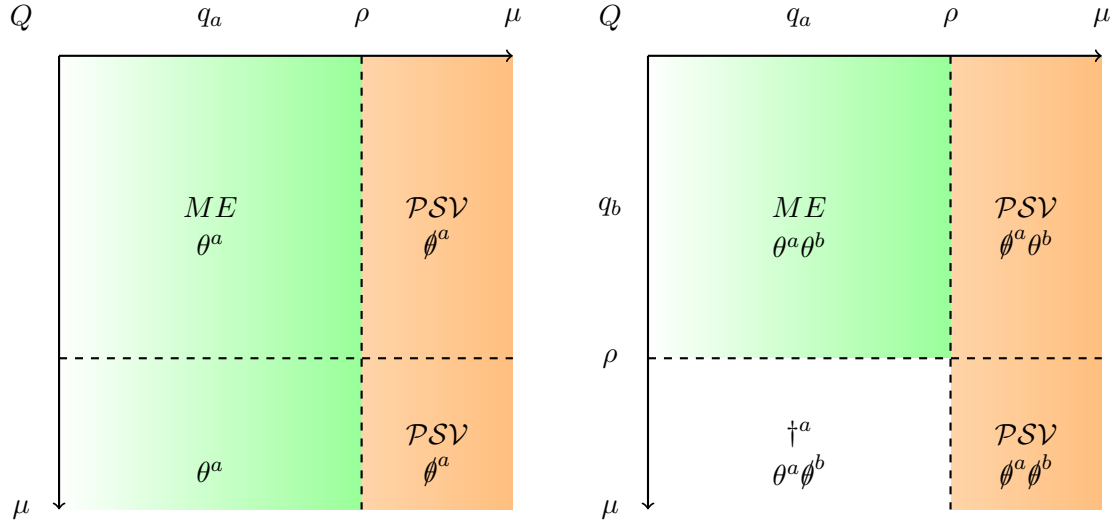


Figure 4.2.: Illustration of the region which is not filled by emissions from emitter a if the vetoed showering is simply vetoing emissions above the scale ρ . While the region can be separated into above and below scale ρ for a single emitter, the division into matrix element region ME and vetoed shower region PSV produces dead regions \dagger_a of individual emitters a by simple vetoing. See Eq. 4.18 for further explanation.

clusterings. Underlying clusterings to construct a history of shower emissions can turn out to be below the merging scale, if the momenta are reshuffled while clustering. In this case it is not a ordered clustering with respect to the shower. Shower histories are constructed by ordered shower emissions only.

For the splitting between ME- and PS-region one needs to construct an algorithm that can produce

$$\mathcal{PS}_\mu[\phi_0] = \mathcal{PSV}_\mu[\mathcal{PS}_\rho[\phi_0]]. \quad (4.15)$$

Here, \mathcal{PS}_μ and \mathcal{PS}_ρ are of the same kind, but with different cutoffs, and \mathcal{PSV}_μ is a construction that fills the rest of the phase space

$$\Phi_{\mathcal{PSV}_\mu} = \Phi_{\mathcal{PS}_\mu} \setminus \Phi_{\mathcal{PS}_\rho}. \quad (4.16)$$

with emissions according to the probability of the parton shower.

If the evolution variable of the shower and the variable which is used to calculate the cut between the two regions are the same, the \mathcal{PSV}_μ can be achieved by starting the shower from the last splitting scale before \mathcal{PS}_ρ ended and veto all emissions with scales above the merging scale ρ . This vetoing then leads to the name 'vetoed shower'.

If the merging scale differs from the shower evolution variable one finds gaps between the two regions, which needs to be filled. The procedure is called a truncated shower [19].

Partly Open Vetoed Showers

In our implementation we see that by merging matrix elements to a CS-dipole shower we need to be careful in the description of the vetoed shower. The vetoed shower described above

assumes that there is a scale to evolve and that emissions can be assigned in a unique way by a jet algorithm to a leg. Emissions from the parton shower can be assigned to one emitter. This is true for angular ordered showers without overlapping phase spaces. CS-like dipole showers and CS dipole subtraction however works in a way that IR/C-enhancement is approximated and divergences are subtracted by the sum of the dipole contributions. Therefore the phase space of dipoles overlap. The assignment of clusterings/splittings is not unique.

As a consequence it can happen that hard wide angled emissions from an emitter can be – also by the effects of recoils – collinear to the spectator of the dipole. So we need to be more detailed in describing the vetoing algorithm.

In order to see the details we split up the Sudakov form factor for a $q\bar{q}$ pair by rewriting it as

$$\Delta_\mu^{q_0} = \exp \left[\int_\mu^{q_0} \sum_{i=a,b} dP_i(q_i, z_i) \right] \quad (4.17)$$

$$= \exp \left[\int_\mu^{q_0} \sum_{i=a,b} dP_i(q_i, z) \left(\theta_\rho^a \theta_\rho^b + \theta_\rho^a \theta_\rho^b + \theta_\rho^a \theta_\rho^b + \theta_\rho^a \theta_\rho^b \right) \right] \quad (4.18)$$

$$= \exp \left[\int_\mu^{q_0} \left(\sum_{i=a,b} dP_i(q_i, z) \theta_\rho^a \theta_\rho^b + dP_b(q_i, z) \theta_\rho^a \theta_\rho^b + dP_a(q_i, z) \theta_\rho^a \theta_\rho^b \right) \right] \quad (4.19)$$

$$\times \exp \left[\int_\mu^{q_0} \left(dP_b(q_i, z) \theta_\rho^a \theta_\rho^b + dP_a(q_i, z) \theta_\rho^a \theta_\rho^b + \sum_{i=a,b} dP_i(q_i, z) \theta_\rho^a \theta_\rho^b \right) \right] \quad (4.20)$$

$$= \exp \left[\int_\mu^{q_0} \left(\sum_{i=a,b} dP_i(q_i, z) \theta_\rho^i \right) \right] \times \exp \left[\int_\mu^{q_0} \left(\sum_{i=a,b} dP_i(q_i, z) \theta_\rho^i \right) \right] \quad (4.21)$$

$$= \Delta_\rho^{q_0} \times \Delta_\mu^{V,q_0} \quad (4.22)$$

In Fig. 4.2 the regions of Eq. (4.18) are illustrated. The θ_ρ^i 's describe regions of the phase space where the scale to emit a parton i is above the scale ρ . θ_ρ^i stands for the region in PS where the emission is below the scale ρ for the splitting i . We have two possibilities to emit a gluon from an colour dipole with overlapping phase spaces. The breakdown of the phase space in Eq. (4.18) can be seen as all/one/no emission are/is above the scale ρ .

If we write the sum explicitly, we can sort the terms such that the emission itself is above the scale ρ , even if the scale with respect to the other emitter is below the scale ρ . In the following we used that $\theta_\rho^a \theta_\rho^b + \theta_\rho^a \theta_\rho^b = \theta_\rho^a$ to separate the phase space into regions where the assigned splitting is above the scale ρ . With this we can split the Sudakov expression $\Delta_\mu^{q_0}$ into a region where the assigned splitting is always above and one where it is always below.

A naive vetoed shower starts with trial emissions that are vetoed if they produce a larger scale than the merging scale. This is exactly the second exponential of Eq. (4.21). We see that in principle and on the first look the vetoed shower Sudakov factor Δ^V factorizes from the previous shower Sudakov factor with the cutoff ρ . But, in Eq. (4.19) we can identify the ME-region $\theta^a \theta^b$. It is defined by the condition, that all splitting scales are above the merging

scale. So only the first part of the line represents the ME-region, while the other two belong to the PS-region. These parts of the Sudakov exponent/phase space are not filled by the ME since they have scales lower than the merging scale. The emission described by the kernel P_a is not performed in a vanilla veto shower, since the scale corresponding to P_a is above ρ . This region is now defined as dead region of emitter a . Even if we use the same scale the shower uses for ordering, the dead region is not filled by a , by the fact of overlapping phase spaces of individual splittings. The region of phase space is still filled by the vetoed showering of emissions from kernel P_b , which are enhanced in this region.

If we would have only one emitter, the region can be separated between above and below the scale ρ . For overlapping dipoles phase spaces the region where both scales are above the scale is the green area on the right graph in Fig. 4.2. Emissions below the scale ρ are not described by matrix element, but the emission of leg a is also not possible by naively vetoing, because it is above the scale ρ .

We can fill the dead region by proposing a partly open vetoed shower, meaning that an emission is accepted if any of the scales calculated for possible splittings – other than the actual splitting – is lower than the merging scale. This fills the dead region with emissions from lower multiplicities.

The parts of the sum in the merging description in Eq. (4.14) that can fill the dead zone is always the lower multiplicities. The lower multiplicity however is weighted with Δ_ρ^i in Eq. (4.22) which already contains the suppression coming from the dead regions. So we need to modify the algorithm in order to not get a double counting of this areas in the suppression.

One way to achieve this would be to calculate the Sudakov factor in the merging formula Eq. (4.14) with a trial shower like the CKKW-L description then calculate all scales for possible reclustering and only suppress the contribution if all scales are above the merging scale. In other words, calculate the Sudakov suppression for exactly the ME-region. With such a procedure one can then fill the dead region and the region below the merging scale with a vetoed shower that accepts emissions in these regions.

4.3. Changes of Inclusive Observables and Restoring Unitarity

In the following a description is given that was introduced to modify the merging in a way that inclusive observables are not modified by the merging procedure. This description will naturally change the way how to calculate the Δ_ρ^i and will solve the described problem automatically.

The ideas presented in this section are mainly founded on the observations made in the LoopSim approach [78], which used unitarity to mimic higher order effects in regions of phase space with expected large corrections. The transfer to parton showers was seen in [22, 30]. The ideas and some extensions are presented in the following.

The approximation made in Eq. (4.8) can also have intermediate steps

$$B_N(q_0) \approx B_{N-1}\alpha_s(q_0) \frac{f_N(q_0)}{f_{N-1}(q_0)} P_N(z) \approx \dots \approx B_0(q_0) \prod_{j=1}^N \alpha_s(q_0) \frac{f_j(q_0)}{f_{j-1}(q_0)} P_j(z), \quad (4.23)$$

where the approximation of B_N gets worse from left to right. In the merging description we replaced order by order in the sum.^{||} With Eq. (4.23) the difference between the shower approximation of multiplicity i and the inclusion of matrix elements in the merging prescription is

$$\Delta_i^0 B_i(q_0) + \Delta_{i-1}^0 \Delta_\rho^{i-1} B_{i-1}(q_0) \approx \Delta_i^0 B_{i-1} \alpha_s(q_0) \frac{f_i(q_0)}{f_{i-1}(q_0)} P_i(z) + \Delta_{i-1}^0 \Delta_\rho^{i-1} B_{i-1}(q_0). \quad (4.24)$$

The change of the scale dependent α_s and PDF ratio is included in the definition of Δ_i^0 . The second summand on both sides is the same and was written out to make the following arguments comprehensible. On the right hand side we have the shower emission in the first contribution and the no emission contribution in the second term. The left hand side receives the matrix element corrected expression to this. The difference is of $\mathcal{O}(\alpha_s)$.

For LO merging this is not a problem, since the correction is not in the accuracy the fixed order calculation is producing. If we want to include NLO corrections to the merging in the second step we need to take care that the LO merging does not change the inclusive expressions at the same order of the NLO corrections.

To fix the difference of Eq. (4.24) but to keep the matrix element corrections to the shower approximations, we can modify the second terms on the left side of Eq. (4.24). The Δ_ρ^{i-1} can be written in an schematic** way as

$$\Delta_{i-1}^0 \Delta_\rho^{i-1} B_{i-1}(q_0) = \Delta_{i-1}^0 \left(1 - \int_\rho^{q_{i-1}} \alpha_s(q) \frac{f_i(q)}{f_{i-1}(q)} P_i(z) \Delta_q^{i-1} \right) B_{i-1}(q_0) \quad (4.25)$$

We replace the no emission probability from the scale q_{i-1} to ρ by one minus the emissions probability^{††}, which is the basic formula for parton showers in Eq. (3.10). This integration in Eq. (4.25) is written explicitly and differs from the implicit phase space integration of the exclusive states. The difference is that the integral has to be performed in a way that the 'emission' described by $P(z)$ is not resolvable, so no additional parton is produced. P_i is not changing u_{i-1} as for shower emissions.

It was identified [22, 30, 78] that the same parts which were used to replace the shower emissions with matrix elements, can be used to restore the unitarity of the cross section. Eq. (4.24) can be modified as

$$\begin{aligned} \mathcal{PS}_{i-1} [\Delta_{i-1}^0 B_{i-1} u_{i-1}] &\approx \Delta_{i-1}^0 \left[\mathcal{PS} \tilde{\mathcal{V}}_\mu [B_{i-1}(q_0) u_{i-1}] - \mathcal{PS} \mathcal{V}_\mu [u_{i-1} \int_\rho^{q_{i-1}} \Delta_i^{i-1} B_i(q_0)] \right. \\ &\quad \left. + \mathcal{PS}_\mu [\Delta_i^{i-1} B_i(q_0) u_i] \right]. \end{aligned} \quad (4.26)$$

^{||}In principal one could only replace individual multiplicities, and use the parton shower for other multiplicities. In such a procedure one would veto parton shower events which exactly produce the multiplicity of the replaced sample.

^{**}Schematic since we do not write out the variables of the phase space integration.

^{††}The implicit sum over all possible emissions may not be forgotten. It is present in the exponent of the Sudakov factor Δ_ρ^{i-1} and implicit in the splitting functions.

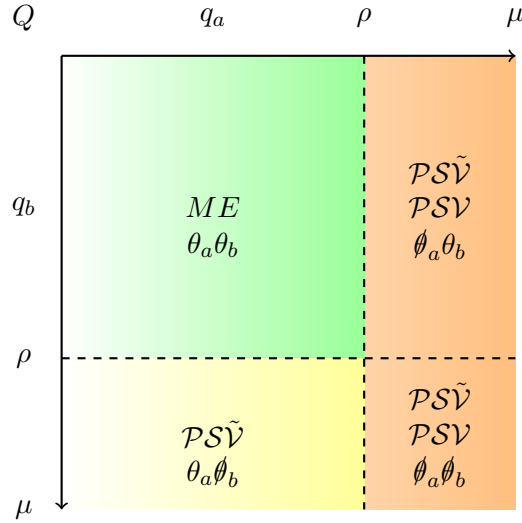


Figure 4.3.: The unitarized merging replaces the matrix element region of the exponentiated phase space of the Sudakov factor. The dead region of Fig. 4.2 can now be filled with the unsuppressed lower multiplicity, see Eq. (4.26).

Notice that the seeming difference in the scales of α_s and the PDFs is absorbed in the difference between Δ_i^{i-1} and Δ_q^{i-1} , see Eq. (4.12). The index of $u_{i/i-1}$ illustrates the numbers of emissions. While the term in the first line are phase space configurations with $i - 1$ extra emissions, the term in the second line on the right hand side is the part with one additional resolvable emission above ρ . The phase space integration is here again implicit.

The two expressions in Eq. (4.26) containing B_i differ only in the phase space configuration u , if the phase space is identical, which is discussed in Sec. 4.6. Inclusive observables, defined by not resolving additional emissions, are not modified by the inclusion of matrix elements, to the merging.

In Eq. (4.25) the replacement of the no emission probability is exact. The replacement in Eq. (4.26) requires that all scales are above the merging scale, so the integration is performed strictly in the matrix element region of the merging. By that we replace the no emissions probability from the last scale to the merging scale with the requirement that the integration in the Sudakov form factor is in the matrix element region. Compared to Eq. (4.18) we replaced the expression

$$\exp \left[\int_\mu^{q_0} \sum_{i=a,b} dP_i(q_i, z) \theta_\rho^a \theta_\rho^b \right]. \quad (4.27)$$

The regions where any of the scales associated with a clustering is below the merging scale can now be filled with the first term on the right hand side of Eq. (4.26).

Therefore we define two types of vetoed parton showers \mathcal{PSV}_μ and $\tilde{\mathcal{PSV}}_\mu$ in the first line of Eq. (4.26). While \mathcal{PSV}_μ allows emissions in the dead regions, $\tilde{\mathcal{PSV}}_\mu$ only emits below the merging scale. Because we subtract with the integral exactly the contributions coming from the ME region, but not the dead regions, the emissions from $\tilde{\mathcal{PSV}}_\mu$ will produce the correct amount of emissions in the dead region. In Fig. 4.3 the regions filled by the various contributions are illustrated.

By construction we see that after phase space integration the terms containing B_i in Eq. (4.26) cancel for inclusive observables $u_i = u_{i-1}$. Since we did not restrict ourself on explicit i this holds for every multiplicity. Inclusive observables therefore are unchanged at $\mathcal{O}(\alpha_s)$. Exclusive observables on the other hand receive matrix element corrections.

The explicit integral on the extra emissions in Eq. (4.26) is written in a schematic way. A way to perform it would be in a POWHEG motivated way. One would produce in a practical implementation phase space configurations u_{i-1} and then produce extra emissions from this to calculate the weight of the 'real emission'. In our implementation we produce phase space configurations for the u_i kinematic and cluster these as

$$\sum_j \int_\rho^{q_{i-1}} \frac{w_j}{\sum_k w_k} \tilde{w}_{i-1}^j \Delta_i^{i-1} B_i(q_0). \quad (4.28)$$

The normalized $w_i / \sum_k w_k$, see Sec. 4.5 for details, is the probability to cluster the phase space configuration u_i to get the 'history' of the parton shower, meaning the sequence of clusterings/splittings the algorithm/shower would assign/produce to get from u_i/u_0 to u_0/u_i .

4.4. Review 1

To review the changes to the parton shower introduced by the LO merging and as described in the previous section by unitarization of inclusive observables we illustrate in Fig. 4.4 the formulas given in the text. Although the arguments given in the description are not completely depicted, the basic ideas can be fetched.

The upper blocks illustrate the pure shower effects acting on an LO contribution. Starting from an Born configuration additional emissions are produced in the shower approximation (orange blocks in the next line). The probability to remain in the starting configuration is expressed by the Sudakov form factor multiplied to the line. The sum of the blocks in the line and the first block in the next line is given by the value of the first block of the line by the unitarity of the parton shower. The inclusive cross section is not changed.

In standard LO merging algorithms (middle blocks) the splitting above the merging scales is replaced by the matrix element and weighted with the Sudakov suppression in order to produce 'exclusive' states above the merging scale. Δ_{i+1}^i contains the scale changes to the α_s and PDF ratios the shower would have produced. Each state is further suppressed – either with analytic expressions or trail showering – to get exclusive states from the last splitting to the merging scale. The cross section is changed by the difference of the parton shower and the matrix elements.

The last Sudakov form factor Δ_ρ^i is replaced by subtraction of the same matrix element corrections used in the merging. This corrects for the changes induced for inclusive observables at the $\mathcal{O}(\alpha_s)$. In order to include NLO corrections the merged LO sample must be controlled to receive no changes at the same $\mathcal{O}(\alpha_s)$ as the corrections will produce. The unitarity of the parton shower is restored.

4.5. Dipole Shower Clustering

The implementation of merging is driven by the Dipole shower described in [57]. For clustering back the emissions the tilde kinematics outlined in [51] are used. All possible flavour

Parton Shower:

B_0	$\cdot \Delta_\rho^0$	
	$P_1 \Delta_1^0 B_0$	$\cdot \Delta_\rho^1$
$P_2 \Delta_2^1 P_1 \Delta_1^0 B_0$		

Standard LO merging:

B_0	$\cdot \Delta_\rho^0$	
	$\Delta_1^0 B_1$	$\cdot \Delta_\rho^1$
$\Delta_2^1 \Delta_1^0 B_2$		

Unitarized LO merging:

B_0	$-\int \Delta_1^0 B_1$	
	$\Delta_1^0 B_1$	$-\int \Delta_2^1 \Delta_1^0 B_2$
$\Delta_2^1 \Delta_1^0 B_2$		

Figure 4.4.: Reviewing the steps of from the pure parton shower over standard LO merging to the unitarization prescription described in the text. The description of the blocks is given in Sec. 4.4. Note that this illustration should only serve as a summary and to guide the eye through the formulas.

combinations are already included in the clustering to tilde kinematics and no clusterings like $uc \rightarrow g$ are described by the CS dipoles. The clustering contain all inverse splittings the shower would also produce if the shower was able to work in the $N_C = 3$ mode with colour correlations. When there are different possibilities to cluster from ϕ_n to $\tilde{\phi}_{n-1}^i$ the clustering should be based on the probability the shower would have produced the emission. To keep the clustering as close to the shower algorithm as possible we are using the p_T definition of the shower as the ordering variable. Also only large N_C colour connected emitter-spectator pairs^{††} are considered in the clustering algorithm, as the shower radiates from large N_C colour dipoles only.

The cluster algorithm in steps:

1. Produce a phase space point for n external momenta ϕ_n .
2. Check if all tilde-Kinematics $\tilde{\phi}_{n-1}^i$ have a p_T^i larger than the merging scale ρ . This defines the ME region.

^{††}To check if a Pair is colour connected we calculate the colour correlator in the large N_C limit and check if the result is not vanishing.

3. Collect all underlying $\tilde{\phi}_{n-1}^i$, with the requirements:

- If $n = 1$: ϕ_1 needs to be in the shower phase space of $\tilde{\phi}_0^i$ for a shower starting scale Q_h ^{§§}. The shower phase space has the requirement that the p_T^i is lower than the last scale (Q_h or previous p_T) and the z -boundaries for the emission are respected. The z -boundaries are given in Tab. (C.1).
- If $n > 1$: There is a $\tilde{\phi}_{n-2}^j(\tilde{\phi}_{n-1}^i)$ with \tilde{p}_T^j (Q_h for $n = 2$) for which ϕ_n is in the shower phase space of $\tilde{\phi}_{n-1}^i$ with starting scale \tilde{p}_T^j .
- The large N_C colour correlator for the emitter spectator pair of $\tilde{\phi}_{n-1}^i$ does not vanish.

4. Select one of the $\tilde{\phi}_{n-1}^i$ collected in step 3. with the normalized probability w_i . In this implementation we chose the weight w_i to be,

$$w_i = |P_i(\phi_n^i, \tilde{\phi}_{n-1}^i)/B_{n-1}(\tilde{\phi}_{n-1}^i)| \quad (4.29)$$

with P_i being CS dipole in the shower approximation [70], which is close to the shower splitting weights.

5. Repeat step 3 and 4 for $\tilde{\phi}_{n-1}^i$ until there are no further next ordered steps.

In [70] it is shown that, if the initial colour lines are chosen proportional to the weights of the squared colour-flow amplitudes, see e.g. [79], the expression expected from the parton shower is proportional to [70, 80]

$$|\mathcal{M}_{\text{PS}}|^2 = \sum_{\alpha, \beta} -\frac{1}{\mathbf{T}_{ij}^2} \frac{\langle \mathcal{M} | \mathbf{T}_k \cdot \mathbf{T}_{ij} | \mathcal{M} \rangle}{|\mathcal{M}|^2} \Big|_{N \rightarrow \infty} P_{ij,k} |\mathcal{M}|^2 , \quad (4.30)$$

with the spin averaged splitting kernels $P_{ij,k}$. $|\mathcal{M}|^2$ is the squared Born matrix elements and the ratios are evaluated in the large N_C colour-flow limit. The shower approximation P_i is therefore the spin averaged CS dipole, evaluated in the large N_C limit and reweighted with the ratio of the full colour and large N_C Born matrix element squared.

After applying the cluster algorithm, we arrived at a given $\hat{\phi}_{n-m}$. If $n = m$ we found a full history of possible shower emissions. In this case we assign the shower starting scale $Q_h(\hat{\phi}_0)$ to the process. In the case that $n > m$ we got a not fully ordered shower history and therefore assume that the shower would not fill these parts of the phase space. In this case we need to define a new starting scale for the process $Q_h^k(\hat{\phi}_{k>0})$. In this implementation we use

$$Q_h^k(\hat{\phi}_{k>0}) = \max(Q_h(\hat{\phi}_k), \min(2p_i p_j)) , \quad (4.31)$$

where $Q_h(\hat{\phi}_k)$ is the scale generated by the same instructions as are applied to the ϕ_0 and $\min(2p_i p_j)$ is the minimum of invariant masses of all coloured particles. This choice is motivated by the fact that the process is treated as a new process the shower would not produce and if the emissions are very hard the scales should take this into account. In Drell-Yan like processes the first hardest emission with $p_T > M_X$ will therefore be evaluated with a scale larger than M_X which would be a natural choice for the process with an additional emission.

^{§§} Q_h is a scale related to $\tilde{\phi}_0^i$, it is calculated as the shower stating scale of a not merged sample.

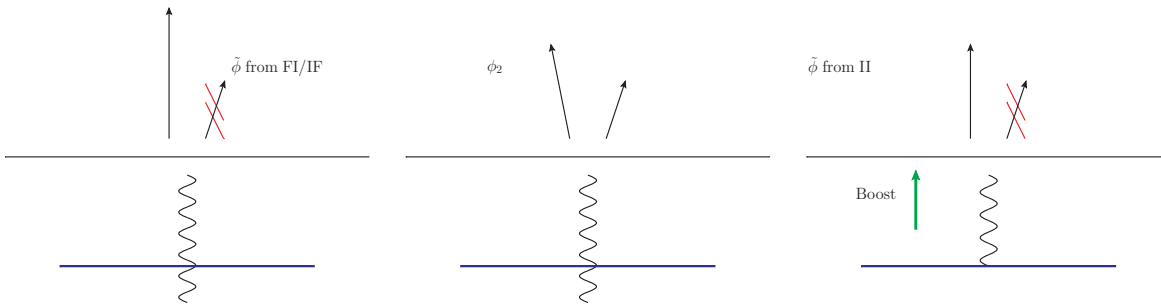


Figure 4.5.: Schematic example event in the middle. Clustering with FI or IF dipoles leads to unchanged momentum of the electroweak system while II dipoles can lead to a boost of the full system. This boost can then lead to 'longer' histories, if the first emission is in the shower phase space due to the boost, depicted by the blue line. This will lead to artifacts of the cluster algorithm so that we conclude that the cluster algorithm must not depend on the length of the history.

Note that in the clustering algorithm the phase space points $\tilde{\phi}_{n-2}^j$ is only used to provide the scale \tilde{p}_T^j or Q_h . We do not require that $\tilde{\phi}_{n-1}^i$ is in the shower phase space of $\tilde{\phi}_{n-2}^j$. Requiring that and choosing only longest histories, would lead to artifacts of the clustering algorithm. An example is given in Fig. 4.5 where an enhanced collinear emission of the first emitted parton can lead to 'longer' histories due to the boost of II dipoles. The probability that the shower would have produced the emission from a II dipole is suppressed, but if the clustering depends on the length of the history the clustering with the II dipole would be preferred. The given cluster algorithm is independent of the length of the history.

4.6. Unordered Histories

In Eq. (4.26) a way to preserve unitarity is introduced. The integral in Eq. (4.26) was defined as the integral which is performed in the Sudakov form factor. Also the boundaries on the phase space are defined in that way. In processes where the parton shower is used for backward DGLAP-evolution, like in LHC processes, there is more energy in the process by emitting a parton, even though the scale is decreasing. The phase space of the process with an additional parton is larger than the assumed parton shower phase space which is restricted by the scale of the hard process, in order to exponentiate the logarithms of the hard scales.

If the parton shower is seen as a solution to the DGLAP equations, see Eq. (3.11), no harder emissions can be produced than the factorization scale used in the PDF weights of the hard process. If the scales of the subsequent clusterings cannot be ordered they are seen to be finite contributions which are not covered by the inclusive measured PDFs.

We therefore add them to the cross section. This type of cluster sequence is then called a unordered history, since it is not ordered in the sense of the parton shower emissions. In the case of multiple emissions it can happen – as already pointed out in Ch. 4.5 – that the clustering does not trace back to the original process. In that case we define the lowest multiplicity with an ordered history to be the new hard process or new seed process. If we find at least one clustering which is ordered this will not change the cross section.

The contributions from first emissions of Z boson production that are above the hard scale, e.g. the mass of the Z boson, are parts which will be included in the real emission of the NLO

calculation. Since we add the finite, unordered contributions, for which no clustering can be found in the LO merging we must be careful to not add them to the merging with higher order matrix elements. This will be achieved by the requirement that if all clustering scales of the real emission are above the merging scale and the clustering of Ch. 4.5 finds no clustering the real emission contribution is set to zero.

An other example for unordered histories is the real emission contribution $q\bar{q} \rightarrow Hg$ to $gg \rightarrow H$ in an effective Model with ggH couplings and strictly massless quarks. The final state gluon cannot be clustered to the incoming partons since no Born process is present. These finite contributions are added without unitarization since they are corrections not covered by the parton shower.

4.7. Remarks on Merging Smoothness and Accuracy

As discussed in Sec. 4.3 we correct the difference of the cross section produced by B_n by subtraction of the B_{n-1} contributions. The effects at the merging scale need to be analysed. Below the merging scale is the region of phase space where the vetoed shower produces emissions from the seed process and the clustered process with one additional emission. Above the merging scale the phase space region is filled by the process with one additional emission. The contributions at the merging scale can be schematically written as

$$\partial\sigma/\partial q|_{\rho-\epsilon} = \left(B_0 - \int_\rho^{Q_0} B_1 \Delta_1^0 \right) P(\rho) \quad \text{and} \quad \partial\sigma/\partial q|_{\rho+\epsilon} = (B_1 \Delta_1^0)|_{q_1=\rho}, \quad (4.32)$$

where the integration of all variables not describing the evolution scale is performed. The expressions for the corresponding parton shower contributions is, since the parton shower is not affected by the merging scale

$$\partial\sigma^{PS}/\partial q|_{\rho\pm\epsilon} = (B_0 \Delta_1^0) P(\rho). \quad (4.33)$$

The difference between pure parton shower and merged expressions from above the merging scale is given by the difference between the explicit matrix element and the corresponding parton shower expansion, $B_1 - B_0 \cdot P$.

Below the merging scale the difference is given by the difference of the Sudakov expressions,

$$\Delta_{\rho-\epsilon} = \int_\rho^{Q_0} (B_1 - P \cdot B_0) \Delta_1^0. \quad (4.34)$$

This strongly depends on the ability of the shower to mimic the matrix element corrections inside the shower phase space. The logarithmic accuracy of this relation is one order higher than the accuracy of the shower. So (N)NLL if the shower is (N)LL accurate. Since the additional emission of the (vetoed) shower is necessary the order is increased again for the difference at the merging scale.

Non logarithmic contributions like interference effects of s -channel with u - or t - channel diagrams in $V+j$ production, or the contribution of final state electro-weak radiation in pure electro weak production are not covered by the shower. These can lead to $\mathcal{O}(\alpha_s)$ differences at the merging scale.

4.8. Notation of Merged Cross Sections

Using the LO merging of multiple LO contributions with a parton shower, we define the merged samples for the Process A as

$$A(0, 1, 2, \dots, N) = A^V(0) + A^V(1) + \dots + A^V(N-1) + A(N) \quad (4.35)$$

if matrix elements where merged up to N additional emissions. The upper index V at the individual multiplicities is labeling the fact that these contributions are vetoed above the merging scale. The last multiplicity $A(N)$ is not vetoed.

Note that e.g. the multiplicity with no additional emission, contains the process itself and the clustered process with one additional emission

$$A^V(0) = A^{\tilde{V}}(0) - A_C^V(1). \quad (4.36)$$

Here the process $A^{\tilde{V}}(0)$, with no additional emission, is showered with possible emissions in the dead region.

CHAPTER 5

Merging Matrix Elements and Parton Showers with NLO Corrections

For NLO merging it is important to distinguish which parts of the NLO calculation are already taken into account by the tree level merging. As in matching of fixed order NLO calculations to a parton shower, the problem of double counting must be solved, see Sec. 3.5. In Sec. 5.1, we show the concepts behind the method and start with a basic NLO matching prescription. Since these are corrections to the first LO we use the notation of the previous section to define the NLO corrections to this process as $A(0^*, 1, \dots, N)$. In Sec. 5.2 we describe the merging prescription in the presence of an additional NLO correction, accordingly defined as $A(0^*, 1^*, 2, \dots, N)$. Here, we describe the corrections and expansions needed to reach NLO accuracy above the merging scale. In Sec. 5.3 we review the merging to achieve $A(0^*, 1^*, 2, \dots, N)$ and show which properties are required to expand the procedure for higher multiplicities with the abbreviation $A(0^*, 1^*, \dots, M^*, M+1, \dots, N)$. The last part of this chapter is used to include scale variation parameters to the merging algorithm, see Sec. 5.4.

5.1. Merging with NLO Corrections to the First LO

For the purpose of matching the merged expressions with corrections to the seed * process, we write the parts of a tree level merging of two LO matrix elements explicitly as

$$A(0, 1) = \mathcal{PS}\tilde{\mathcal{V}}_0[u_0 B_0(q_0)] \quad (5.1)$$

$$- \mathcal{PS}\mathcal{V}_0 \left[\sum_i \tilde{u}_0^i \int_{\rho}^{q_0} \frac{w_i}{\sum_j w_j} B_1(q_0) \Delta_1^0 \right] \quad (5.2)$$

$$+ \mathcal{PS}_1 \left[\sum_i u_1 B_1(q_0) \frac{w_i}{\sum_j w_j} \Delta_1^{0,i} \theta_{PS} \right] \quad (5.3)$$

$$+ \mathcal{PS}_1 [u_1 B_1(q_1) \theta_{PS}] \quad (5.4)$$

*We are dealing with multiple Born processes, so the seed process is the Born process of the lowest multiplicity.

The first line is the vetoed parton shower, allowed to emit into the dead region. Eq. (5.2) is produced by the unitarization prescription. Corresponding to the unitarized part, the third line are the parts from the LO merging above the merging scale. The last term contains phase space regions which are not available by the shower emissions, namely the unordered histories of Sec. 4.6. As a short notation this is labelled with \emptyset_{PS} .

To match this 'resummed' parton shower formula with the NLO calculation we make use of the matching formula (2.80)

$$d\sigma^{\text{matched}} = d\sigma^{\text{resummed}} - d\sigma^{\text{res, expanded}} + d\sigma^{\text{fixed order correction}} .$$

To perform the matching this requires an α_s -expansion, also below the merging scale and in the dead region. We expand Eq. (5.1) to get

$$\mathcal{PS}\tilde{\mathcal{V}}_0[u_0B_0(q_0)] = u_0B_0(q_0)\Delta_\mu^{V,0}\Delta_\rho^{D,0} \quad (5.5)$$

$$+ u_1B_0(q_0) \sum_i P_i \theta_{PS} \theta(q_i < \rho) \Delta_{q_i}^{V,0} \Delta_\rho^{D,0} \Delta_\mu^{q_i} \quad (5.6)$$

$$+ u_1B_0(q_0) \sum_i P_i \theta_{PS} \theta(q_i > \rho) \left(1 - \prod_j \theta(q_j > \rho) \right) \Delta_{q_i}^{D,0} \Delta_\mu^{q_i} + \mathcal{O}(\alpha_s^2) \quad (5.7)$$

$$= u_0B_0(q_0) \left(1 - \sum_i \int_\mu^{q_0} P_i \theta_{PS} \left(1 - \prod_j \theta(q_j > \rho) \right) \right) \\ + u_1B_0(q_0) \sum_i P_i \theta_{PS} \theta(q_i > \mu) \left(1 - \prod_j \theta(q_j > \rho) \right) + \mathcal{O}(\alpha_s^2). \quad (5.8)$$

Eq. (5.6) is the expansion of the emissions below the merging scale produced by the vetoed shower, Eq. (5.7) belongs to the dead region emissions. Both satisfy the bracket in Eq. (5.7) so that these can be collimated. It is worth to make clear that if any scale is below the merging scale the sum over all Shower approximations has to be taken. It should also be mentioned that the large- N_C colour structure the shower produces has to be taken into account. Both vetoed showers are not changing the cross section, so that $\Delta_\mu^{V,0}$ and $\Delta_\rho^{D,0}$ are the no emission probabilities for emitting outside the matrix element region. Their explicit form is given by the exponentiation of Eq. (5.6) and Eq. (5.7). Their $\mathcal{O}(\alpha_s)$ expansion is therefore the same as for the explicit emissions into the shower regions.

The expansion of Eqs. (5.2) and (5.3) leads to

$$(5.2) + (5.3) = - \sum_i \tilde{u}_0^i \int_\rho^{q_0} \frac{w_i}{\sum_j w_j} B_1(q_0) + u_1 B_1(q_0) \theta_{PS} . \quad (5.9)$$

Note, that the weights $w_{i/j}$ disappear in the second addend, since here only the Sudakov weight depends on the shower history, but still are present in the first term. In the first term the phase space configurations \tilde{u}_0^i depends on the clustering path of the LO merging.

We recall the NLO correction as

$$d\sigma_0^{NLO} = [B_0 + \bar{V}_0(\mu_R, \mu_F) + IPK_0] u_0 + \sum_i D_i \tilde{u}_0^i + B_1 u_1$$

with \bar{V}_0 being the UV-renormalized virtual correction and IPK_0 being the sum of integrated dipoles and collinear remainder from PDF renormalization. B_1 is the real emission contribution and is integrated over the ϕ_1 phase space. The dipoles D_i however must be added in a fixed order calculation into the tilde-kinematics \tilde{u}_0^i to cancel against their integrated counterparts.

If we precisely add the NLO $\mathcal{O}(\alpha_s)$ contributions and subtract the expanded ones we get the matched/merged $A(0^*, 1)$ compared to the merged $A(0, 1)$ as

$$A(0^*, 1) = A(0, 1) + u_0 (\bar{V}_0 + IPK_0) \quad (5.10)$$

$$+ \sum_i \tilde{u}_0^i \int_\rho \left(\frac{w_i}{\sum_j w_j} B_1(q_0) \theta_{PS} - D_i \right) \prod_j \theta(k_T^j > \rho) \quad (5.11)$$

$$+ \sum_i \tilde{u}_0^i \int_{\tilde{\mu}} (P_i B_0 \theta_{PS} - D_i) \left(1 - \prod_j \theta(k_T^j > \rho) \right) \quad (5.12)$$

$$+ u_1 \left(B_1(q_0) - \sum_i P_i B_0 \theta_{PS} \theta(q_i > \tilde{\mu}) - \sum_i D_i \theta(q_i < \tilde{\mu}) \right) \left(1 - \prod_j \theta(k_T^j > \rho) \right) \quad (5.13)$$

θ_{PS} assures that we are not double counting contributions occurred as finite contributions of the LO-merging process as well as it keeps the shower approximation in the region where the shower can produce emissions. θ_{PS} enters Eq. (5.11) in an integral where all dipoles have scales above the merging scale. So if we perform the same clustering as we did in the LO clustering and find that the real contribution cannot arise from a parton shower emission we counted this already and need to set $\theta_{PS} = 0$ in order to prevent double counting. Since all individual scales are above the merging scale we know that the contributions in Eq. (5.11) are finite. The sum over the individual tilde-kinematics is weighted with the clustering weights. If we sum all contributions into the same \tilde{u}_i it would destroy either the α_s expansion of the resummed expression or the fact that dipoles and Insertion operators cancel. We point out that at this point the Real emission contribution is always clustered to dipoles which are colour correlated in the large N_C limit, if the Shower also works in the large N_C approximation.

Eq. (5.13) contains contributions which are below the merging scale. Since there is no matrix element correction from the merging, this must be added in the real emission kinematic. A subtraction of the shower approximation like in MC@NLO takes place. This happens only below the merging scale compared to the MC@NLO approach where the shower approximation subtracts in the full shower phase space.

We introduced the variable $\tilde{\mu}$ which should be close to the shower cutoff μ . However one can also set $\tilde{\mu}$ larger than μ to gain numerical stability. The stability suffers from the fact that the shower approximations are calculated in the large- N_C limit and with spin averaged splitting functions which are also used in the shower.

Note that the parts of Eq. (5.13) below $\tilde{\mu}$ can also be stored in the Born kinematics below the cutoff as,

$$u_0 \theta(\tilde{\mu} > q_1) \left(B_1(q_0) - \sum_i D_i \right). \quad (5.14)$$

This is the same part as Eq. (3.16) and was already discussed in Sec. 3.5. There it was discussed that one is able to choose without destroying the accuracy of the shower nor the inclusive NLO calculation in which kinematic configuration the expressions should be included. In the following we choose the Born-like kinematics[†].

The formulas given in Eqs. (5.10)-(5.13) are based on the expansion after the showering/resummation process. As a consequence no showering should be performed after the replacement. But again as in the matching description described in Sec. 3.5 one can argue that the contributions should be showered after performing the matching. So to be clear what is done in the merging algorithm for $A(0, 1)$ and $A(0^*, 1)$, we renew the definition of $A(0^*, 1)$ to be

$$A(0^*, 1) := \mathcal{PS}[A(0^*, 1)] . \quad (5.15)$$

As discussed in Sec. 3.5 the reapplication of the shower operator does not change already showered contributions. It only effects the subtracted expanded and NLO contributions.

To see the effect of writing the NLO correction in this way, we should take a look at the properties if we vary the merging scale ρ .

Restoring standard NLO matching for $\rho \rightarrow q_0$

If $\rho = q_0$ there is no merging scale and no vetoed shower, so we end up with

$$A(0^*, 1) = \mathcal{PS}_0 [u_0(B_0(q_0) + \bar{V}_0 + IPK_0)] \quad (5.16)$$

$$+ \mathcal{PS}_0 \left[\sum_i \tilde{u}_0^i \int_{\tilde{\mu}} (P_i B_0 \theta_{PS} - D_i) \right] \quad (5.17)$$

$$+ \mathcal{PS}_1 \left[u_1 \left(B_1(q_0) - \sum_i P_i B_0 \theta_{PS} \theta(q_i > \tilde{\mu}) - \sum_i D_i \theta(q_i < \tilde{\mu}) \right) \right] \quad (5.18)$$

$$+ \mathcal{PS}_1 [u_1 B_1(q_1) \theta_{PS}] . \quad (5.19)$$

This is exactly the expression for the matched cross section in Eqs. (3.13)-(3.16) with additional showering of the $\mathcal{O}(\alpha_s)$ parts. The merging with an enhanced merging scale is therefore as accurate as the MC@NLO or POWHEG approach, which is an important feature.

At the merging scale ρ

At the merging scale we have for tree level merging the difference

$$\delta_\rho = B_1 \Delta_\rho^0 - \sum_i P_i \cdot B_0 \tilde{\Delta}_\rho^0 \quad (5.20)$$

where $\tilde{\Delta}_\rho^0$ is for unitarized merging part of the right hand side of Eq. (4.26) and for standard tree level merging part of the left hand side. The two Sudakov form factors differ in non

[†] Since after the calculation on parton level the particle momenta are reshuffled to their constituent mass in order to enter the cluster hadronization, which can lead to event rejections for very collinear or soft emissions we decided to store these contributions in the Born-like kinematics in favour of the inclusive cross section. Also the fact that in principal arbitrary non singular power corrections can be added to the subtraction dipoles, which need to cancel against their integrated counterparts favours the choice of Born-like kinematics.

singular parts and are identical for standard tree level merging. The difference between B_1 and $\sum_i P_i B_0$ appears in the way how the NLO corrections are inserted to the tree level merging in Eq. (5.13) without the Sudakov form factor and thus compensates for the difference in the tree level merging up to order α_s . δ_ρ is of order NNLL if the shower is NLL and thus an improvement on the α_s is as good as it can be, since no logarithmic improvement at the merging scale due to NLO insertions should be expected, if the shower catches the logarithmic structure of the process.

In the middle left plot of Fig. 7.7 we can see that the NLO corrections improve the behaviour by a smoother continuation below and above the merging scale. We further see that the MC@NLO result is similar to the results of the matched/merged NLO inclusion described above.

We state again that the NLO calculation must be independent of the dipoles and the corresponding integrated counter part, so we need to ensure that the dipoles are clustered in a sensible way. An algorithm, which aims to do this is given in Appendix A.

5.1.1. Review 2

The formulas can, as it is done in Sec. 4.4, be illustrated to review the steps so far. The upper blocks in Fig. 5.1 illustrate the LO merged sample with emissions below and above the merging scale. The shower emissions are produced in the full shower phase space with the exclusion of the matrix element region. The θ_{PS} in the purple block illustrates, that the LO sample is unitarized if the additional emission is in the shower phase space of the underlying configuration. The θ_{PS} is implicitly defined in P_i .

The LO merged sample is expanded up to $\mathcal{O}(\alpha_s)$. Emissions of the unitarized expressions are $\mathcal{O}(\alpha_s^2)$. Expansion of the shower emission and the Sudakov expression for emissions outside the matrix element region produces subtraction terms for this region labelled with ϕ_{ME} . The expanded LO merging expressions in the matrix element region produces the real emission of the fixed order calculation itself. The unitarized expression has a reduced multiplicity due to the clustering to the underlying Born configuration.

$\mathcal{O}(\alpha_s)$ expressions of the fixed order NLO correction are illustrated by the blocks in the middle of Fig. 5.1. Dipole expressions are included with Born-like kinematics (tilde kinematics), which is effectively a clustering/integration. Notice, that they need to cancel against their analytic, integrated counterparts in the IPK -operators.

Adding the $\mathcal{O}(\alpha_s)$ expressions of the fixed order NLO correction and subtracting the $\mathcal{O}(\alpha_s)$ expansion of the shower, produces a picture close to the matching description of MC@NLO. Each contribution has a counterpart, collected into the same block. Contributions that are added as finite corrections to the LO merging are not double counted, since the 'real emissions' is clustered solely inside the shower phase space. These blocks must now be added to the LO merged sample.

As a comparison we can also illustrate the matching for fixed order NLO corrections and parton shower, see Eqs. (3.13)-(3.16), with this building blocks. Here the shower expansion needs to be subtracted in the full shower phase space and since no merging scale is applied all building blocks receive a showering in the full parton shower phase space.

We introduced the merging of LO matrix elements with up to one additional NLO correction. By preserving the LO cross section it is possible to match NLO corrections without destroying the accuracy of the aimed precision. In the next section we show how to include NLO

LO merging (with emissions outside ME region):

B_0	$-\int \Delta_1^0 B_1 \theta_{PS} \theta_{ME}$	$\cdot \Delta_\mu^V$
	$P_1 \Delta_1^{0,V} B_0 \phi_{ME}$	$P_1 \Delta_1^{0,V} (-\int \Delta_1^0 B_1 \theta_{ME}) \theta_<$
	$\Delta_1^0 B_1 \theta_{ME}$	

$\mathcal{O}(\alpha_s)$ expansion:

$\mathcal{O}(\alpha_s^0)$	$-\int B_1 \theta_{PS} \theta_{ME}$	$-\int P_1 \phi_{ME} B_0 \theta_{PS}$
	$P_1 B_0 \phi_{ME}$	$\mathcal{O}(\alpha_s^2)$
	$B_1 \theta_{ME}$	

$\mathcal{O}(\alpha_s)$ of NLO contributions:

$\bar{V}_0 + IPK_0$	$-\int D_1$	
	B_1	

Adding $\mathcal{O}(\alpha_s)$ NLO contributions and subtracting $\mathcal{O}(\alpha_s)$ expansion:

$\bar{V}_0 + IPK_0$	$\int (B_1 \theta_{PS} - D_1) \theta_{ME}$	$\int (P_1 B_0 - D_1) \phi_{ME}$
	$(B_1 - P_1 B_0) \phi_{ME}$	

As a comparison NLO matching, see Eqs. (3.13)-(3.16):

B_0	$\bar{V}_0 + IPK_0$	$\int (P_1 - D_1) B_0$
	$(B_1 - P_1 B_0)$	

Figure 5.1.: Reviewing the steps to get from unitarized LO merging to the inclusion of the NLO correction to the seed process. The description of the blocks is given in Sec. 5.1.1. As in Fig. 4.4: Note that this illustration should only serve as a summary and to guide the eye through the formulas.

corrections by following the procedure of expanding the shower expressions and including the fixed order corrections.

5.2. NLO Merging with Two NLO Corrections

For the purpose of merging multiple NLO calculations, we start again with explicit merging of two NLO corrections. Therefore we write the LO merged expression for the LO merged cross section with up to two additional emissions described by matrix elements as

$$A(0, 1, 2) = \mathcal{PS}\tilde{\mathcal{V}}_0[u_0B_0(q_0)] \quad (5.21)$$

$$- \mathcal{PS}\mathcal{V}_0 \left[\int_{\rho}^{q_0} \sum_i \frac{w_i}{\sum_j w_j} \tilde{u}_0^i B_1(q_0) \Delta_1^{0,i} \theta_{PS}^1 \right] \quad (5.22)$$

$$+ \mathcal{PS}\tilde{\mathcal{V}}_1 \left[u_1 B_1(q_0) \sum_i \frac{w_i}{\sum_j w_j} \Delta_1^{0,i} \theta_{PS}^1 \right] \quad (5.23)$$

$$- \mathcal{PS}\mathcal{V}_1 \left[\int_{\rho}^{q_1} \sum_{i,k} \frac{w_{ik}}{\sum_{j,l} w_{jl}} \tilde{u}_1^k B_2(q_0) \theta_{PS}^1 \theta_{PS}^2 \Delta_2^{0,ik} \right] \quad (5.24)$$

$$+ \mathcal{PS}\tilde{\mathcal{V}}_1 \left[u_1 B_1(q_1) \theta_{PS}^1 \right] \quad (5.25)$$

$$- \mathcal{PS}\mathcal{V}_1 \left[\int_{\rho}^{q_1} \sum_k \frac{w_k}{\sum_l w_l} \tilde{u}_1^k \theta_{PS}^1 \theta_{PS}^2 B_2(q_0) \Delta_2^{1,k} \right] \quad (5.26)$$

$$+ \mathcal{PS}_2 \left[u_2 \sum_{i,k} \frac{w_{ik}}{\sum_{j,l} w_{jl}} \Delta_2^{0,ik} B_2(q_1) \theta_{PS}^1 \theta_{PS}^2 \right] \quad (5.27)$$

$$+ \mathcal{PS}_2 \left[u_2 \sum_k \frac{w_k}{\sum_l w_l} \Delta_2^{1,k} B_2(q_1) \theta_{PS}^1 \theta_{PS}^2 \right] \quad (5.28)$$

$$+ \mathcal{PS}_2 \left[u_2 B_2(q_1) \theta_{PS}^1 \theta_{PS}^2 \right]. \quad (5.29)$$

The first three lines and the fifth line are already present in Eq. (5.1). The expressions of Eq. (5.24) and Eq. (5.27) correspond to the phase space configurations for which a full ordered shower history can be found. Eq. (5.24) is the clustered contribution originating from the unitarization prescription. The weights have two indices for the first and for the second clustering. We can also label each history with just one index, but we will see below, that in many cases we can sum over all subsequent clusterings, leaving just a dependence on the first clustering weight. The expression in Eq. (5.26) and (5.28) describe regions of phase space, for which a first clustering above the merging scale can be found, but no second within the shower phase space of the seed process. Eq. (5.29) contains all the phase space configurations for which all scales are above the merging scale, but no first clustering can be found within the phase space of the underlying process, no unitarization expression is subtracted since this is added as an finite addition to the LO merging.

To match with fixed order calculations we need to expand this expression in α_s as for the case of the first NLO correction.

Eqs. (5.21) and (5.22) are used to include the first NLO correction in order to correct for B_0 . Additional emissions from these contributions can be of the same $\mathcal{O}(\alpha_s)$ as the second NLO correction but are always below the merging scale or in the dead region in the first place. If we aim to merge NNLO this contributions will need an α_s expansion up to α_s^2 . For the second NLO correction we require that we find a first emission which is above the merging scale.

The next term that needs to be expanded to $\mathcal{O}(\alpha_s^2)$ with respect to B_0 is Eq.

$$(5.23) \quad = \quad u_1 B_1(q_0) \sum_i \frac{w_i}{\sum_j w_j} \theta_{PS}^1 \left(1 + \alpha_s \partial_{\alpha_s}^1 \Delta_1^{0,i} + \alpha_s \partial_{\alpha_s}^1 \Delta_\rho^{q_1,D,i} \Delta_\mu^{q_1,V,i} \right) \quad (5.30)$$

$$+ \sum_k u_2^k P_k(q_0, q_2^k) \left(1 - \prod_l \theta(k_T^l > \rho) \right) B_1(q_0) \sum_i \frac{w_i}{\sum_j w_j} \theta_{PS}^{1,i} + \mathcal{O}(\alpha_s^2). \quad (5.31)$$

The $\partial_{\alpha_s}^1$ must be read as an operator projecting out the $\mathcal{O}(\alpha_s)$ part in an Taylor expansion, which was introduced in Eq. (2.76). The appearance of the product of θ -functions is analog to Eq. (5.8).

We use the expression Eq. (4.12) to get

$$\alpha_s \partial_{\alpha_s}^1 \Delta_1^{0,i} = \alpha_s \left[\partial_{\alpha_s}^1 \frac{f_1^i(q_1)}{f_1^i(q_0)} + \partial_{\alpha_s}^1 \frac{f_0^i(q_0)}{f_0^i(q_1)} + \partial_{\alpha_s}^1 \frac{\alpha_s(q_1^i)}{\alpha_s(q_0^i)} + \partial_{\alpha_s}^1 \sum_k \Delta_{q_1}^{k,i,q_0} \right] \quad (5.32)$$

Note that u_1 is independent but the expansion depends on the weights w_i . We expand the 'path' the LO merging has gone. In the algorithm this can be respected by clustering the u_1 contributions in the same way as the LO cluster algorithm and then expand the terms along this clustering history. This implies that if the clustering found a splitting in a II dipole, which only changes the PDF of the emitter, the PDF expansion is only performed for this. But also if the spectator parton changes the momentum fraction, the expansion is needed.

A similar result was found in [29] where they point out that the α_s expansion from the PDF-ratio can be, using the DGLAP-equation

$$\frac{\partial}{\partial \log(q^2)} f_i(x, q) = \sum_j \int_x^1 \frac{dz}{z} \frac{\alpha_s}{2\pi} \hat{P}_{ij}(z) f_j(x/z, q) - \frac{\alpha_s}{2\pi} f_i(x, q) \sum_j \int_0^1 dz \hat{P}_{ji}(z),$$

written as

$$\frac{f_i(x, q_1)}{f_i(x, q_0)} = 1 + \frac{\alpha_s}{2\pi} \log \left(\frac{q_1^2}{q_0^2} \right) \left(\sum_j \int_x^1 \frac{dz}{z} \hat{P}_{ij}(z) \frac{f_j(x/z, q_0)}{f_i(x, q_0)} - \sum_j \int_0^1 dz \hat{P}_{ji}(z) \right) + \mathcal{O}(\alpha_s^2). \quad (5.33)$$

In [29] both initial state PDFs are expanded for each step, what is not done in this work. We will go into detail on this choice in the discussion of Eq. (5.44) at the end of this section.

The expansion of the α_s -ratio is

$$\frac{\alpha_s(q_1)}{\alpha_s(q_0)} = 1 - \frac{\alpha_s}{2\pi} \beta_0 \log \left(\frac{q_1^2}{q_0^2} \right) + \mathcal{O}(\alpha_s^2), \quad \text{with } \beta_0 = \frac{11}{6} N_c - \frac{2}{3} T_R N_f. \quad (5.34)$$

The expansion of $\Delta_{q_1}^{k,q_0}$ for a DGLAP-like shower is for

$$\text{final states } \Delta_{q_1}^{k,q_0} = 1 - \frac{\alpha_s}{2\pi} \sum_i \int_{q_1^2}^{q_0^2} \frac{dq^2}{q^2} \int_{z_-}^{z_+} dz \hat{P}_{ik}(z) + \mathcal{O}(\alpha_s^2) \quad (5.35)$$

and for

$$\text{initial states } \Delta_{q_1}^{k,q_0} = 1 - \frac{\alpha_s}{2\pi} \sum_i \int_{q_1^2}^{q_0^2} \frac{dq^2}{q^2} \int_x^{z_+} \frac{dz}{z} \hat{P}_{ki}(z) \frac{f_i(x/z, \mu_F)}{f_k(x, \mu_F)} + \mathcal{O}(\alpha_s^2) \quad (5.36)$$

Comparing Eq. (5.36) and Eq. (5.33) one can see the correspondence between the DGLAP Equation and the backward evolving initial state shower up to phase space effects given by z_+ and the difference of splitting kernels used in the shower compared to the AP kernels. In our implementation we keep these expansions clearly separated, since phase space effects and changed kernels both contribute at $\mathcal{O}(\alpha_s)$, although they are not logarithmically enhanced.

Finally the last part in (5.30) is a pure no emission probability which is the counter part to the emissions in (5.31). The α_s expansion is

$$\partial_{\alpha_s}^1 \Delta_{\rho}^{q_1, D, i} \Delta_{\mu}^{q_1, V, i} = - \int_{\mu}^{\rho} \sum_k P_k(q_0, q_2^k) \theta_{PS} \left(1 - \prod_l \theta(k_T^l > \rho) \right) + \mathcal{O}(\alpha_s^2). \quad (5.37)$$

The sum over weights and phase space constraints in Eq. (5.31) translates into the restriction that q_2^k must be reachable from any underlying clustering. This is why the sum over the weights and θ_{PS}^i is replaced by the i -independent θ_{PS} . Also in Eq. (5.31) the i dependence drops and is replaced by θ_{PS} .

To finalize the expansion of the $A(0, 1, 2)$ cross section, we need to expand the contribution proportional to B_2 as

$$(5.24) + (5.26) = - \int_{\rho}^{q_1} \sum_{i,k} \frac{w_{ik}}{\sum_{j,l} w_{jl}} \tilde{u}_1^k B_2(q_0) \theta_{PS}^1 \theta_{PS}^2 \quad (5.38)$$

$$\begin{aligned} & - \int_{\rho}^{q_1} \sum_k \frac{w_k}{\sum_l w_l} \tilde{u}_1^k B_2(q_0) \theta_{PS}^1 \theta_{PS}^2 + \mathcal{O}(\alpha_s^2) \\ & = - \int_{\rho}^{q_1} \sum_k \frac{\tilde{w}_k}{\sum_l \tilde{w}_l} \tilde{u}_1^k B_2(q_0) \theta_{PS}^2 + \mathcal{O}(\alpha_s^2), \end{aligned} \quad (5.39)$$

and

$$\begin{aligned} (5.27) + (5.28) & = u_2 B_2(q_1) \theta_{PS}^1 \theta_{PS}^2 + u_2 B_2(q_1) \theta_{PS}^1 \theta_{PS}^2 + \mathcal{O}(\alpha_s^2) \\ & = u_2 B_2(q_1) \theta_{PS}^2 + \mathcal{O}(\alpha_s^2). \end{aligned} \quad (5.40)$$

We used that there is no dependence on the first emission, respectively the second clustering i in Eq. (5.38). We therefore define $\tilde{w}_k = \sum_i w_{ik}$. In Eq. (5.40) we use the obvious $\theta_{PS}^1 + \theta_{PS}^2 = 1$.

So with this we have all the expressions for expansions of the merged cross section with three combined LO contributions. These are not all contributions of the order of the second NLO

correction above the merging scale. While merging the first NLO correction we argued that the $\mathcal{O}(\alpha_s)$ expressions which where added should be showered with the phase space available for the Born-like contributions. So acting with the shower on this contributions will lead to emissions above the merging scale, which are of $\mathcal{O}(\alpha_s^2 L^2)$, so formally from the fixed order point of view $\mathcal{O}(\alpha_s^2)$ with respect to the seed Born-like process. These parts must be subtracted.

From the practical point of view it is convenient to veto emissions from the first NLO corrections if they are above the merging scale. We are not subtracting the exact $\mathcal{O}(\alpha_s)$ expansion but the full contribution from these emissions above the merging scale, which is of the same order as the expansion. All effects due to this vetoing are of higher order. For the algorithm, this implies that if a NLO correction to an higher multiplicity is present, we act on the first NLO corrections with a vetoed shower instead of the full shower.

In addition we preserve the inclusive NLO cross section, by subtracting the second NLO correction contributions in an integrated form from the B_0 contributions. Which is along the line of the LO merging description, but shifted in $\mathcal{O}(\alpha_s)$. The idea is driven by the LoopSim approach [78] were multiple NLO corrections where combined by adding and subtracting the higher multiplicity NLO corrections.

The inclusive NLO cross section to the B_1 part can be expressed as

$$d\sigma^{NLO} = [B_1 + \bar{V}_1(\mu_R, \mu_F) + IPK_1] u_1(k_T^j > \rho, \forall j) + \sum_i D_i \tilde{u}_1^i(k_T^{j,i} > \rho, \forall j) + B_2 \Theta u_2 \quad (5.41)$$

where the arguments of the Born-like measurement functions are cuts on the clustering to the \tilde{u}_0^j kinematics. This has to be done for the dipoles for each configuration separately to ensure that the integrated dipoles in IPK_1 cancel correctly against the clustered dipoles. The multiplicity of the dipoles is given by the phase space configuration \tilde{u}_k , for general k it is the multiplicity of the u_0 configuration with k additional partons, here $k = 1$. Note that this dipole corresponds to the real emission with two additional partons with respect to the u_0 configuration.

For the real emission we require that either all possible clusterings are above the merging scale or at least one dipole fulfils the property that all underlying clusterings j are above the merging scale. The mathematical formulation is

$$\Theta = \theta \left(\sum_k \prod_i \theta(k_{T,1}^{i,k} > \rho) \theta(k_{T,2}^k < \rho) + \prod_k \theta(k_{T,2}^k > \rho) \right) > 0 \quad (5.42)$$

This choice is based on the idea that single unresolved emissions are allowed for the real emission, but double unresolved emissions are not allowed. The merging scale in this respect acts as the resolution parameter. If we require that at least one of the underlying clusterings fulfils the property of having all underlying kinematics above the merging scale, than it is possible to cluster this contribution, so that a unitarization of the second NLO correction will preserve the cross section up to unordered histories.

For the merged $A(0^*, 1^*, 2)$ this leads to[†]

$$A(0^*, 1^*, 2) = A(0, 1, 2) + A(0^*, 1) - A(0, 1) \quad (5.43)$$

$$+ u_1 \left(-B_1(q_0) \sum_i \frac{w_i}{\sum_j w_j} \partial_{\alpha_s}^1 \Delta_1^{0,i} \theta_{PS}^1 + \bar{V}_1 + IPK_1 \right) \prod_i \theta(k_{T,2}^i > \rho) \quad (5.44)$$

$$+ \sum_k \tilde{u}_1^k \int_{\rho}^{\hat{s}} \left(\frac{\tilde{w}_k}{\sum_l \tilde{w}_l} \theta(q_2 < q_1) \Theta B_2(q_0) - D_k \right) \prod_i \theta(k_{T,1}^{i,k} > \rho) \quad (5.45)$$

$$\cdot \left(\prod_l \theta(k_{T,2}^l > \rho) \right)$$

$$+ \sum_k \tilde{u}_1^k \int_{\mu}^{\hat{s}} (P_k B_1 \theta(q_2 < q_1) - D_k) \prod_i \theta(k_{T,1}^{i,k} > \rho) \quad (5.46)$$

$$\cdot \left(1 - \prod_l \theta(k_{T,2}^l > \rho) \right) \left(\prod_l \theta(k_{T,2}^l > \mu) \right)$$

$$+ u_2 \left(B_2(q_0) \Theta - \sum_k P_k B_1 \theta(q_2 < q_1) \prod_i \theta(k_{T,1}^{i,k} > \rho) \right) \quad (5.47)$$

$$\cdot \left(1 - \prod_l \theta(k_{T,2}^l > \rho) \right) \left(\prod_l \theta(k_{T,2}^l > \mu) \right)$$

$$+ \int_0^{\hat{s}} \tilde{u}_1 \left(B_2(q_0) \Theta - \sum_k D_k \prod_i \theta(k_{T,1}^{i,k} > \rho) \right) \quad (5.48)$$

$$\cdot \left(1 - \prod_l \theta(k_{T,2}^l > \rho) \right) \left(1 - \prod_l \theta(k_{T,2}^l > \mu) \right)$$

$$+ \text{clustered unitarization} . \quad (5.49)$$

This merged expression contains the NLO correction of the subleading process and adds NLO corrections of the first emission. Compared to the Eqs. (5.31) and (5.37) the requirement, that all first clusterings should be above the shower cutoff was included to Eqs. (5.46) and (5.47). This cuts on the phase space of the corrections below the merging scale for splittings, not described by the corresponding splitting function/dipole.

The understanding of the given $A(0^*, 1^*, 2)$ requires more explanation:

- Eq.

$$(5.44) = u_1 \left(-B_1(q_0) \sum_i \frac{w_i}{\sum_j w_j} \partial_{\alpha_s}^1 \Delta_1^{0,i} \theta_{PS}^1 + \bar{V}_1 + IPK_1 \right) \prod_i \theta(k_{T,2}^i > \rho) ,$$

contains the virtual corrections, the integrated Dipole contributions, collinear remainders from PDF renormalization as well as the $\mathcal{O}(\alpha_s)$ -expansion of the shower (resummation) related parts.

[†]We will discuss in the following that additional weights should be applied. See discussion below.

All these parts can be calculated together for individual phase space configuration u_1 . The Virtual contribution is calculated with the scale of the seed Born process[§], which is not intuitive, since the scale could also be the scale of the first splitting.

The expansion of the α_s -ratio Eq. (5.34) produces exactly this property. The renormalization scale compensating terms of the NLO calculation, have the same form as this expansion, see Eq. (2.77). Here only one, and later multiple scale compensating parts for each emission are produced. This multiple scale improved NLO cross section is close to the idea in [77]. The example given in Sec. 2.6 has this form, see Eq. (2.79).

The expansion of the first PDF ratio in Eq. (5.32) contains the same parts as the P -operator in the CS subtraction formalism, where the factorization scale is related to process dependent scales. So in close analogy to the α_s -running this part of the PDF expansion relates the scale of the splitting to the scale used for the shower.

Both running expansions show the property that the large logarithms expected in the NLO correction calculated with the scale of the seed process is compensated by the logarithms of the shower expansion, and therefore related to the shower scales. We now expect logarithms of the shower splitting scales and the process dependent scales. These should be moderate if the shower is produces the logarithms which are expected. Finite K -factors will not be covered.

We are left with the second and the last expression of Eq. (5.32). One is the expansion of the initial PDF ratio and the other contains the expansions of the initial and final Sudakov form factors.

The final state Sudakov expressions are all time-like. We see that the PDF expansion of the initial PDF of the Born process f_0 together with the Sudakov factor expansion of this leg produces also – up to phase space effects and power corrections – the expression of an expanded time like correction. This can be understood since the evolution from the splitting, described by the ME to the subleading process is independent of PDF running. The initial state that was not assigned with a splitting by the clustering algorithm, should be corrected with the space like Sudakov expression, containing PDF ratios, since we evolve the PDF at this leg together with the shower scale. So only one expansion of the PDF ratio is present.

- Eq.

$$(5.45) = \sum_k \tilde{u}_1^k \int_{\rho}^{\hat{s}} \left(\frac{\tilde{w}_k}{\sum_l \tilde{w}_l} \theta(q_2 < q_1) \Theta B_2(q_0) - D_k \right) \prod_i \theta(k_{T,1}^{i,k} > \rho) \\ \cdot \left(\prod_l \theta(k_{T,2}^l > \rho) \right),$$

reveals dipoles and real emission for phase space configurations, where all scales of the first clusterings are above the merging scale. The dipoles originate from the NLO subtraction and are therefore clustered to the tilde kinematics. The matrix element corrections due to the real emission matrix elements are already present in the LO merging. They are clustered according to the weight of the LO merging and therefore compensate for the unitarization contributions of the LO merging.

[§]If a full history is found, this is the scale one would assign to the B_0 process. In the case of unordered history it should be the scale of the new defined seed process given by the LO merging.

The weight ratio effectively is described by the first backward clustering. Here it can happen that all weights vanish, which is the case if no ordered clustering can be found. In this case, which is made explicit by $\theta(q_2 < q_1)$ the LO merging already added this as a finite contribution, see Sec. 4.6. This restriction cannot be made for the Dipole parts since the integrated counterparts contain no cuts on ordering.

- Eq.

$$(5.46) \quad = \sum_k \tilde{u}_1^k \int_{\mu}^{\hat{s}} (P_k B_1 \theta(q_2 < q_1) - D_k) \prod_i \theta(k_{T,1}^{i,k} > \rho) \\ \cdot \left(1 - \prod_l \theta(k_{T,2}^l > \rho) \right) \left(\prod_l \theta(k_{T,2}^l > \mu) \right) \quad (5.50)$$

includes the Dipole contributions for which at least one Dipole has a resolution scale lower than the merging scale. The counterpart to this is, as in the case of $A(0^*, 1)$, the integrated Shower contributions from the Sudakov expansions of either the dead zone or the vetoed shower below the merging scale. The 'integration' of this part starts at the infrared cutoff of the shower. The shower expansion requires that the phase space point corresponding to the real emission, is inside the shower phase space of the tilded \tilde{u}_1^k kinematics.

- Eq.

$$(5.47) \quad = u_2 \left(B_2(q_0) \Theta - \sum_k P_k B_1 \theta(q_2 < q_1) \prod_i \theta(k_{T,1}^{i,k} > \rho) \right) \quad (5.51) \\ \cdot \left(1 - \prod_l \theta(k_{T,2}^l > \rho) \right) \left(\prod_l \theta(k_{T,2}^l > \mu) \right)$$

collects real emission with the subtracted shower approximation below the merging scale but above the IR cutoff of the shower produced by the expansion of the vetoed shower. All cluster scales below for secondary clusterings i need to be above the merging scale. This requirement also applies to the real emission contributions via the Θ cut, if the corresponding first clustering is below the merging scale.

- Eq.

$$(5.48) \quad = \int_0^{\hat{s}} \tilde{u}_1 \left(B_2(q_0) \Theta - \sum_k D_k \prod_i \theta(k_{T,1}^{i,k} > \rho) \right) \quad (5.52) \\ \cdot \left(1 - \prod_l \theta(k_{T,2}^l > \rho) \right) \left(1 - \prod_l \theta(k_{T,2}^l > \mu) \right)$$

represents the 'bridge' cross section as it is needed for NLO matching to parton showers. The shower is not emitting below the IR cutoff, so if one of the dipoles reveals a scale lower than the IR cutoff the dipole contributions need to be subtracted from the real emission, as in fixed order calculations. For the event interpretation one of the dipole kinematics \tilde{u}_1 needs to be chosen. This choice and clustering corresponds to the integral \int_0^{μ} . The choice contains an ambiguity, which will be addressed below.

- Eq. (5.49) contains the clustered contributions of all the corrections for the $A(0^*, 1^*, 2)$ compared to $A(0^*, 1, 2)$. This is done to preserve the NLO cross section of the seed process as in the LO merging. Since we know that all underlying kinematics to all $A(0^*, 1^*, 2)$ contributions are above the merging scale by construction, we can always cluster the underlying kinematics if they are inside the reachable shower phase space of any $n - 2$ kinematic configuration.

Cancellation of the subtraction related contributions

The modifications required the inclusion of cuts on the phase space to separate the individual parts. The subtraction terms, included to regularize the NLO calculation, need to cancel between the dipole contributions and the integrated insertion operators. Collecting only the dipole contributions of Eqs. (5.45)-(5.48), this gives

$$\begin{aligned} & \sum_k \tilde{u}_1^k \int_{\rho}^{\hat{s}} (-D_k) \prod_i \theta(k_{T,1}^{i,k} > \rho) \cdot \left(\prod_l \theta(k_{T,2}^l > \rho) \right) \\ & + \sum_k \tilde{u}_1^k \int_{\mu}^{\hat{s}} (-D_k) \prod_i \theta(k_{T,1}^{i,k} > \rho) \cdot \left(1 - \prod_l \theta(k_{T,2}^l > \rho) \right) \left(\prod_l \theta(k_{T,2}^l > \mu) \right) \\ & + \int_0^{\hat{s}} \tilde{u}_1 \left(- \sum_k D_k \prod_i \theta(k_{T,1}^{i,k} > \rho) \right) \cdot \left(1 - \prod_l \theta(k_{T,2}^l > \rho) \right) \left(1 - \prod_l \theta(k_{T,2}^l > \mu) \right) \end{aligned}$$

which collapse to

$$\sum_k \tilde{u}_1^k \int_0^{\hat{s}} (-D_k) \prod_i \theta(k_{T,1}^{i,k} > \rho) \quad (5.53)$$

if the individual kinematics \tilde{u}_1^k are picked randomly/flat. So that each dipole is integrated over the full single emission phase space with the requirement that secondary clusterings are above the merging scale. The insertion operators integrate the full phase space analytically and require that all primary clusterings show scales above the merging scale, see Eq. (5.44). The secondary clusterings of the dipoles correspond directly to the primary clusterings of the insertions, when no ordering of the second clustering with respect to the first clusterings is required. So the subtraction related contributions cancel with this choice.

Cancellation of the shower approximation for inclusive observables

The shower related subtraction related contributions in Eqs. (5.46) and (5.47) can be summarized as

$$\begin{aligned} & \left(\sum_k \tilde{u}_1^k \int_{\mu}^{\hat{s}} P_k B_1 - u_2 \sum_k P_k B_1 \right) (\theta(q_2 < q_1)) \\ & \cdot \prod_i \theta(k_{T,1}^{i,k} > \rho) \left(1 - \prod_l \theta(k_{T,2}^l > \rho) \right) \left(\prod_l \theta(k_{T,2}^l > \mu) \right) \end{aligned} \quad (5.54)$$

so that they cancel for inclusive observables, not resolving additional emissions. The structure is the same as it is used to construct the MC@NLO procedure. The difference to MC@NLO

are the cuts on subsequent clusterings. These are the contributions which are used to remove the double counting of shower emissions and real emission contributions. In the merging they only apply for the phase space below the merging scale.

Further Improvements

With the $\mathcal{O}(\alpha_s)$ expansions of the shower configurations and the addition of the NLO corrections to the first emission we control terms of this order above the merging scale from the fixed order point of view. From the resummation point of view we can now think of modifications which are beyond $\mathcal{O}(\alpha_s)$ but include the shower effects to the matched/merged expressions. The first part of this considerations was to perform a showering of the NLO contributions in the case of $A(0^*, 1)$ like in MC@NLO. This leads to similar shapes between LO+PS and NLO matched simulations for small scales. As discussed, these (showered) contributions need to be subtracted above the merging scale since they are of the same order as the NLO contributions to the first emission. By vetoing these emissions we effectively subtract the $\mathcal{O}(\alpha_s)$ and terms of higher order above the merging scale. Vetoing – not subtraction – means that we add the NLO correction to the first emission below the merging scale of the first emission.

Another way how to subtract $\mathcal{O}(\alpha_s)$ (and terms of higher order) from the showered NLO contributions of $A(0^*, 1)$ would be to reweight the NLO contributions with Sudakov suppression from the hard scale to the merging scale, and then shower the contribution below the merging scale. By this construction we would not be able to preserve the NLO cross section for inclusive observables. By vetoing the NLO contributions of $A(0^*, 1)$ and by clustered-subtraction of the additional NLO contributions of $A(0^*, 1^*, 2)$ we preserve the $A(0^*, 1)$ inclusive cross section. If the K -factor for the inclusive $A(0^*, 1)$ and the corrections of $A(0^*, 1^*, 2)$ above the merging scale are both larger (lower) than one we get a suppression (enhancement) in the same direction as we would assume from the Sudakov suppression. If the K -factor are different this can lead to discontinuities.

Since we truncate the perturbative series, we get scale cancellations between different orders of the series. The renormalization scale choice of $B_1(\mu_R)$ above the merging scale should be cancelled by the contributions of $A(0^*, 1^*, 2)$. The scale choice of B_1 is due to the shower reweighting shifted for one of the $\alpha_s(\mu_R)$. This shift was corrected in the $A(0^*, 1^*, 2)$ sample due to the expansion of the α_s ratio. In order to get an improved scale compensation between B_1 and the corrections we reweight the history of the corrections in $A(0^*, 1^*, 2)$ with the same factors as B_1 . So for B_1 like parts, Eq. (5.44), we calculate the same reweights as for B_1 . For the real emission above the merging scale that are calculated together with the subtraction dipoles, Eq. (5.45), the weight is calculated for the underlying Born process of the dipole. For the real emission below the merging scale, Eqs. (5.47) and (5.48) we pick one of the underlying kinematics that fulfils the condition that all scales below the last scale are above the merging scale, randomly and reweight the history producing this configuration. The piece, where dipoles and shower approximation meet, Eq. (5.46), is reweighted with the history weight of the dipoles. Note the important features of this choices:

- Since we cluster all contributions, this will not change the cross section.
- Dipoles – above the shower cutoff – are always reweighted with the history weight of their underlying Born process. So the same reweighting is applied for the integrated dipoles in IKP.
- The history weight is by definition of the type $1+\mathcal{O}(\alpha_s)$, so reweighting the NLO parts will not destroy the NLO accuracy.

- The suppression coming from the Sudakov factor of the history will stabilize the contribution if we go to smaller merging scales.

This history reweighting of the NLO contribution is also done in the MINLO approach[77], where the Sudakov suppression is calculated analytically. The suppression leads in this case to Sudakov peaks in fixed order calculations. Also the UNLOPS and NL³ [29] approach performs this reweighting. In the MEPS@NLO [25, 26] formalism the Sudakov reweighting is also applied for the 'last' real emission scale. This leads to numerically more stable results, since it is an effective cutoff applied to the real emission. Since this is formally also of higher order, the 'NLO accuracy' is not violated. In this work we keep closer to the previous ideas of reweighting the real emission not differently from the virtual corrections.

The algorithms how to generate the corrections are given in Appendix B.

5.2.1. Review 3

As for the introduction of the unitarized LO merging and the inclusion of the NLO correction to the seed process we give a pictorial review of the changes made so far. Note that the building blocks in Fig. 5.2 contain, especially in this review much less information as the previous text in the last section.

The NLO correction to the first additional emission above the merging scale follows the same idea as the inclusion of the $\mathcal{O}(\alpha_s)$ corrections to the seed process. We start by expanding the unitarized LO merged expressions for the sample with two additional emissions.

Therefore the LO merging is explicitly written with emissions outside the matrix element region, which is labelled with θ_{ME} . These are the upper blocks in Fig. 5.2. Since we describe two emissions with matrix elements, we have matrix element regions for the first and for the second emission. The θ_{ME} without index are always related to the higher index of B_i or P_i . θ_{ME}^i or $\theta_{ME}^{i'}$ with index require that the i 'th emission is inside or outside the matrix element region. The symbolic integrals over in the purple blocks are the clustered contributions from the unitarization description of Sec. 4.3. For readability we define the θ_{PS} of Sec. 5.1.1, in the blocks of this review to be part of the symbolic integrals.

With the condition that the first emission is in the matrix element region, the expansion up to $\mathcal{O}(\alpha_s^2)$ of these expressions leads to the second block structure. The first line contains no emission from the parton shower and the second only emissions outside the matrix element region. The last three rows are similar to the expansion that leads to the inclusion of the NLO correction of the seed process. Two differences appear:

- Conditions on the cluster sequence are required. A phase space point with $\theta_{ME}^2 \theta_{ME}^1$ requires that there is a cluster sequence with the first clustering is outside the matrix element region but then all direct next clustering scales are above the merging scale.
- The $\mathcal{O}(\alpha_s)$ expansion of the shower weight Δ_1^0 needs to be calculated. Δ_1^0 is defined in Eq. (4.12) and contains beside the Sudakov form factors for the shower history also α_s and PDF ratios. After the expansion ,as described in the (5.2), it is subtracted with the virtual contributions. This produces a multi-scale improved NLO calculation close to the one described in [77].

NLO corrections to the process with an additional emission need to be defined with cuts for the real emission contribution and on the first emission of for the Born-like kinematic

LO merging (with expansion outside ME region):

B_0	$-\int \Delta_1^0 B_1 \theta_{ME}$	$\cdot \Delta_\mu^{0,V}$	
	$P_1 \Delta_1^{0,V} B_0 \theta_{ME}$	$P_1 \Delta_1^{0,V} (-\int \Delta_1^0 B_1 \theta_{ME}) \theta_<$	
	$\Delta_1^0 B_1 \theta_{ME}$	$-\int \Delta_2^0 B_2 \theta_{ME}$	$\cdot \Delta_\mu^{1,V}$
		$P_2 \Delta_2^{1,V} \Delta_1^0 B_1 \theta_{ME}$	$P_2 \Delta_2^{1,V} (-\int \Delta_2^0 B_2) \theta_<$
		$\Delta_2^0 B_2 \theta_{ME}$	

$\mathcal{O}(\alpha_s^2)$ expansion with first emission in ME region ($\mathcal{O}(\alpha_s)$ expansion counted from B_1):

No	first	emission	
	θ_{ME}	$\theta_<$	
	$(\partial_{\alpha_s}^1 \Delta_1^0) B_1 \theta_{ME}$	$-\int B_2 \theta_{ME}$	$-\int P_2 B_1 \theta_{ME}^2 \theta_{ME}^1$
		$P_2 B_1 \theta_{ME}^2 \theta_{ME}^1$	$\mathcal{O}(\alpha_s^3)$
		$B_2 \theta_{ME}$	

$\mathcal{O}(\alpha_s^2)$ of second NLO contributions ($\mathcal{O}(\alpha_s)$ expansion counted from B_1):

$(\bar{V}_1 + IPK_1) \theta_{ME}$	$-\int D_2 \theta_{ME}$	
	$B_2 \Theta$	

Adding $\mathcal{O}(\alpha_s)$ NLO contributions and subtracting $\mathcal{O}(\alpha_s)$ expansion:

$(\bar{V}_1 + IPK_1 - (\partial_{\alpha_s}^1 \Delta_1^0) B_1) \theta_{ME}$	$\int (B_2 - D_2) \theta_{ME}^2 \theta_{ME}^1$	$\int (P_2 B_1 - D_2) \theta_{ME}^2 \theta_{ME}^1$
	$(B_2 \Theta - P_2 B_1) \theta_{ME}^2 \theta_{ME}^1$	

Figure 5.2.: Reviewing the steps to get from unitarized LO merging to the inclusion of the NLO correction to the process with one additional emission. The description of the blocks is given in Sec. 5.2.1. As in Fig. 4.4 and Fig. 5.1: Note that this illustration should only serve as a summary and to guide the eye through the formulas.

configurations. For the contributions with Born-like kinematics we require that all clustering scales are above the merging scale, which defined the matrix element region. The Θ , in the blocks describing the $\mathcal{O}(\alpha_s^2)$ of the NLO contributions, requires that either all clustering scales are above the merging scale, or for all first clusterings that if the clustering scale is below the merging scale all secondary clusterings are above the merging scale.

5.3. Extending the NLO Merging to Multiple NLO Corrections

We now give the properties that are needed to extend the NLO merging to multiple NLO corrections. In the merging of two NLO cross sections we required that the scales of all underlying clusterings of the Born-like (virtual, IPK and subtraction dipole contributions) are above the merging scale. This assures, that these phase space configurations are also present in the LO merging. Also the cut Θ in Eq. (5.42) is constructed in a way, that either all direct clusterings are above the merging scales or all scales of the underlying clusterings are above the merging scale if the first clustering is below. This assures that each underlying Born configuration that was obtained by clustering a real emission configuration is available by the LO merging. In any case we get parton states which have one additional separated parton by the merging scale. If we require the same cuts and procedure for n 'th NLO corrections we will always get phase space configurations that have $n - 1$ additional partons separated by the merging scale. For example, in the last section we included the second NLO correction and required cuts on the first emission.

For the $n - 1$ additional separated partons we calculated in the LO merging history weights, which now, in the aim of producing NLO corrections, need to be expanded and subtracted. Additional we get from the merging of n additional separated partons at LO the subtraction parts for the real emissions above the merging scale. In this respect it is necessary that the clustering of the B_{n+1} only depends on the last clustering step, which is the case if we see that the \tilde{w}_k in Eq. (5.45) sums all underlying cluster sequences.

We need to take care that the NLO corrections of the processes with lower multiplicities interfere not with the higher multiplicities. This can be achieved by either expanding or vetoing. As already seen for $A(0^*, 1^*, 2)$ the vetoing will then keep the contributions proportional to the Born process below the merging scale, which can be compensated by the contributions of the higher multiplicity by unitarization, if the K -factors are both larger/smaller than one.

The same algorithm can be applied to $A(0^*, 1^*, \dots, M^*, \dots, N)$ as it is applied to $A(0^*, 1^*, 2)$ with the difference that the algorithm must expand the previous history steps of the shower emissions. So for each clustering step the Sudakov suppression, α_s -ratios and PDF-ratios must be calculated as in the case of LO merging and in addition the NLO corrections must be subtracted with the appropriate shower approximations and the expansion of the history weights. Since the scales are given by the LO clustering algorithm, the difference of $A(0^*, 1^*, \dots, M^*, \dots, N)$ and $A(0^*, 1^*, \dots, (M - 1)^*, \dots, N)$ is given by

$$\begin{aligned} A(0^*, 1^*, \dots, M^*, \dots, N) &= A(0^*, 1^*, \dots, (M - 1)^*, \dots, N) \\ &\quad + u_M \left(-B_M(q_0) \sum_i \frac{w_i}{\sum_j w_j} \partial_{\alpha_s}^1 \Delta_M^{0,i} \theta_{PS}^M + \bar{V}_M + IPK_M \right) \prod_i \theta(k_{T,2}^i > \rho) \end{aligned}$$

$$\begin{aligned}
&+ \sum_k \tilde{w}_M^k \int_{\rho}^{\hat{s}} \left(\frac{\tilde{w}_k}{\sum_l \tilde{w}_l} \theta(q_{M+1} < q_M) \Theta B_{M+1}(q_0) - D_k \right) \prod_i \theta(k_{T,M}^{i,k} > \rho) \\
&\cdot \left(\prod_l \theta(k_{T,M+1}^l > \rho) \right)
\end{aligned} \tag{5.55}$$

$$\begin{aligned}
&+ \sum_k \tilde{w}_M^k \int_{\mu}^{\hat{s}} (P_k B_M \theta(q_{M+1} < q_M) - D_k) \prod_i \theta(k_{T,M}^{i,k} > \rho) \\
&\cdot \left(1 - \prod_l \theta(k_{T,M+1}^l > \rho) \right) \left(\prod_l \theta(k_{T,M+1}^l > \mu) \right)
\end{aligned} \tag{5.56}$$

$$\begin{aligned}
&+ u_{M+1} \left(B_{M+1}(q_0) \Theta - \sum_k P_k B_M \theta(q_{M+1} < q_M) \prod_i \theta(k_{T,M}^{i,k} > \rho) \right) \\
&\cdot \left(1 - \prod_l \theta(k_{T,M+1}^l > \rho) \right) \left(\prod_l \theta(k_{T,M+1}^l > \mu) \right)
\end{aligned} \tag{5.57}$$

$$\begin{aligned}
&+ \int_0^{\hat{s}} \tilde{u}_M \left(B_{M+1}(q_0) \Theta - \sum_k D_k \prod_i \theta(k_{T,M}^{i,k} > \rho) \right) \\
&\cdot \left(1 - \prod_l \theta(k_{T,M+1}^l > \rho) \right) \left(1 - \prod_l \theta(k_{T,M+1}^l > \mu) \right)
\end{aligned} \tag{5.58}$$

$$+ \text{clustered unitarization .} \tag{5.59}$$

Here the subtraction and shower approximations are always corresponding to the individual multiplicity. The \tilde{w} in the real emission above the merging scales are the probabilities that is given by the LO clustering algorithm and the $\partial_{\alpha_s}^1 \Delta_M^{0,i}$ is the expansion of the full history up to α_s . The Θ for the M 'th real emission only takes into account the first and/or secondary clusterings. Also the other cuts take into account not more than two clusterings, so that the algorithm for two NLO corrections is portable to M , with the same construction. The weight construction for the shower history related expansion is described for general M in Appendix B. We spare to review the expansion from two to M additional NLO corrections. The building blocks in the simplified notation correspond to the blocks in Sec. 5.2.1 with the replacement of $1 \rightarrow M$ additional emissions.

5.4. Scale Choice and Variation

After constructing the algorithm to merge multiple NLO cross sections, we define the scales and their variation used in the different parts of the calculation. We use the scales already included in the **Matchbox** [70] framework and include them into the merging. In a LO calculation with parton shower evolution we can choose various scales. The renormalization[¶] scale μ_R for α_s and the factorization scale μ_F for the PDFs defining the scales of the hard process. The shower starting scale Q_H defines the scale of the hardest possible emission. Other than that,

[¶]If other parameters than α_s were renormalized with scale depended schemes like the $\overline{\text{MS}}$ -scheme also one scale for each parameter could be used, after evolving the parameters with the appropriate RGEs.

we can change the scales used in the shower. The scales here are the arguments of the scale dependent α_s used in the shower splittings and the scale used in the PDF ratios [81].

We collect the scale dependent expressions used and insert scale variation parameters as:

- All matrix elements are calculated with

$$(\mu_R, \mu_F) \rightarrow B_i(\xi_R \mu_R, \xi_F \mu_F), V_i(\xi_R \mu_R, \xi_F \mu_F), IPK_i(\xi_R \mu_R, \xi_F \mu_F)$$

where μ_R and μ_F are calculated from the variables of the seed process if a full ordered shower history could be found. If not they are calculated according to Eq. (4.31), where we defined a 'new' starting scale^{||} for not fully ordered histories.

- The Sudakov form factor are calculated with, and radiation is created according to

$$\text{Eq. (3.8)} \rightarrow \Delta_f(\xi_H Q_H \rightarrow \mu) = \exp \left(\sum_{f'} \int_{\mu}^{\xi_H Q_H} \frac{dq}{q} \int_{z_-}^{z_+} dz \frac{\alpha_s(\xi_A q)}{2\pi} P_{ff'}(z) \right), \quad (5.60)$$

and

$$\text{Eq. (3.9)} \rightarrow \Pi_i(\xi_H Q_H \rightarrow \mu; x_i) \quad (5.61)$$

$$= \exp \left(\sum_{i'} \int_{\mu}^{\xi_H Q_H} \frac{dq}{q} \int_{x_i}^{z_+} \frac{dz}{z} \frac{\alpha_s(\xi_A q)}{2\pi} \frac{f_{i'}(x_i/z, \xi_f q)}{f_i(x_i, \xi_f q_1)} P_{i'i}(z) \right), \quad (5.62)$$

if it is the first emission. For further emissions we define the scales as fixed by the scale q where the emission is produced. Note that z_+ and z_- in general also depend on the boundaries of q , so are ξ_H dependent. In the dipole shower of `Herwig++` they depend on the upper scale, as can be read of Tab. (C.1).

- Accordingly we get

$$\text{Eq. (4.12)} \rightarrow \Delta_i^0 = \quad (5.63)$$

$$\frac{f_i(\xi_f q_i^{ls})}{f_i(\xi_F \mu_F)} \prod_{j=0}^{i-1} \frac{\alpha_s(\xi_A q_{j+1})}{\alpha_s(\xi_R \mu_R)} \left[\delta_{j0} \frac{f_0(\xi_F \mu_F)}{f_0(\xi_f q_1)} \Delta_{q_1}^{\xi_H Q_H} + (1 - \delta_{j0}) \frac{f_j(\xi_f q_j)}{f_j(\xi_f q_{j+1})} \Delta_{q_{j+1}}^{q_j} \right] \quad (5.64)$$

for the shower weights. The Kronecker delta δ_{j0} distinguish between first and multiple emissions. This shower weights are then expanded as shown in Sec. 5.2. For this we then use $\alpha_s(\mu_R)$ and the PDFs at scale μ_F . The scales in the logarithms and the boundaries for the expanded Sudakov suppression receive the ξ_i factors.

We included the five parameters ξ_R , ξ_F , ξ_H , ξ_A and ξ_f into the merged expression. In Ch. 7 the results are shown with variations of the first three parameters. Interfaces exists to vary all parameters independently.

Conclusion

In this and the previous chapter, we followed the idea of matching resummed calculations to fixed order calculations. The unitarized, resummed expressions for LO merging have been expanded and subtracted from the $\mathcal{O}(\alpha_s)$ expressions of the NLO corrections. This leads to

^{||}Other choices for this 'new' scale are possible but not yet implemented.

direct subtraction below the merging scale, as compared to the matching of fixed order NLO calculations to parton showers in the full shower phase space.

We implemented the expressions for general additional LO N and NLO corrections M in the `Matchbox` framework of `Herwig++` [3] with the dipole shower [57]. Some detail of this implementation and the efforts of interfacing external program packages to generate an automated matching and merging are given in the next chapter.

CHAPTER 6

Implementation and Validation

In the following we describe the practical implementation of the needed weights to perform the previously described (N)LO merging of matrix elements to parton showers. Since the algorithms were detailed in the previous chapter, we concentrate more on the individual parts, their implementation and validation. Starting with one of the key ingredients of merging algorithms being the Sudakov form factor reweighting of ordered shower histories this chapter continues with a description on the calculation of the expanded shower expressions. The chapter ends with a short overview on the matrix element interfaces developed to produce automated NLO matching and merging in `Herwig++/Matchbox`.

6.1. Sudakov Form Factor Reweighting

One of the important features of merging matrix elements to parton showers are the weights to produce 'exclusive' states. The matrix elements that correct the shower emissions need to be reweighted with the expressions given in Eq. (4.12). While in the classic CKKW approach this was produced by analytic Sudakov expressions, the CKKW-L produced the suppression with trial showers as described in Sec. 4.2. The first does not respect the actual shower structure and is only applicable if the shower correctly reproduces the expected Sudakov suppression, the latter can be applied to any shower algorithm and respects the phase space boundaries of the shower. Since the trial showering produces the suppression by discarding events it can produce strongly fluctuating weighted events. One can avoid this fluctuation by multiple trials and weighting the event with the fraction of the trials that did not emit above the next history scale. Both will produce correct no emission probabilities the shower would have produced.

The idea that was followed in the implementation was to implement two types of suppression factors, which then can also serve as a cross check. On the one hand the CKKW-L approach by constructing underlying fake events that are then showered and on the other hand to calculate the suppression with an explicit Monte Carlo integral of the exponent of the Sudakov factors respecting the phase space boundaries and scales used in the shower. The explicit integration can be performed faster to give more stable results and can be used, in a modified way, to

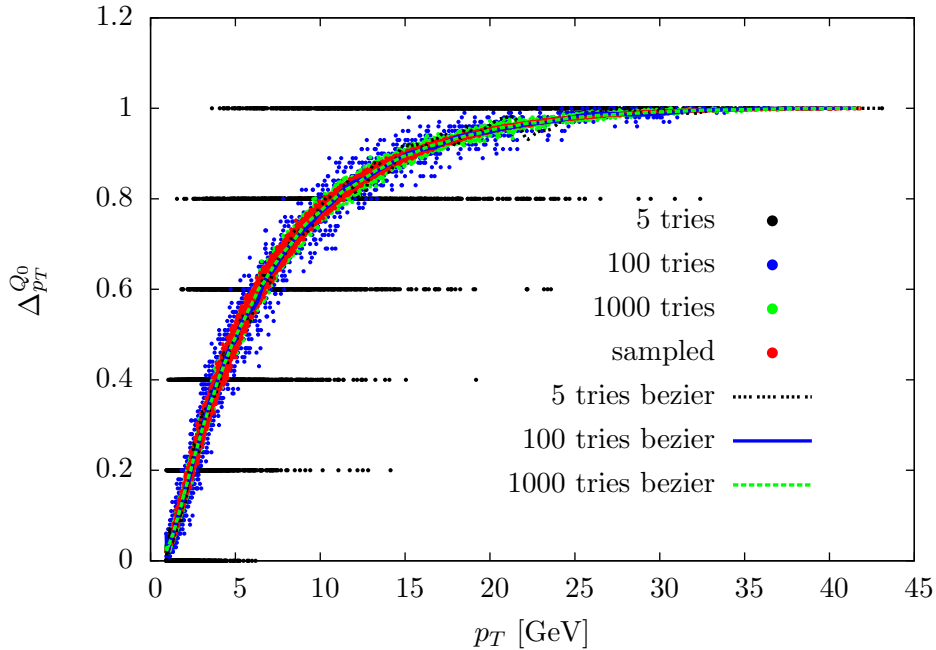


Figure 6.1.: Comparison of the implementation of a Sudakov form factor for a $q\bar{q}$ pair with $Q_0=91.2$ GeV. The blue, black and green points correspond to CKKW-L type Sudakov suppression, where the number of no emissions above the scale p_T is counted. The fraction then produces the density of no emissions. While five trials lead to visible stripes, the grid of 100 trial events is much more centered around the average value and the spread of 1000 trials is close to the spread gotten from sampling the exponent with a Monte Carlo error off 5%. The average, produced by the bezier function of gnuplot, agrees for both methods and various numbers of trials.

calculate the shower expansions needed for the NLO merging. The shower expansion of the Sudakov factors, see Eq. (5.30), are the same integrals with fixed scales in the α_s and PDF arguments. The advantage of calculating the Sudakov suppression together with the matrix elements is from a technical point of view superior to the reweighting or discarding large event files. The integrator can adapt with algorithms similar to the Vegas algorithm [82] or Monaco algorithm* to the combined matrix element and Sudakov suppression weight. Strongly singular regions which would produce large parts of the cross section are suppressed naturally by the shower/Sudakov suppression and if the integrator adapts the behaviour, it produces less phase space points in this regions.

The Sudakov exponents are simple 3-dimensional integrals with simple (except of numerical PDF ratios), but scale and initial state momentum fraction x dependent functions. In addition the phase space boundaries need to be taken into account. Since these functions/phase space boundaries were already implemented with proper substitutions to sample the Sudakov exponent efficiently in the `Herwig++`-dipole shower a single routine can perform the integration after setting up the used dipole kernels that the shower would have used from the shower history to produce the next emission.

*A modified Vegas algorithm implemented in `VBFNLO` [83].

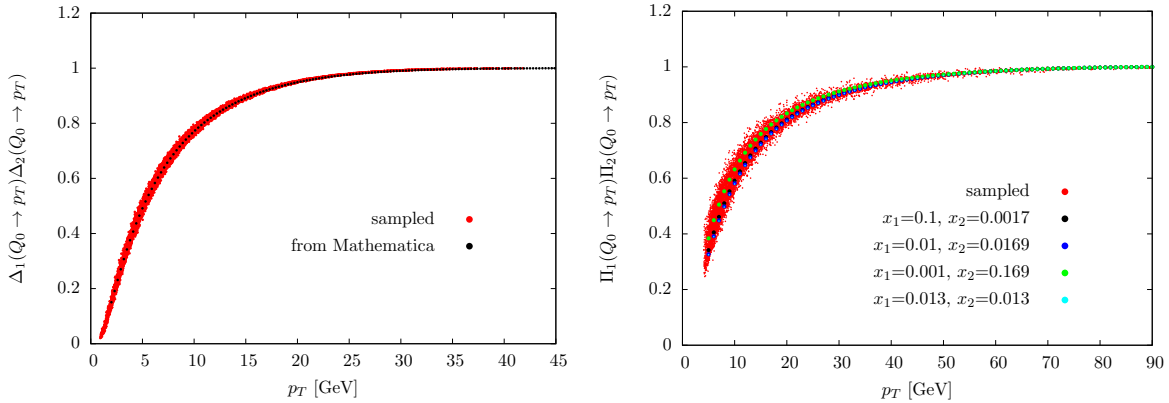


Figure 6.2.: Sudakov suppression as a function of p_T . Left: The comparison of the sampling implementation (red dots), against the **Mathematica** implementation (black dots) for a $q\bar{q}$ -pair building a FF-dipole with $Q_0 = M_Z$. Right: The suppression for $q\bar{q}$ -pair building a II-dipole with $Q_0 = M_Z$ and different $x_{1/2}$ values so that $x_1 x_2 S = M_Z^2$. The backward Sudakov factor depends on $x_{1/2}$. All other factors vary in the splitting functions used but not in the sampling algorithm.

The CKKW-L approach can be implemented by producing the fake events and running the shower algorithm with aborting after the first emission. If the emission is above the next scale of the shower history the phase space point is discarded.

To have a third comparison the Sudakov suppression expected by the dipole shower was implemented in **Mathematica** for FF- and II-dipoles. The implementation of II-dipoles required the calculation of PDF ratios which was interfaced with the NNPDF **Mathematica** interface [84].

In Fig. 6.1 a comparison is shown for the difference between the CKKW-L like implementation and the sampling of the Sudakov exponent. The CKKW-L Sudakov suppression is shown for 5, 100 and 1000 trial emissions, while for the 5 and 100 trial emissions the ratios are still visible the 1000 trial emissions are overlapping with the sampled exponent. The average of the suppression achieved by the procedures is identical.

The comparison against the **Mathematica** implementation for a FF and an II dipole with PDF ratios is shown in Fig. 6.2. Since the PDF ratio depends on the value of the incoming momentum fraction, the Sudakov suppression is broader than the one coming from the FF dipole.

6.2. α_s -Expansion of Shower Related Weights

For the NLO merging it was explained in Sec. 5.2 that the weights produced by the shower in the LO merging need to be subtracted from the merged sample to $\mathcal{O}(\alpha_s)$ in order to get NLO accuracy above the merging scale. In the previous section the results for CKKW-L like and sampled Sudakov are shown to give similar results. In order to produce the weights needed for the expansion of the shower expressions, the sampling routines can be reused without exponentiation. In the calculation, the arguments of the scale dependent components are kept fixed.

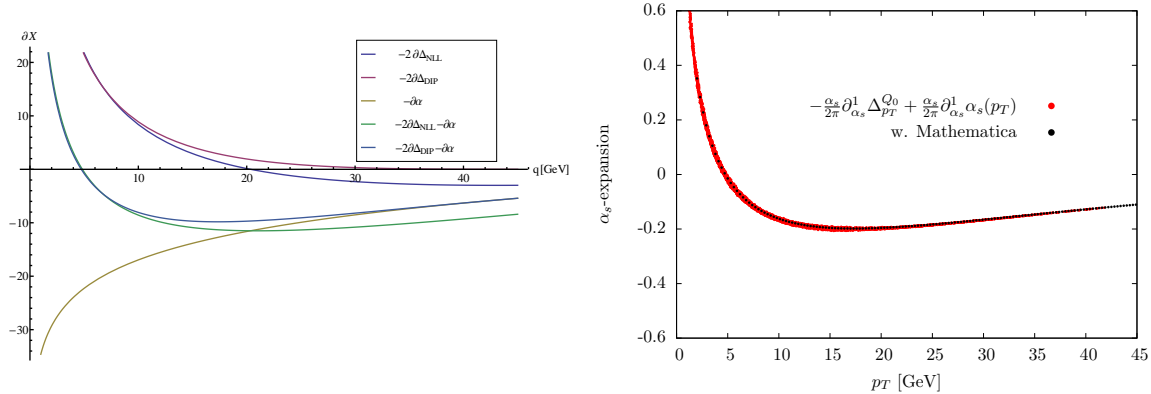


Figure 6.3.: Expansions of the shower related contributions. Left: The expected results as implemented in **Mathematica**. Right: The results from the sampling of the Sudakov exponent with a fixed scale. The PDF ratios produce a wide $x_{1/2}$ dependent band and are not included in this comparison. The dark blue line in the left plot is the $\mathcal{O}(\alpha_s)$ expansion of the NLL Sudakov expression, the purple the one expected from the dipole shower. The yellow line is the logarithm from the α_s -running. Green and light blue line are the sum of α_s and Sudakov expansion for Δ_{NLL} and Δ_{DIP} .

The expansion of the α_s ratio is given in Eq. (5.34). Due to the sign of the β -function, subtracting the α_s expansion of the ratio leads to a negative contribution. The Sudakov expansion leads to positive weights in the sum of Eq. (5.32).

Eq. (5.33), giving the expansion of the PDF ratio is closely related to the P operator of the CS subtraction formalism. With the substitution given in Eq. (2.73), the same expressions can be used here. In the implementation of the integrated regularized AP-splitting function, one can either throw one random number handled by the integrator or use multiple points to average the integral. While α_s and the Sudakov expansion have definite sign the PDF ratio expansion depends on the x_{in} value and the flavour of the incoming parton. Here the $+$ -distribution in combination with the PDF can lead to positive and negative contributions.

To double check the implementation the expressions were implemented in **Mathematica**, with the results for the Sudakov and α_s expansion shown in Fig. 6.3. Here also the expansion of the NLL Sudakov expression used in the MINLO [77] approach is shown. Since the NLL Sudakov for large values of p_T can become larger than one, see Fig. 4.1, the expansion needs to produce negative weights.

For small values of the scales the Sudakov expansion dominates since the α_s expansion is a subleading logarithm and the integrated splitting functions lead to squared logarithmic dependence.

6.3. Phase Space Boundaries and Definitions

Merging matrix elements to parton showers in a way, like it is described in Ch. 4 requires the 'reconstruction' of the assumed showering history. Phase space boundaries and transverse momentum p_T definitions are the same in clustering of the momenta of the matrix elements and shower emissions. The dipole shower of **Herwig++**[57] has two run modes. The collinear mode uses inverted kinematics of the tilded kinematics given in [41]. Here the incoming

momenta of II/IF dipoles are fixed to be collinear to the beam and shower emissions will only change the momentum fraction of incoming partons. In the non collinear mode, described in [57], shower emissions produce also initial states with transverse momenta. In the latter mode the clustering of the higher multiplicity phase space points with the usual tilded kinematics will not reconstruct the emissions coming from the showering. Since some of the definitions have changed from the first introduction of the dipole shower [57], the restrictions on phase space boundaries and the definitions of variables are listed in Appendix C.

6.4. Smearing

In the merging algorithm the scale where to split the phase space into matrix element and shower domain plays an important role. Discontinuities at this scale are expected and shall be beyond the accuracy of the shower. Small discontinuities can be smeared if we choose the merging scale for each phase space point as

$$\rho = \rho_C(1 - \kappa + 2\kappa r) , \quad (6.1)$$

where ρ_C is the central merging scale and $r \in [0, 1]$ is a flat random number. If the corrections due to the merging are large kinks at the merging scale are still possible and can be seen as an error estimate of the method. The results in Ch. 7 have been generated with $\kappa=0.1$.

6.5. External Matrix Element Provider

For NLO matching and merging the interplay of parton shower and NLO corrections is important. In the last decade huge efforts have been made to automatize the computation of NLO cross sections. Many programs were developed to create libraries, which can compute UV renormalized virtual corrections, e.g. [10, 85–87]. The automatized generation of LO matrix elements which are needed to produce the real emission and subtraction was developed much earlier, e.g. [88, 89].

In order to match NLO with parton shower, it is of great interest to have full control over phase space generation/population, matrix element calculation, subtraction and parton shower evolution. The **Matchbox**[70] module of **Herwig++** is aiming to provide a fully automated matching to the parton showers (angular ordered and dipole). Since the **Herwig++** event generator had neither a fully automated LO matrix element generator, which fits into the framework of **Matchbox**, nor the generation of NLO corrections automatically, the interfacing to external providers of these parts was needed.

LO Matrix elements – on amplitude level

In collaboration with the **MadGraph** [10] team an interface was implemented which is able to build a library, fitting into the framework of **Matchbox**. **MadGraph** internally uses the same colour basis as the **ColorFull** package[90] that provides a native interface to the routines used by **Matchbox**. The fully automatized generation, linking and mapping of internal orderings between **Matchbox** and **MadGraph** is provided. With these ingredients tree level amplitudes and colour correlated matrix elements can be calculated. In order to provide spin colour correlations, needed for CS subtraction of processes with external gluons, the internally used plus polarization vector for gluons ε_+^μ are constructed with the **HELAS** routine [91] `vxxxxx(...)` used in **MadGraph**.

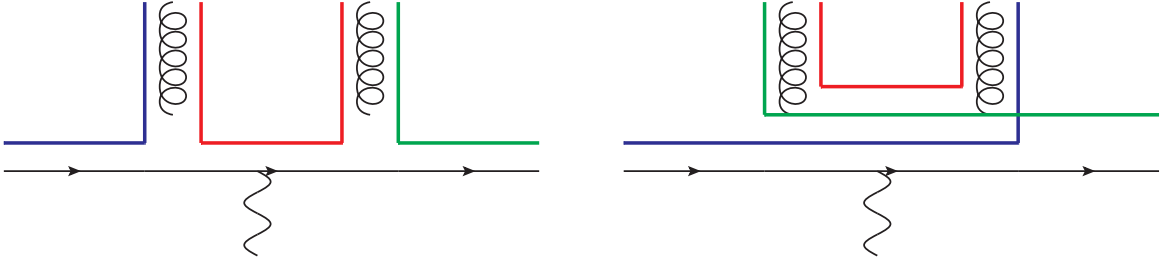


Figure 6.4.: Pictorial representation of the large- N_C colour dipoles. The $q\bar{q}$ -pair is not connected after emitting a gluon. While CS subtraction contains dipoles with colour correlations between the $q\bar{q}$ -pair, the shower does not emit from the quark with the anti-quark being the spectator. The initial colour dipoles are picked by the weight of the squared large- N_C colour-flow amplitudes, as shown in [70].

As outlined in [70] the spin-colour correlations of the form

$$\langle \mathcal{M}_\mu | \mathbf{C}_{ij} C^{\mu\nu} | \mathcal{M}_\nu \rangle = \langle \mathcal{M}_\mu | \mathbf{C}_{ij} | \mathcal{M}_\nu \rangle \left(C\eta^{\mu\nu} + \frac{q^\mu q^\nu}{Q^2} \right)$$

can be calculated efficiently by

$$\begin{aligned} \langle \mathcal{M}_\mu | \mathbf{C}_{ij} C^{\mu\nu} | \mathcal{M}_\nu \rangle &= \frac{1}{Q^2} \left[\langle \mathcal{M} | \mathbf{C}_{ij} | \mathcal{M} \rangle (-CQ^2 + |\epsilon_+ \cdot q|^2) \right. \\ &\quad \left. + 2\text{Re} \left((\epsilon_+ \cdot q)^2 \begin{cases} \langle \mathcal{M}_- | \mathbf{C}_{ij} | \mathcal{M}_+ \rangle & \text{outgoing } g \\ \langle \mathcal{M}_+ | \mathbf{C}_{ij} | \mathcal{M}_- \rangle & \text{incoming } g \end{cases} \right) \right], \quad (6.2) \end{aligned}$$

where $\mathbf{C}_{ij} = \mathbf{T}_i \cdot \mathbf{T}_j / \mathbf{T}_i^2$ is the colour correlator and $\langle \mathcal{M} |$ are the amplitudes with open colour indices and μ, ν and \pm are the helicities of the gluon.

The showers in **Herwig++** are using the large N_C colour information to choose the initial colour flows according to the weight of the squared large N_C colour amplitude, see Fig. 6.4. This information can be produced with the **MadGraph** interface and the large N_C mode of the **ColorFull** package.

NLO Matrix elements – squared amplitude level

For an automated matching/merging of NLO corrections to the partons showers of **Herwig++**, the NLO providers **GoSam**[86], **NJet**[92], **OpenLoops**[87] and **VBFNLO**[93][†] are available, using the standard interface **BLHA2** [94], which is an extension to the **BLHA** [95]. In **BLHA2** the external programs are expected to provide, beside the renormalized virtual corrections, also treelevel and (spin-)colour correlated amplitudes. In addition to the LO interface to **MadGraph** the automated interface to the one loop corrections provided by the **MadGraph/aMC@NLO** [10] was developed. With this extension to the **Matchbox** framework processes provided by the external programs can be consistently matched to the parton showers. In addition to calculate the matrix elements also parameter choices used in the event generation are handled fully by the event generator and communicated to the external program. The various interfaces have been tested and validated extensively among each other and to external packages like **MCFM**[96].

[†]The author was mainly involved in the interfacing of **GoSam**, **MadGraph** and **OpenLoops**

CHAPTER 7

Phenomenological Results and Improvements

In this chapter, the results of LO and NLO merging will be discussed. First, in Sec. 7.1, the clean environment, in terms of pure final state QCD radiation, at e^+e^- colliders like LEP is used to validate the merging scheme at parton level without the effects of hadronization. With the results seen for NLO merging we discuss the value and choice of α_s in Sec. 7.1.1. Sec. 7.2 is dedicated to the comparison of LEP data to these results with hadronization effects. The next step, in Sec. 7.3, is then the environment of LHC physics as a hadron collider. Comparisons of the merging algorithm to the W^\pm and Z boson at LHC and the effects of merging on Higgs production are discussed. The last comparison is then using dijet production with LHC conditions. All plots in this chapter have been produced with **Rivet** [97].

7.1. Parton Production in $e^+ e^-$ Annihilation

The following discussion provides also a validation of the implementation, since we compare to constructed pseudo observables which are not measurable at colliders. The clean environment (from the QCD point of view) at an e^+e^- collider is perfectly suited to validate the clustering algorithm for ordered histories. Since the phase space is given by the initial center of mass energy $\hat{s} = s$, mostly full ordered histories can be found.

LO-merging:

The first pseudo-observable is constructed to precisely show the behaviour at the merging scale. For this reason, we select from all parton level events those with exactly three partons in the final events. We start with a $q\bar{q}$ pair so the first emission must be a gluon. For this gluon with momentum p_j we calculate the transverse momenta p_T^i that would correspond to the emission of either the quark or the anti-quark with momentum p_i . The other parton serves as a spectator, see Sec. 2.5, with momentum p_k as

$$p_T^i = \sqrt{yz(1-z)s} \quad \text{with} \quad z = \frac{p_ip_k}{p_ip_k + p_jp_k} \quad \text{and} \quad y = \frac{p_ip_j}{p_ip_j + p_kp_j + p_ip_k} \quad (7.1)$$

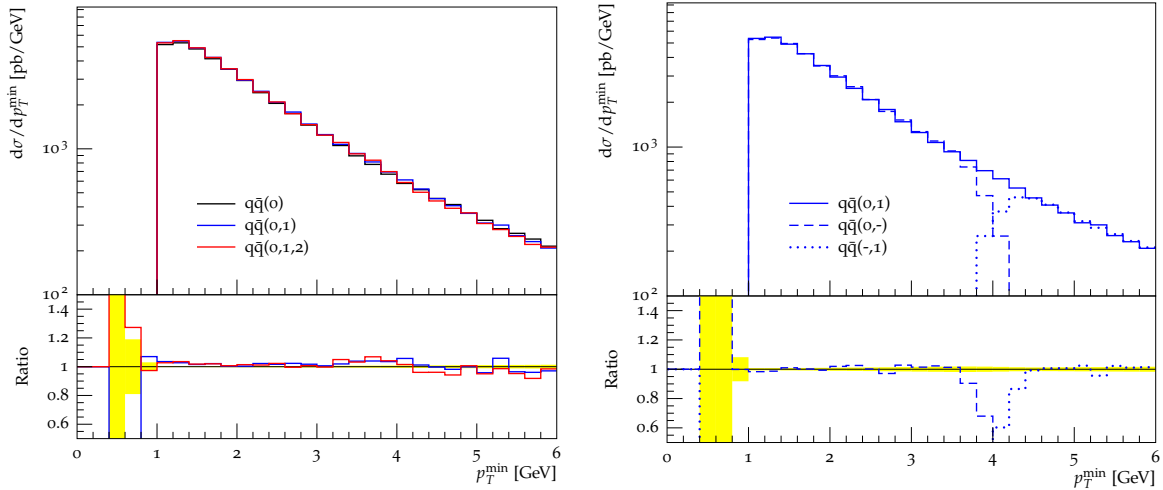


Figure 7.1.: Constructed pseudo observable p_T^{\min} , defined as the minimum dipole-transverse momentum in exclusive $q\bar{q}$ -events. Left: Differential cross section of the merged samples with zero, one and two additional emissions for the process $e^+e^- \rightarrow q\bar{q}$. Right: Sample with one additional emission split up into the vetoed part, where no additional emissions above the merging scale takes place and the parts above the merging scale. The center of mass energy is $\sqrt{s} = 91.2$ GeV merging scale is $\rho = 4$ GeV with a smearing of 10%.

The events are then binned for $p_T^{\min} = \min(p_T^q, p_T^{\bar{q}})$ to get the differential cross section with respect to p_T^{\min} .

The results were obtained with a center of mass energy of $s = 91.2$ GeV, with an $\alpha_s^{\overline{\text{MS}}}(M_Z) = 0.118$ and without electron PDFs* simulating energy loss due to initial state photon radiation. In Fig. 7.1 the result for the fraction of three parton events is shown for one and two additional partons in the merging. Higher multiplicities would not change this 'pseudo' observable since we require exactly three partons. The smooth transitions at the merging scale $\rho = 4$ GeV with a shower cutoff at $\mu = 1$ GeV indicates that the veto algorithm, α_s reweighting, Sudakov suppression and the shower history choice is implemented properly for pure final state emissions. Also the merged sample for two additional emissions, which are handled by the correct matrix elements $q\bar{q}(0, 1, 2)^\dagger$, shows a smooth behaviour at the transition from the matrix element region to the parton shower domain. This shows that also the emissions from the merged sample $q\bar{q}(-, 1, -)$ with three partons, before the vetoed shower is applied, produced enough emissions to disappear in the distribution in the left picture of Fig. 7.1. So also the starting scales and vetoed shower work as they should.

In Fig. 7.2 the differential cross section is plotted with respect to the y_{34} parameter, which separates a three jet configuration from a four jet configuration when a Durham jet algorithm [61, 62] is applied. In the hard tail – larger y_{34} values – the algorithm resolves four jet events which are separated clearly and should therefore be described by the matrix element. The distribution rises for smaller values of y_{34} , resolving the enhanced softer and/or more collinear emissions. Below $y_{34} \approx 2 \cdot 10^{-4}$ the probability drops to find the transition from

*Also the comparison against data in Sec. 7.2 will be without the effects of electron PDF, since the data is often corrected for the effects of these, see e.g. Sec. 2 in [98] or Sec. 4.1.2. in [99].

[†]For notation see Sec. 4.8.

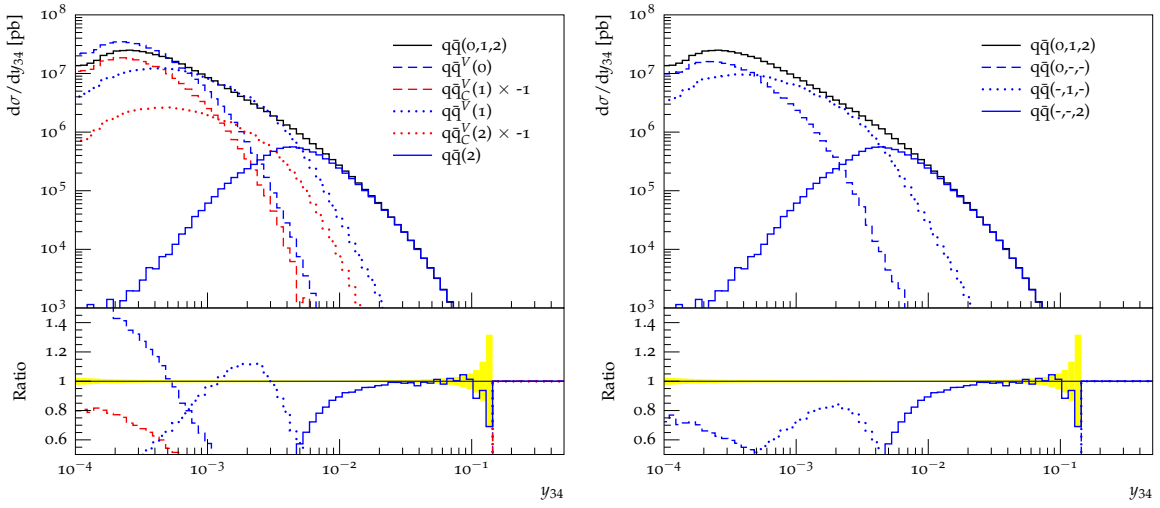


Figure 7.2.: Differential cross section as a function of y_{34} , which separates three jet events from four jet events in a Durham jet algorithm. The cross section is split up into the different contributions leading to the combined $q\bar{q}(0, 1, 2)$ merged sample. The blue contributions in the left picture are compensated by the red, clustered subtraction terms. The red lines are multiplied by a factor minus one. In the right picture the blue contributions are the sum of the red and blue lines in the left plot, e.g. $q\bar{q}(0, -, -) = q\bar{q}^V(0) + q\bar{q}_C^V(1)$.

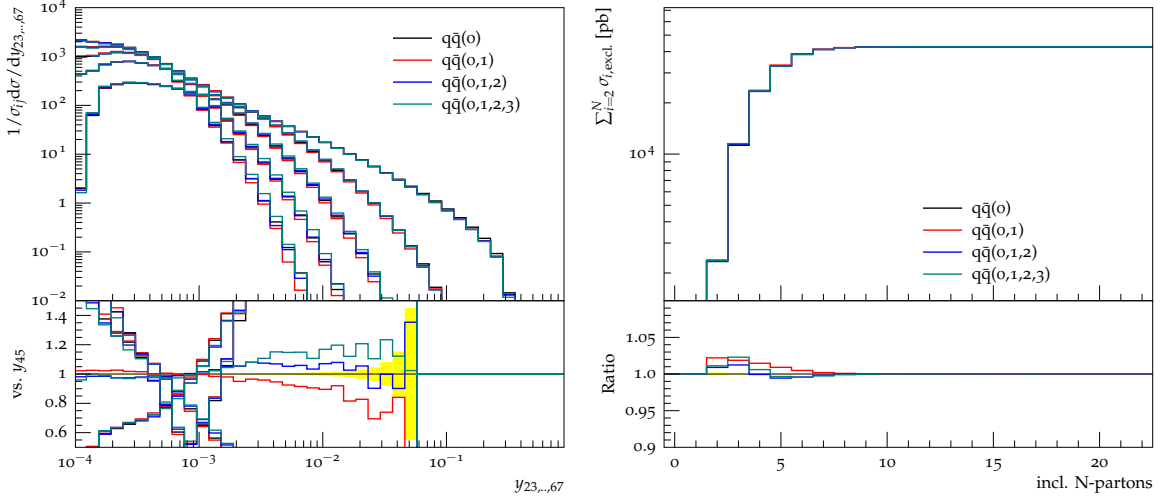


Figure 7.3.: Left: Differential jet rates as a function of the various Durham $y_{a,a+1}$ parameter, where a particular event changes the multiplicity from an a -jet to an $a+1$ -jet configuration within the Durham jet algorithm. The differential cross sections have been normalized to their individual integrated cross section and the ratio is with respect to y_{45} of $q\bar{q}(0)$. Right: The cross section as a function of inclusive N -parton states.

three to four jet events. The different distributions are plotted leading to $q\bar{q}(0, 1, 2)$. Here, we split the distribution according to Eqs. (4.35) and (4.36). On the left hand side of Fig. 7.2, the dashed lines correspond to configurations entering the vetoed shower with no additional emission. These are (before the vetoed showering) the pure $e^+e^- \rightarrow q\bar{q}$ events (blue dashed), which are compensated by the clustered events with one additional emission (red dashed)

that are multiplied with minus one. The sample with one gluon emission above the merging scale and then vetoed further emissions populates the intermediate region of this observable. The one additional jet $q\bar{q}^V(1)$ (blue dotted) contribution is compensated by the clustered $q\bar{q}^C(2)$ contributions, originating from clustered four parton configurations. The hard tail is filled with emissions described by the reweighted matrix element with two additional emissions (blue solid). Summing the compensating distributions of the left panel of Fig. 7.2, leads to the distributions in the right panel. The ratio plot shows the smooth transition between the different samples. Since the dipole p_T , which is used in the showering as the evolution parameter, does not directly correspond to the Durham resolution parameter no hard cuts in the samples are expected in the distribution of y_{34} .

The unitarization of the merged cross sections is shown in the right panel of Fig. 7.3 where the pseudo-observable of the cross section with inclusive N -partons is shown, which is defined as the sum of the exclusive parton cross sections up to N -partons. The merging does not change the inclusive cross section but can lead to variations in small multiplicities.

Even though the inclusive cross section does not change, the shapes of exclusive observables can change. This can be seen from the left picture of Fig. 7.3, where the transitions for two to three, up to six to seven jets are plotted normalized to their individual integral. The ratio shows the distributions, which get corrections from the merged contribution with up to three additional partons so $e^+e^- \rightarrow 5$ partons, with respect to $d\sigma/dy_{45}$ of the pure shower $q(0)$. No large discontinuities in the differential distributions are observed.

NLO-merging

The addition of NLO merged samples to the LO merging produces stronger shape distortions than the LO merging, since the shower approximates only the logarithmic contributions of the corrections. Finite contributions or higher order logarithms can lead to discontinuities at the merging scale. Due to the unitarization of the NLO cross section this will also affect the contributions below the merging scale.

In Fig. 7.4 the NLO corrections to the seed and the process with one additional emission is plotted for merging scales $\rho = 4$ GeV and $\rho = 6$ GeV. Unitarization of the NLO corrections leads to a reduction in the y_{23} distribution at low scales due to the large K -factor of the NLO correction to the $e^+e^- \rightarrow 3$ jet cross section. For smaller merging scales this has a larger effect, since the reduction is smeared over less phase space. The description of the hard tail is unaffected by the merging scale. The variation of the merging scale can be seen as an error estimate of the method.

7.1.1. Discussion of the α_s Value and Improving the Behaviour

The merged samples were produced using a two loop running $\alpha_s^{\overline{\text{MS}}}$ in the $\overline{\text{MS}}$ -scheme, see Eq. (2.43), with an input value $\alpha_s^{\overline{\text{MS}}}(M_Z) = 0.118$. This is close to the world average 0.1185 ± 0.006 [100] and used as central value of many PDF fitting collaborations. It was done because the NLO calculations are also calculated in the $\overline{\text{MS}}$ -scheme. By changing the $\alpha_s^{\overline{\text{MS}}}(M_Z)$ value to 0.128 as input, one can see that the hard tail of the NLO merged contributions can be mimicked by pure shower emissions, see Fig. 7.4. It is not surprising that tunes for event generators using LO emissions led to larger $\alpha_s(M_Z)$ input values. Tuning to LEP data with **Herwig++** [3] led to $\alpha_s(M_Z) = 0.127$ and Pythia's Monash [101] tunes use even higher $\alpha_s(M_Z) = 0.1365$.

The reason is well known and used in the **Herwig++** default shower for predictions [3]. In [102], it is shown that in the $z \rightarrow 1$ region of the splitting functions NLO effects can be absorbed

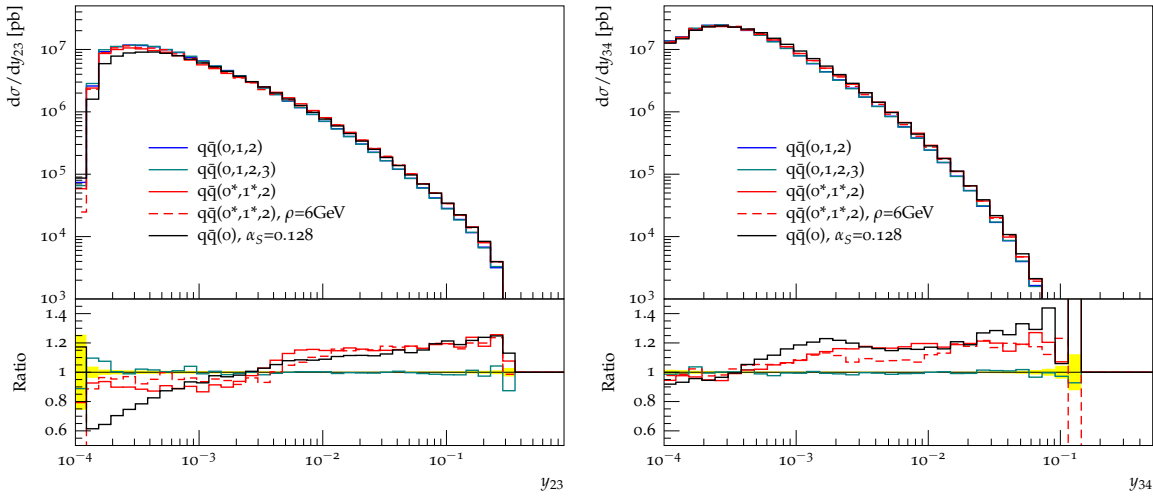


Figure 7.4.: As Fig. 7.2, the differential cross section with respect to the y_{23} (left) and y_{34} (right) resolution with a Durham jet algorithm. The ratio is normalized to the LO merged result with up to two additional matrix element emissions $q\bar{q}(0, 1, 2)$. The blue, green and red-solid lines are produced with merging scale $\rho = 4$ GeV, while the red-dashed sample was produced using $\rho = 6$ GeV. The LO merged and the NLO merged contributions result in using an $\alpha_s(M_Z) = 0.118$. The comparison can be made to the pure shower result $q\bar{q}(0)$ for an increased $\alpha_s(M_Z) = 0.128$ (black line). The NLO merged samples increase the cross section in the hard tail compared to the LO merged contributions. The pure shower with increased α_s leads to similar behaviour for these observables in the hard tail, but differs for small y_{23} or y_{34} .

for coherent showers into a redefinition of α_s^{MC} and using the two loop definition of $\alpha_s^{\overline{\text{MS}}}$. In the $z \rightarrow 1$ limit, also the regularized AP splitting functions, are dominated as [42]

$$P_{gg}(z) \rightarrow \frac{2C_A}{(1-z)_+} \left(1 + \frac{\alpha_s^{\overline{\text{MS}}}}{2\pi} K_g\right) \quad \text{and} \quad P_{qq} \rightarrow \frac{2C_A}{(1-z)_+} \left(1 + \frac{\alpha_s^{\overline{\text{MS}}}}{2\pi} K_g\right). \quad (7.2)$$

K_g is a constant term in the diagonal part of $\mathcal{O}(\alpha_s^{\overline{\text{MS}}})$ correction to the splitting function [3] of P_{gg} and P_{qq} . Redefining $\alpha_s^{\overline{\text{MS}}}$ to α_s^{MC} is called the Monte-Carlo scheme [3]. The relation between α_s^{MC} and $\alpha_s^{\overline{\text{MS}}}$ is then given by [102]

$$\alpha_s^{\text{MC}} = \alpha_s^{\overline{\text{MS}}} \left(1 + \frac{\alpha_s^{\overline{\text{MS}}}}{2\pi} K_g\right) \quad \text{with} \quad K_g = C_A \left(\frac{67}{18} - \frac{1}{6}\pi^2\right) - \frac{5}{9}N_F \overbrace{\approx 3.454}^{N_f=5}. \quad (7.3)$$

An $\alpha_s^{\overline{\text{MS}}}$ of 0.118 translates into an α_s^{MC} of 0.126 with this description, so close to the tuning values. It is emphasized in [102] that the change of α_s and therefore the measurement of $\Lambda_{QCD}^{\overline{\text{MS}}}$ is restricted to phase space regions where $z \rightarrow 1$.

In the MINLO approach [77] analytic Sudakov form factors are used to weight events in order to merge NLO cross sections. The improved NLL Sudakov form factor, given in Appendix A. of [77] and plotted in Fig. 4.1, exactly contains the expression given in Eq. (7.3) as a prefactor

of the leading logarithmic contribution. This naturally leads to a stronger suppression as can be seen in Fig. 4.1.

Also in the expansion of the UNLOPS method to UN²LOPS [35] the effects of K_g have been included to the matching with NNLO matrix element corrections.

This motivates to change the $\alpha_s^{\overline{\text{MS}}}$ expression in the shower to be evaluated with the expression given in Eq. (7.3) with scale dependent $\alpha_s^{\overline{\text{MS}}}(pt)$. This absorbs NLO effects of the $z \rightarrow 1$ phase space region. For the merging algorithm it is crucial to understand this change as an $\mathcal{O}(\alpha_s)$ effect. Changing the input value of the $\alpha_s^{\overline{\text{MS}}}$ which is used to calculate cross sections, would change the cross section itself, but changing the expression in the splitting kernels of the shower has advantages.

The advantages become clear already when we rethink the matching of NLO corrections to parton showers. Here the expression of the shower is expanded up to $\mathcal{O}(\alpha_s)$. Since the modification with K_g in Eq. (7.3) is in this sense an $\mathcal{O}(\alpha_s^2)$ contribution, the subtraction for the real emission contribution is calculated with $\alpha_s^{\overline{\text{MS}}}$, see Eq. (3.15). Also the corresponding counterpart in Eq. (3.14) is then calculated with $\alpha_s^{\overline{\text{MS}}}$. The inclusive cross section is exactly the $\overline{\text{MS}}$ cross section, but the shape of the Sudakov peak corresponds to the improved that resums the K_g contribution like in analytic resummation and absorbs the diagonal parts of the $\mathcal{O}(\alpha_s^{\overline{\text{MS}}})$ correction to the splitting function into the AP splitting functions.

If we want to implement the change of the $\overline{\text{MS}}$ -scheme to the MC-scheme into the merging of multiple NLO cross sections we can use the same technique of expanding the shower expressions. The expansion of the shower expressions with respect to $\alpha_s^{\overline{\text{MS}}}$ does not change the expansion of the PDF in Eq. (5.33) nor the expansion of the Sudakov expansion in Eqs. (5.35) and (5.36), but both are calculated with the fixed $\alpha_s^{\overline{\text{MS}}}$ instead of α_s^{MC} . Calculating the Sudakov expansions and the PDF-ratio expansion with α_s^{MC} would induce formally higher orders. The leading expansion of the shower expressions can be seen as an approximation to the virtual corrections. Calculating the NLO corrections with $\alpha_s^{\overline{\text{MS}}}$ and the expansions of the shower related expression with α_s^{MC} would lead to a mismatch. The α_s ratios in the leading order merging are reweighted to be the same α_s^{MC} as it is used in the shower. To be explicit, in the merging Eq. (4.12) is replaced by

$$\Delta_i^0 = \frac{f_i(q_i^{ls})}{f_i(q_0)} \prod_{j=0}^{i-1} \frac{\alpha_s^{\text{MC}}(q_{j+1})}{\alpha_s^{\overline{\text{MS}}}(q_0)} \frac{f_j(q_j)}{f_j(q_{j+1})} \Delta_{q_{j+1}}^{q_j} \quad (7.4)$$

and with this the expansion of Eq. (5.34) becomes

$$\frac{\alpha_s^{\text{MC}}(q_j)}{\alpha_s^{\overline{\text{MS}}}(q_0)} = 1 - \frac{\alpha_s^{\overline{\text{MS}}}}{2\pi} \beta_0 \log \left(\frac{q_j^2}{q_0^2} \right) + \frac{\alpha_s^{\overline{\text{MS}}}}{2\pi} K_g + \mathcal{O}(\alpha_s^{\overline{\text{MS}}}{}^2), \quad (7.5)$$

from the leading $\overline{\text{MS}}$ -running and the expansion of Eq. (7.3). The $\alpha_s^{\overline{\text{MS}}}$ expansions are again subtracted from the NLO corrections, which compensates for the enhanced α_s^{MC} in the LO description. The same modifications are presented in the modified UN²LOPS prescription [35].

All matrix elements are calculated with the $\alpha_s^{\overline{\text{MS}}}$ expression and the cross section is still ($\overline{\text{MS}}$ -) NLO correct above the merging scale.

In fact only the flavour diagonal P_{qq} and P_{gg} behave in the soft $z \rightarrow 1$ region like Eq. (7.3). Nevertheless these splittings produce the double logarithms due to soft and collinear gluon emissions. In the merging the order α_s expansion of the shower is subtracted to be NLO accurate above the merging scale.

So for N additional emissions, we subtract

$$\frac{\alpha_s^{\overline{\text{MS}}}}{2\pi} N \cdot K_g \cdot B_N \quad (7.6)$$

from the NLO contributions. In CS subtraction [41] the same factor is defined in the I operator coming from the phase space restrictions of the dipole splitting [3]. So for pure gluon emissions from the seed process the subtraction cancels against the corresponding term in the I Operator. For processes with more $q\bar{q}$ -pairs this does not hold. Since these processes are suppressed due to colour factors and 'only' single logarithms in the $g \rightarrow q\bar{q}$ splitting, the change made in Eq. (7.3) for parton showers covers the leading behaviour of this part of the I operator.

The question is, if this can be applied also to hadron collisions. A priori this is not obvious, since the $\alpha_s^{\overline{\text{MS}}}$ value used to fit the PDFs to data now differs from the one used in the shower process. This appears inconsistent when we think of the initial state shower as a DGLAP evolution of the PDF, see Sec. 3.4. The scale evolution performed by the PDF evaluation programs can correct the evolution with higher order splitting functions, which also behave like Eq. (7.2), without changing the accuracy of the PDF measurement. The one loop splitting functions, where the factor K_g appears, effectively enlarge the α_s value for large z values. With this argument it is consistent to choose a larger α_s^{MC} value in the showering process, also for initial state emissions. In LO calculations it is still an $\mathcal{O}(\alpha_s)$ effect and since it is not changing the cross section the NLO accuracy is also not affected.

In the UN²LOPS the K_g factor is included into as a prefactor of the scale choice of $\alpha_s(q) \rightarrow \alpha_s(bq)$ with $b = \exp(-K_g/\beta_0) \approx 0.4$. Reviewing the choices for initial state radiation and final state radiation in [69] this explains the good agreement of LEP data with an α_s value of 0.125 and of Tevatron data with an α_s value of 0.118 together with the scale choice of initial state radiations of $p_T/2$, see Sec. 3.3.

We consistently include the enhanced α_s^{MC} into the NLO merging process, which resums leading effects of soft gluon emissions. Thereby the inclusive NLO cross section, as well as the merged NLO accuracy above the merging scale are preserved by subtracting the expanded expressions. The effects are compared to data in the next section.

7.2. Comparison to LEP Data

In the following the comparison to LEP data is shown and discussed. In Fig. 7.5 the differential 2- and 3-jet rate as it was measured by the OPAL collaboration [99] is plotted against results governed by the merging algorithm. The red lines are the results obtained by pure showering. The improvement from changing the α_s value used in the showering process from the $\alpha_s^{\overline{\text{MS}}}$ to the K_g -improved α_s^{MC} are clearly visible and expected. The tails of the distributions, where well separated jets have been measured require the enhanced α_s value.

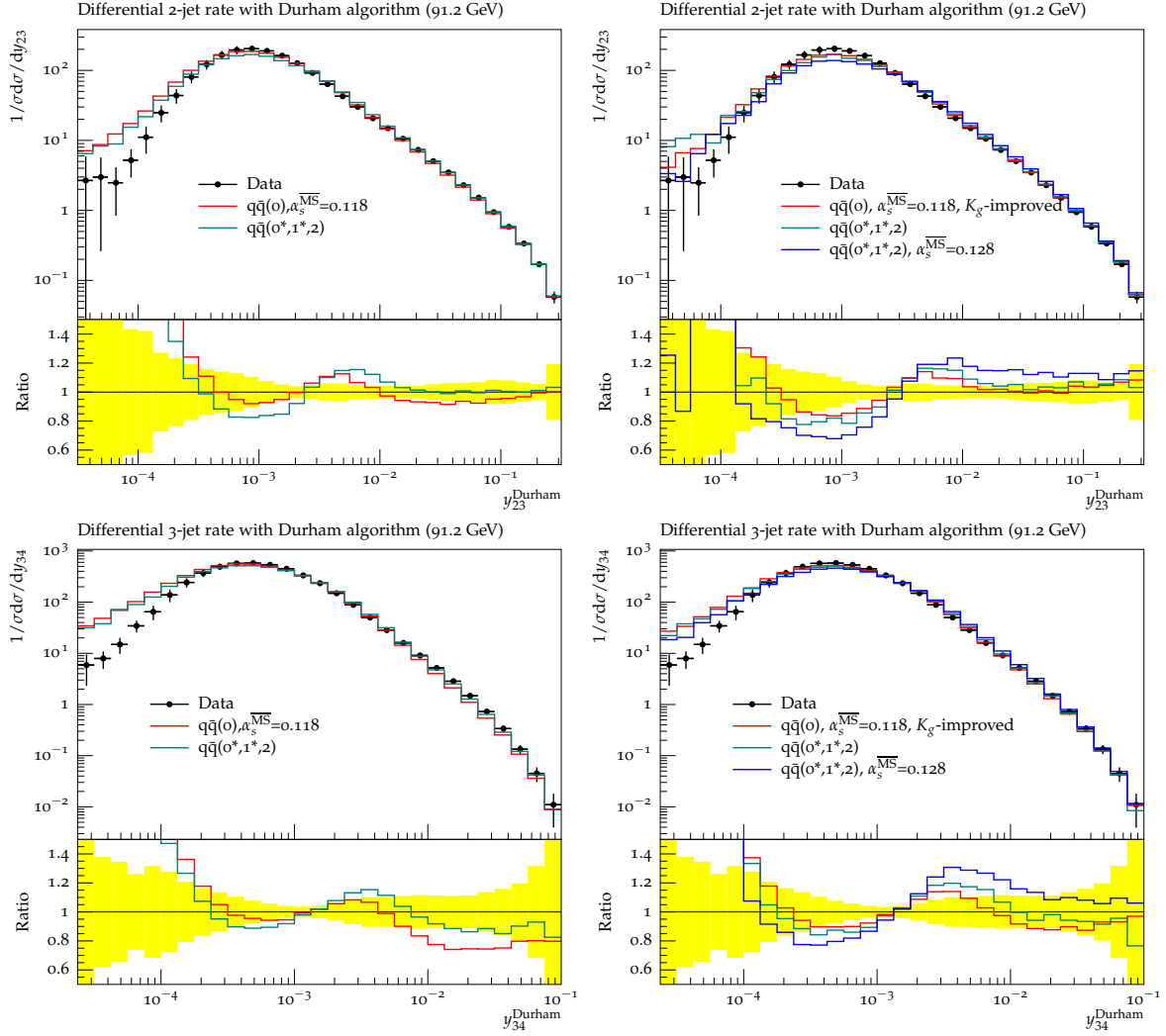


Figure 7.5.: Comparison to OPAL data [99]. Left: The shower process and merging is performed with $\alpha_s^{\overline{\text{MS}}}(M_Z) = 0.118$. The pure shower emissions produce to less hard emissions. The NLO merged sample compensates for this. Right: The factor K_g of Eq. (7.3) was included in the shower process and consistently treated in the merging of $q\bar{q}(0)$ and $q\bar{q}(0^*, 1^*, 2)$ (teal line). Changing only the input value of $\alpha_s^{\overline{\text{MS}}}$ to α_s^{MC} (blue line), without subtracting the additional expressions, produces to hard QCD emissions for the NLO merging.

The NLO merged sample $q\bar{q}(0^*, 1^*, 2)$ – green line – where the seed process and the first emission process was corrected with NLO contributions, improve the description of the well separated jets. The corrections obtained in the $\overline{\text{MS}}$ -scheme are large if the showering process is not improved with the α_s^{MC} corrections. Due to unitarization of the NLO corrections, the region below the merging scale is decreased in order to preserve the inclusive cross section.

As a result of the consistent treatment of the K_g factor by changing from the $\alpha_s^{\overline{\text{MS}}}$ to α_s^{MC} in the splitting Kernels as discussed in the previous section, the correction due to the NLO merging are reduced. This is because leading K_g corrections are already absorbed into the LO expressions. As a result the corrections in the tail are moderate and as a consequence the unitarization changes below the merging scale are also decent. A naive change of the input

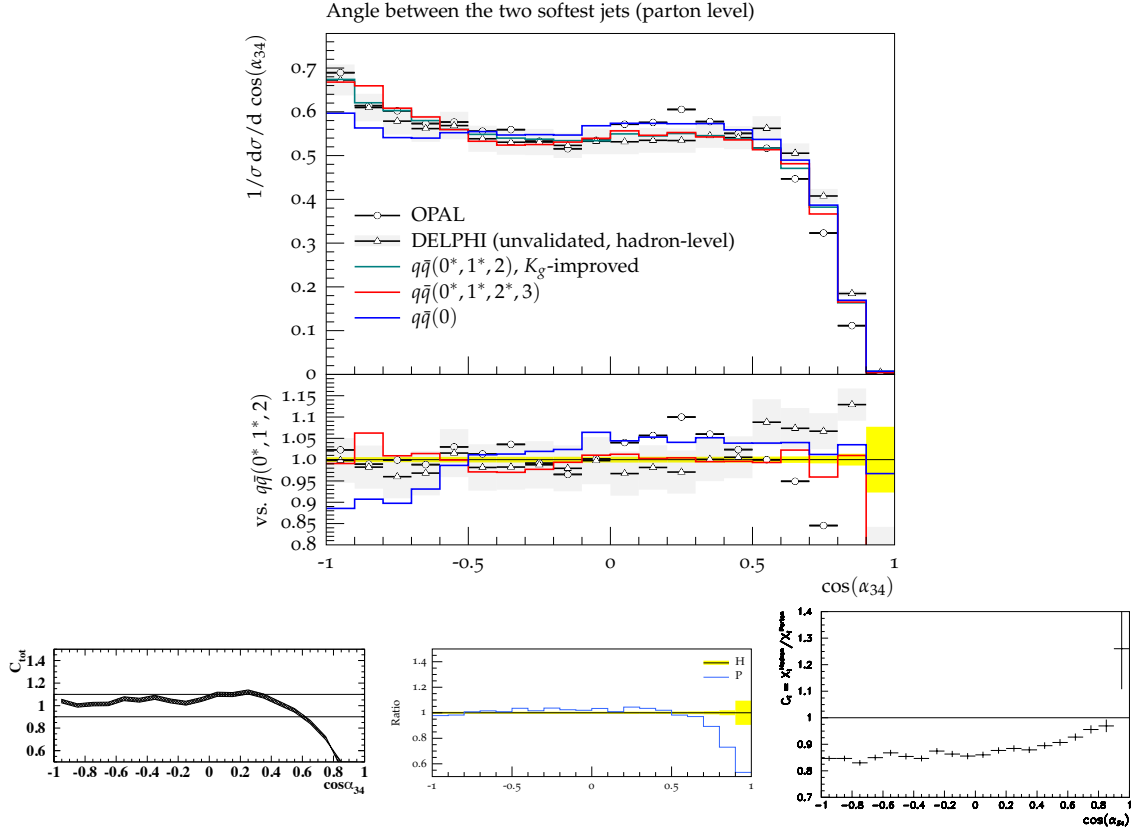


Figure 7.6.: Top: Comparison to data taken by the OPAL [103] and DELPHI [104] collaborations at LEP. The simulation was produced at parton level with NLO merging of up two additional emissions and a merging scale of $\rho = 4$ GeV. The observable is the cosine of the angle between the two softest jets in four jet events with a resolution of the Durham jet algorithm of $y_{Dur} = 0.008$. The ratio plot is with respect to the $q\bar{q}(0^*, 1^*, 2)$ result. The OPAL data is corrected to parton level with the distribution on the lower left. The DELPHI data is corrected to hadron level for detector effects. The lower right distribution is the correction factor in [104] that was applied to the simulation but not to the data. The lower middle panel is the ratio of parton level over hadron level for $q\bar{q}(0, 1, 2)$. All simulations are done with K_g inclusion as described in Sec. 7.1.1.

$\alpha_s^{\overline{\text{MS}}}$ would produce too much QCD radiation as can be seen by comparing with the blue line of Fig. 7.5.

In Fig. D.2 more simulation results are shown as ratio plots, where an overall improvement of the NLO merged sample in the comparison to [103] is seen.

The data comparison in Fig. 7.6 was produced without hadronization since the data measured by the OPAL collaboration [103] has been corrected for experimental and hadronization effects. In the publication the differential total correction factors C^{tot} , which was applied to the angular distributions of four jet configurations are given. The correction plot for the angle of the two softest jets with a resolution of $y_{cut} = 0.008$ is copied from the publication and added as the lower left panel in Fig. 7.6. The statistical error from the data measured at LEP is negligible [103] and set to zero in the validated Rivet [105] analysis.

Another (in Rivet labelled as unvalidated) analysis is provided in the Rivet framework from the data collected from the DELPHI collaboration. It contains the results of the diploma thesis of H. Hoeth [104]. The jet resolution in this analysis is also given by $y_{cut} = 0.008$. Other than a small additional cut on the energy of the jets after applying the Durham jet algorithm of 3 GeV no difference in the source of the Rivet analyses was found. In [104] the correction factor for hadronization effects was applied to the parton shower results, other than on the data itself. The correction they use to include hadronization effects are given in the lower left plot of Fig. 7.6. The DELPHI data is not corrected to parton level, but to hadron level for experimental effects.

The ratio between hadron- and parton-level simulation for the sample $q\bar{q}(0, 1, 2)$ with the dipole shower merging and the cluster hadronization model of Herwig++, see [3] and the references therein, is plotted in the lower middle panel of Fig. 7.6.

While the OPAL correction factor (including experimental effects) starts to rapidly decrease at $\cos \alpha_{34} \sim 0.3$, the corrections from the cluster model are roughly half the size of the C^{tot} from OPAL and start decreasing moderately at $\cos \alpha_{34} \sim 0.4$. The (inverse to the other two) corrections in [104], that are not applied to the data distribution, are mildly increased from $\cos \alpha_{34} = -1$ to ~ 0.4 , and then increase stronger up to $\cos \alpha_{34} = 1$.

We compare the data on parton level with NLO corrections up to the second additional emission $q\bar{q}(0^*, 1^*, 2^*, 3)$. So including NLO corrections to the $e^+e^- \rightarrow 4$ partons. Here we used the `OpenLoops` [87] library for the virtual matrix elements and the `MadGraph` [10] tree-level matrix elements interfaced with the `ColorFull` package [90], as described in Sec. 6.5. For all simulation distributions in Fig. 7.6 the α_s^{MC} was used according to Sec. 7.1.1. The merging scale is $\rho = 4$ GeV and the ratio is with respect to the $q\bar{q}(0^*, 1^*, 2)$ distribution.

The blue sample $q\bar{q}(0)$, containing pure parton shower emissions form the LO seed contribution with two partons, fails to describe the region of jets with large angles. Especially the back-to-back configurations for the softest jets at $\cos \alpha_{34} = -1$ are poorly described. The parton shower underestimates these regions.

Inclusion of matrix elements, suited to describe the large angle emissions more properly, and inclusion of the higher order loop contributions shows a better description of the back-to-back configurations. Already the $q\bar{q}(0^*, 1^*, 2)$ containing tree level corrections to the four parton state agrees well in the $\cos \alpha_{34} \approx -1$ region. The $q\bar{q}(0^*, 1^*, 2^*, 3)$ shows in general the same behaviour as $q\bar{q}(0^*, 1^*, 2)$. The bin at $\cos \alpha_{34} = -0.9$ shows a statistical fluctuation.

The agreement to both data sets is, up to the region with large hadronization effects, within 10 %. However the OPAL distribution shows a significant shape difference in the region of $\cos \alpha_{34} \approx 0.3 \pm 0.1$ to the simulated contribution, where the correction factor shows a peak. Even though the statistical error on the data is negligible the difference between the merged samples and the DELPHI data on parton level is not too alarming.

To conclude:

Parton showers are, with a good tuning and inclusion of known higher order effects, in good agreement with large parts of the LEP data. The inclusion of LO and NLO merging provides a better description in the region of well separated emissions. Without the unitarization description of the NLO merging and understanding the change to the MC-scheme as an $\mathcal{O}(\alpha_s)$ effect, the subtraction of the K_g expressions is unmotivated and leads to bad description of the data. We want to emphasize that the K_g expressions are finite corrections to the NLO

corrections of the process with an additional emission, which is of $\mathcal{O}(\alpha_s^2 L^2)$ and therefore a NNLL effect.

7.3. LHC Results

In this section, results of the merging of LO and NLO matrix elements are discussed and compared to LHC data. First as the standard candles of the LHC, Z- and W-boson production is discussed and compared to data. The discovered Higgs boson challenges Monte Carlo and resummation due to the large perturbative corrections. The results for Higgs production with NLO merging are presented.

7.3.1. Z Boson Production at LHC

Changing the regime from pure QCD final state emissions at e^+e^- collisions to the more challenging environment of hadron collisions requires the interplay of more and more components. Especially the interplay with the measured PDFs, but also the fact that the phase space of additional emissions is not restricted by the initial interaction leads to a more complicated description.

The results shown in this section have been produced with a collider energy of 7 TeV and a NLO NNPDF [106] set[‡] with an $\alpha_s^{\overline{\text{MS}}}(M_Z) = 0.118$. The PDF set is restricted to be positive definite. The invariant Lepton-Pair mass was restricted by $66 \text{ GeV} < m_{e^+e^-} < 116 \text{ GeV}$. The renormalization and factorization scale $\mu_{R/F}$ is the invariant lepton pair mass, which have been varied by a factor two, in order to estimate scale uncertainties. The shower starting scale is the central scale $m_{e^+e^-}$, also for the simulation with varied $\mu_{R/F}$. The matrix elements interfaces to `MadGraph` [10] and `OpenLoops` [87] have been used for tree level and one loop corrections respectively. We show results with $\alpha_s^{\overline{\text{MS}}} = 0.118$ in all expressions and how the distributions change if we use α_s^{MC} instead of $\alpha_s^{\overline{\text{MS}}}$. All scale variations have been produced for the $\alpha_s^{\overline{\text{MS}}} = 0.118$ choice. The scale variation of the changed MC-scheme are expected to be of the same order of magnitude.

7.3.1.1. Transverse Momentum of the Z boson at LO

The distributions in Fig. 7.7 all show the transverse momentum of the lepton pair, which we call, due to the restriction on the invariant mass, the Z boson in this section. Except for the data comparison, the ratio plots of the differential cross sections are all normalized to the LO contribution with a strongly enhanced shower starting scale $Q_H = 5m_{e^+e^-}$. The upper left panel shows, beside the LO with pure parton shower emissions with and without enhanced shower starting scale, the distribution of the sample $Z(0,1)$ with one additional emission merged. In addition the LO distribution for $Z+\text{jet}$ production is plotted. The scale choice of the LO distribution is the transverse momentum of the Z boson, which is close to the scales used in the showering process.

The fact that the parton shower tends to undershoot the real matrix elements is known [69, 109]. Since the parton shower does not include final state emissions it is not expected that the parton shower can reproduce the matrix element correctly. The merged sample follows the contribution of the fixed order above the merging scale. The changes to the inclusive cross sections due to the mismatch are subtracted in this approach below the merging scale,

[‡]The LHAPDF [107] name of the set is NNPDF30_nlo_as_0118_mc.

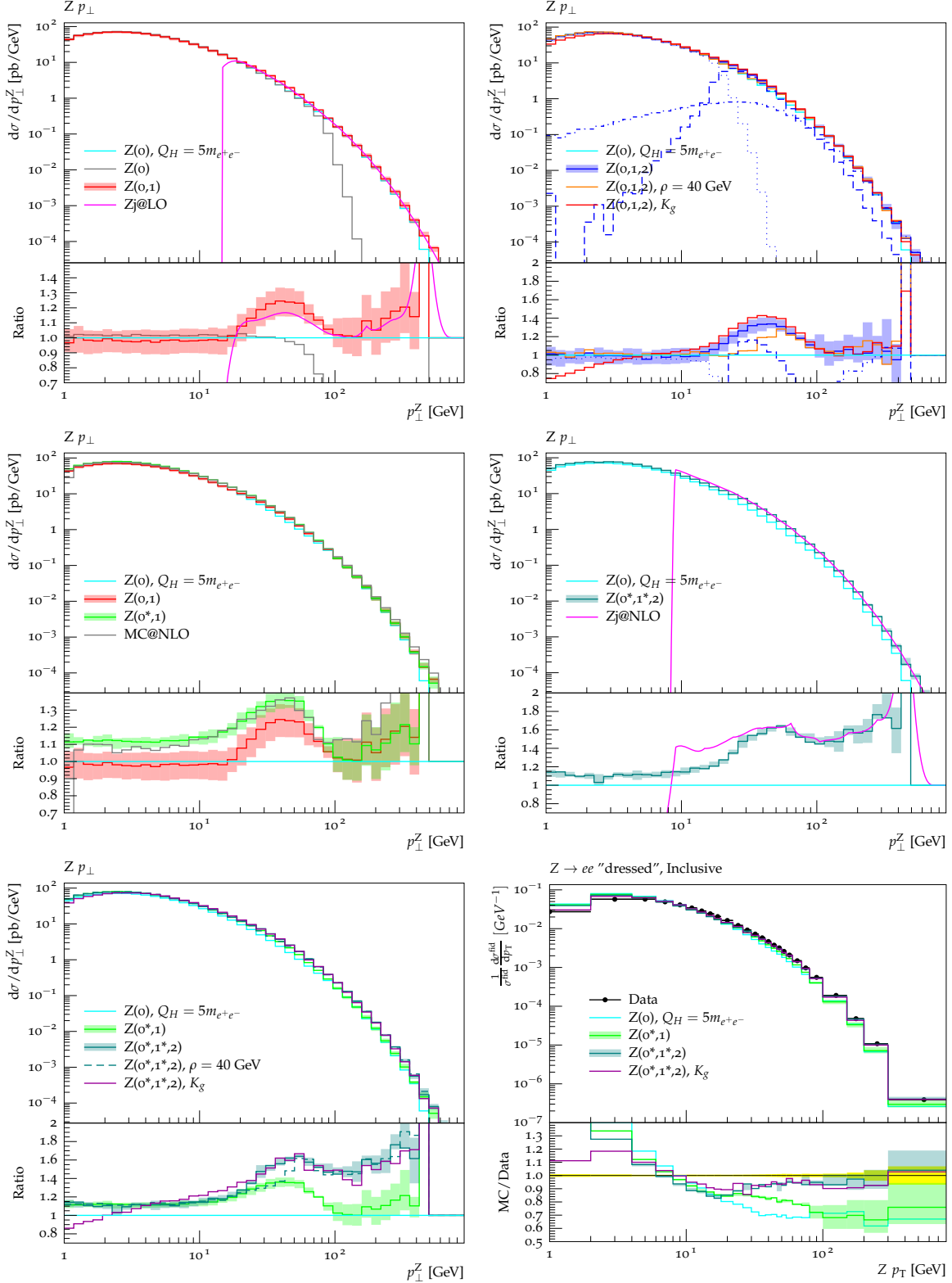


Figure 7.7.: The observable in this figure is the transverse momentum of the Z boson in proton-proton collisions at a collider energy of 7 TeV. The ratios are with respect to the LO shower with enhanced starting scale. Lower right panel shows the comparison to ATLAS data [108]. The individual panels are explained in Sec. 7.3.1.1 and Sec. 7.3.1.2.

which results in a reduction in this region. Above the hard scale the shower with enhanced starting scale and the merged samples approach for this observable which is the same effect seen in [109]. The restriction of the phase space leads to a drop of the shower emissions without enhanced starting scale.

The upper right panel in Fig. 7.7 shows the the $Z(0, 1, 2)$ contribution in blue. The individual merging samples $Z(0, -, -)$, $Z(-, 1, -)$ and $Z(-, -, -2)$ are separated as dotted, dashed-dotted and dashed lines respectively, without label. The $Z(0, 1, 2)$ sample shows the same behaviour as the $Z(0, 1)$ for this observable. Including the LO merging to the second emission in $Z(0, 1, 2)$, additional contributions arise that can lead to small or vanishing transverse momenta of the Z boson, so that the sample $Z(-, -, 2)$ contributes also to the small p_T^Z region. These contributions, where the two additional partons are balancing their transverse momenta are necessary to describe LHC data. The same effect happens in W boson production, where these contribution are discussed, see Sec. 7.3.2.2.

Additional to the splitted $Z(0, 1, 2)$ distribution, also the merged sample with an enhanced merging scale to 40 GeV is plotted. Here the enhancement effect due to the matrix element corrections above the merging scale enter the distribution for higher values of the transverse momentum of the Z boson.

Changing from $\alpha_s^{\overline{\text{MS}}}$ to α_s^{MC} , labelled with K_g leads to a shift of the Sudakov peak to higher values. With this also the shape change at the merging scale $\rho = 20$ GeV is decreased.

7.3.1.2. Transverse momentum of the Z boson at NLO

The distribution with included NLO corrections to the seed process $Z(0^*, 1)$ are shown in the middle right panel in Fig. 7.7. The inclusion is described in Sec. 5.1. Corrections below the merging scale, due to subtracted real emission contributions with parton shower approximations, lead to a reduction of the large rise at the merging scale. The transition is smoother compared to the LO sample with enhanced starting scale. The $Z(0^*, 1)$ is very close to the MC@NLO result produced with the **Matchbox**. Below the hard scale of the shower, the NLO corrections lead to an enhancement of the distribution and to a scale reduction for the $Z(0^*, 1)$ sample. Above the hard scale of the shower the merged sample and MC@NLO differ because of the different scale choice. MC@NLO continues to choose the hard scale of the Born process, here $m_{e^+e^-}$. The merged sample chooses the scale according to Eq. (4.31), which is larger than the scale used in MC@NLO.

The scale variation above the hard scale $Q_H = m_{e^+e^-}$, is not reduced due to the NLO corrections to the seed process. Above the hard scale of the shower the same contributions describe the LO merged $Z(0, 1)$ and the matched/merged $Z(0^*, 1)$ since they were added as finite contributions to the LO merging, see Sec. 4.6.

NLO corrections above the merging scale are included in the $Z(0^*, 1^*, 2)$ sample in the middle right panel of Fig. 7.7. They show a good agreement compared to the fixed order NLO calculation as it was seen in the case of LO merging compared to the fixed order LO calculation.

It is not obvious why the distribution of $Z(0^*, 1)$ and $Z(0^*, 1^*, 2)$ in the lower left panel of Fig. 7.7, are so close below the merging scale. The clustered (to the seed process kinematics) contributions of $Z(0^*, 1)$ and the contributions calculated with seed process kinematics are allowed to emit in the full shower phase space of the seed process. The same contributions also appear in the $Z(0^*, 1^*, 2)$ sample and are vetoed above the merging scale. On the other hand

the NLO corrections to the one jet contributions are also clustered to the zero jet configurations by the unitarization description, see Sec. 5.2. This reduces the NLO contributions below the merging scale, since the K -factor above the merging scale is larger than one.

In addition to the distribution for an enhanced merging scale of $\rho = 40$ GeV, also the distribution with replaced α_s is shown. As in the LO merging the enhancement of the merging scale leads to an delay of the corrections obtained by the matrix element corrections to higher values of the transverse momentum. The replacement of $\alpha_s^{\overline{\text{MS}}}$ to α_s^{MC} leads to a smoother continuation below and above the merging scale, as it is in the LO merged samples. Like the LEP results and as it is constructed, the consistent inclusion of α_s^{MC} mildly changes the $Z(0^*, 1^*, 2)$ where the NLO correction to the first emission is included.

In the lower right panel of Fig. 7.7 the distributions are now compared to the data taken by the ATLAS [108] collaboration at the LHC. The description of the hard tail of the differential cross section is strongly improved by the inclusion of the NLO contributions. The region of small transverse momentum of the Z boson is improved by treatment of α_s^{MC} . Note that we did not retune the parameters of the intrinsic k_T , see [3], and use the same PDF set in all parts of the calculation. The description is improved compared the inclusion of the first NLO correction in $Z(0^*, 1)$, which corresponds to a MC@NLO description, see middle left plot in Fig. 7.7.

7.3.2. W Boson Production at LHC

The production of W^\pm bosons is the largest cross section including heavy bosons measured at the LHC. The production process is very similar to the Z boson production. Beside the hadronic decay ($\sim 66\%$), W^\pm decay into lepton-neutrino pairs ($\sim 11\%$ per generation) [47]. The merging is compared to measurements of the W^\pm boson decaying into a $\mu^\pm\nu_\mu$ pairs. Since we are more interested in the QCD radiation part of the process the CKM matrix [110, 111] is set to $\mathbb{1}$ in the generation of the event samples. Same parameters and matrix element providers as in the Z boson production were used. The distributions of the transverse momentum show a similar picture as for the Z boson, and is not discussed here.

7.3.2.1. k_\perp Splitting Scales and the Effects of Multiple Parton Interactions

The k_\perp splitting scales measured by the ATLAS collaboration [112] are shown in Fig. 7.8. The observables are similar to the jet rates shown for LEP results, see Sec. 7.2 with the expansion of the k_T -jet finding algorithm to hadron colliders [63, 114]. Also distance to the beam must be taken into account in the jet clustering process. See Sec. 1.1. of [112] for a detailed outline of the clustering algorithm. In Fig. 7.8 we observe that the merged sample $W(0^*, 1^*, 2)$ is able to describe the hard region of the first splitting scale $\sqrt{d_0}$ within the experimental uncertainty. In the tail drops to fast compared to data.

Changing the α_s to α_s^{MC} also above the hard scale of the shower and using LO PDFs for the showering process as it is done in [112] may help to describe tail of the second emission $\sqrt{d_2}$, but is part of further investigations. The peak at 40-50 GeV in the $\sqrt{d_2}$ distribution is also visible in [112] compared to the theoretical predictions.

While the hard tail of the contributions is described by the merged samples, the intermediate region (scales between 5 GeV and 30 GeV) needs secondary hard scatterings, described by the multiple parton interaction model (MPI)[3]. The MPI model produces extra emissions from secondary vertices that contribute to the soft activity in the event simulation. After

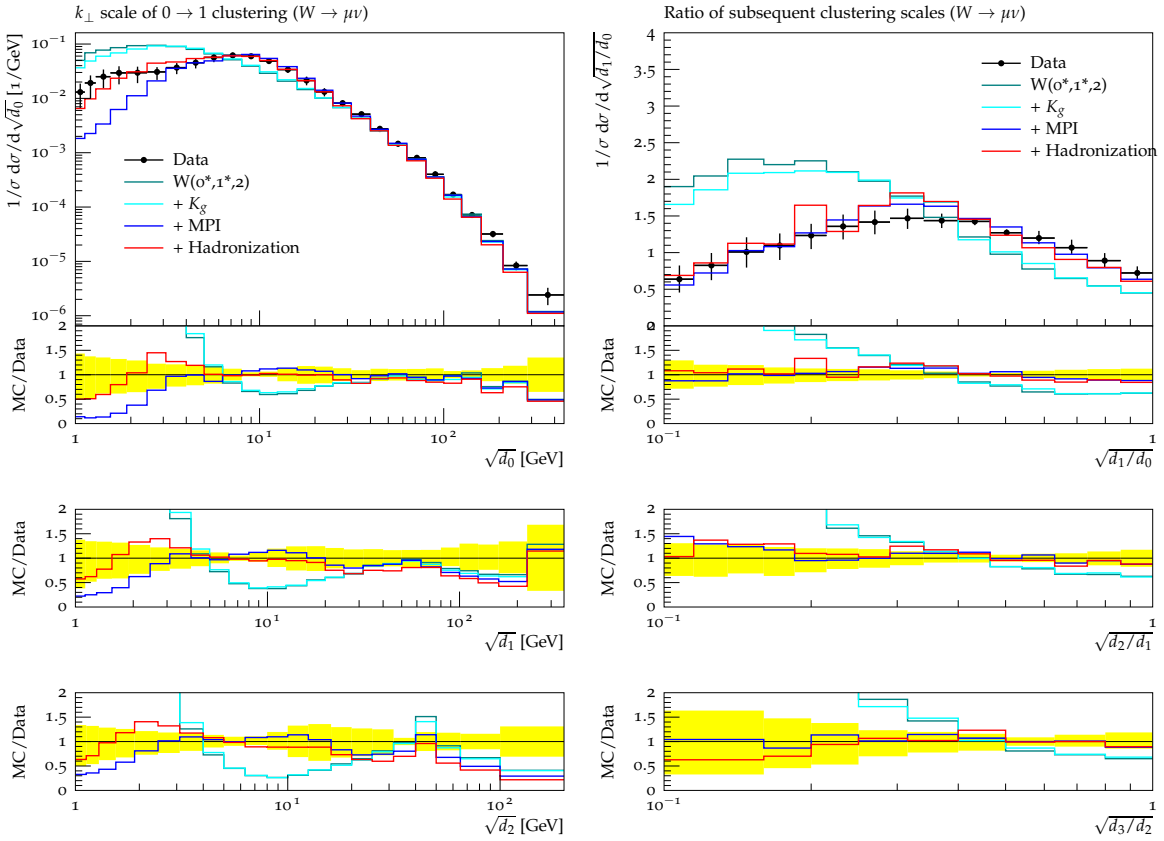


Figure 7.8.: Effects of multiple interactions and the hadronization model in the interplay with the merged samples compared to ATLAS data [112] in sensitive to hadronic activity k_T splittings in W^\pm production. Beside the multiple interaction (MPI) also the hadronization model is needed to describe these observables. In the ratio of different splitting scales the hadronization effects are suppressed.

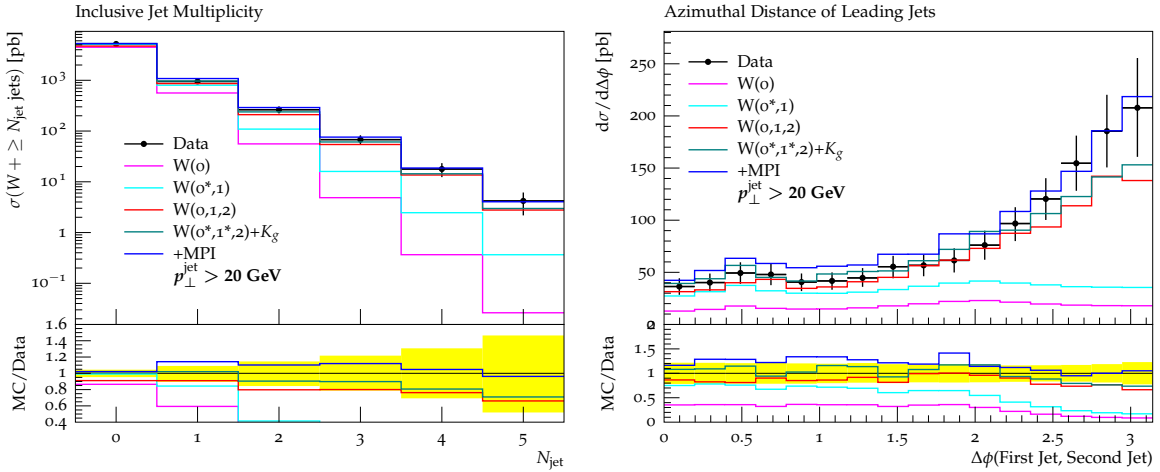


Figure 7.9.: Jet multiplicities and the angle between the two hardest jets, measured by ATLAS [113]. The pure shower and MC@NLO like merging $W(0^*, 1)$ fails to describe data. The contributions from back-to-back scattering jets are important to induce initial dijet like configurations. These open the phase space for more jets and higher multiplicities. $W(0, 1, 2)$ and $W(0^*, 1^*, 2)$ perform equally well besides the normalization, which is improved due to the NLO corrections.

applying the MPI model there are fewer events with very soft hadronic activity, which is then compensated by the modelling of hadronization. Only the interplay of the hard perturbative parts, additional secondary soft emissions and modelling formation of measurable hadronic final states is able to describe the full range of scales from 1 GeV to several 100 GeV.

Ratios of different k_\perp splitting scales shown on the right hand side of Fig. 7.8 suppress hadronization effects but still need the MPI modelling. Although the MPI model is tuned for the default Herwig++ shower, the ratios show differences within two σ .

7.3.2.2. Jet Multiplicities and Back-to-Back Configurations

In Fig. 7.9 the cross sections for inclusive jet multiplicities are plotted against ATLAS data [113]. Pure shower emissions $W(0)$ are not capable to describe the higher jet multiplicities. Also the LO inclusive cross section in the first bin needs the NLO correction included in $W(0^*, 1)$ to get close to the measured cross section. In the $W(0^*, 1)$ distribution the inclusive cross section is corrected to NLO and the first jet is described by LO corrections. These are able, due to unordered histories, to fill the phase space above the shower starting scale. Still the included correction to the first emission fails to describe higher multiplicities.

When the first emission is performed by the showering process in a Drell-Yan process (this also holds for multiple boson production), momentum conservation requires that the electro weak system compensates for the transverse momentum of the emission. A balancing second emission is not strongly ordered and unlikely. These back-to-back configurations have large angles between the two jets. The right plot in Fig. 7.9 illustrates this region of the recoiling dijet system. The LO+PS and NLO+PS samples $W(0)$ and $W(0^*, 1)$ are strongly suppressed for larger angles. The samples including LO matrix element corrections for the second emission fill this region. Additional MPI activity also contributes to this back-to-back configurations but tends to overshoot the region for small angles.

Another approach how to produce these events is a combination of electroweak and QCD showering [115]. Here the dijet events radiate W-bosons leading to the same picture. In [78] giant K -factors are reported and described with the LoopSim method. Back-to-back configurations obviously lead to a large correction in specific regions of phase space and observables like the sum of transverse momenta $H_T = \sum p_T^j$ get enhanced by the to recoiling hard jets. Cutting on the angle between visible dijet systems strongly suppresses the underlying QCD induced, soft electro weak radiation.

The inclusion of the matrix elements with additional two partons is now capable to describe also high multiplicities. The inclusion of NLO corrections to the first emission $W(0^*, 1^*, 2)$ corrects the one jet inclusive cross section to NLO accuracy above the merging scale. Compared to the $W(0, 1, 2)$ sample the K-factor of the subsequent NLO corrections helps to describe data at lower multiplicities. In the four and five jet inclusive cross section the NLO corrected and LO merged samples are again close. The back-to-back configurations are not corrected with NLO matrix elements, so are describes formally with LO accuracy.

The additional emissions generated by the MPI model tend to produce too many jets compared to data. The parameters of the MPI model are tuned with LO predictions and the inclusion of higher orders already includes parts that the MPI tune tries to accommodate for missing contributions in the hard process.

7.3.3. Higgs Boson Production at LHC

With the Higgs boson the last missing piece of the SM was discovered at LHC [1, 2]. From the theoretical point of view, production of a Higgs boson is interesting since large NLO [116, 117] and NNLO [118] corrections are seen for inclusive cross sections.

The dominant production channel is via gluon fusion. Since the massless gluon does not directly couple to the colourless Higgs boson, already the LO contains loop diagrams. In the limit of a large top mass, the $gg \rightarrow h$ process can be described by a Higgs Effective Field Theory model (HEFT) with an additional ghg -vertex, e.g. [119]. The additional operator in the Lagrangian takes the form[§]

$$\mathcal{L}_h = -\frac{1}{4}g_h G_{\mu\nu}^a G^{a,\mu\nu} h \quad \text{with} \quad g_h = \frac{\alpha_s}{3\pi v}, \quad (7.7)$$

where the field strength $G_{\mu\nu}^a$ contains linear and quadratic expressions of the gluon fields, leading to Feynman rules for the ghg -coupling. The `OpenLoops` libraries were used for the one loop corrections and `MadGraph` for tree-level amplitudes in the HEFT model.

7.3.3.1. The Transverse Momentum of the Higgs Boson and the Kink

In Fig. 7.10 the results are shown for the transverse momentum of the Higgs boson at 8 TeV LHC energies. For this distribution the shower starting scale, as well as renormalization and factorization scale are varied simultaneously by factors of two around the central value $M_H = 125$ GeV. The merging scale is set to $\rho = 20$ GeV for the scale variations.

While the LO+PS sample $H(0)$ drops rapidly above the shower starting scale, the merged sample $H(0, 1)$ shows a smooth continuation to transverse momenta above the shower starting scale. The cross section with decreased scale is enhanced and simultaneously the shower phase space is smaller. This leads to an intersection of the scale variation band in the $H(0)$ case. For the merged sample the emissions above the hard shower scale are seen as unordered emissions and added as finite contributions. The scale choice for these contributions is also reduced by the scaling factors as it is now the 'new' hard scale, see Sec. 5.4. This leads to a smooth continuation of the scale uncertainty band.

NLO corrections to the cross section include the large K -factor of the Higgs production cross section. In the merged sample $H(0^*, 1)$ the NLO corrections enter as an addition below the hard scale of the shower. Since the real emission above the hard scale of the shower was already added to the LO merging as a finite, unordered contribution, the tail of $H(0^*, 1)$ above the shower starting scale coincide with the LO merged $H(0, 1)$. The finite NLO contributions which are proportional to the Born process receive the same shower phase space as the $H(0)$ contributions. This leads to a similar drop of the corrections as for $H(0)$ in the left plot in Fig. 7.10. This behaviour is expected as it is also seen in Fig. 3.3 for the MC@NLO result. The logarithmic x -axis amplifies the impression of a 'kink' at the hard scale.

In [72] the origin of the large NLO corrections where identified as the π^2 contributions originating from analytic continuations of $\log^2(-1)$ terms. Whether these contributions exponentiate in the form proposed in [72] or not, at the one loop level the corrections are large and proportional to the Born contributions. This leads to the 'kink' at the shower starting scale.

[§]In the HEFT model of `MadGraph` g_h is multiplied by $\left(1 + \frac{7}{30}\tau + \frac{2}{21}\tau^2 + \frac{26}{525}\tau^3\right)$, and $\tau = m_h^2/(4m_t^2)$ to include top mass effects. Since the results presented here are calculated with the `OpenLoops` libraries for the virtual amplitudes, the top mass is set in both programs to 10^6 GeV in order to avoid ambiguities.

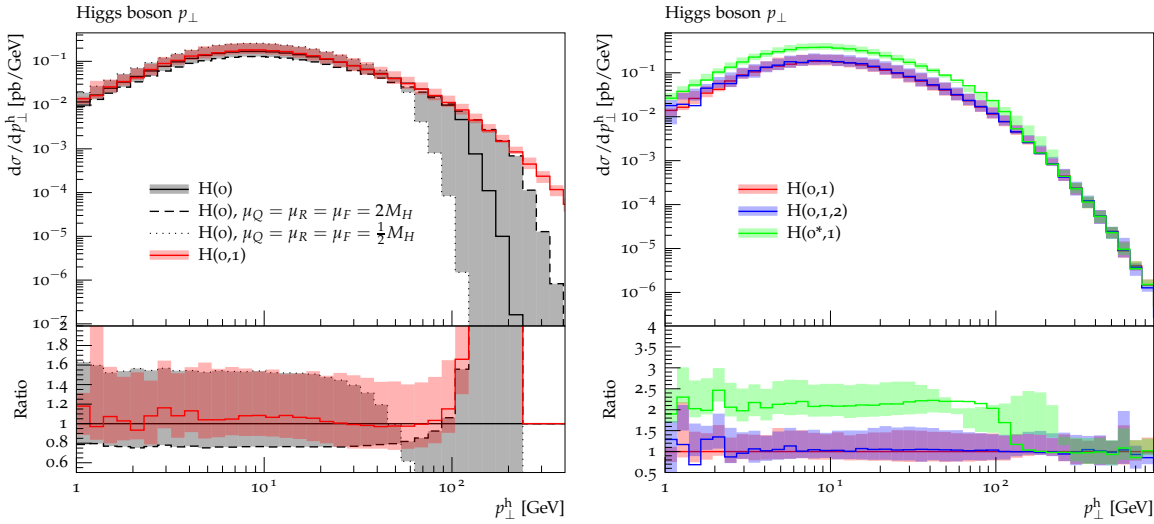


Figure 7.10.: Differential cross section as a function of the transverse momentum of a Higgs boson produced in gluon-fusion. Left: Comparison between pure shower emissions and LO merged contribution with the merging of one additional parton. The error band is showing the variation of simultaneously varying the renormalization, factorization and hard scale of the shower by factors of two. Right: In addition to the LO merged $H(0, 1(, 2))$, with one and two emissions corrected by the matrix elements, the merged cross section with an NLO corrections to the $gg \rightarrow H$ process in the effective field theory with infinite top mass is shown. Restrictions on the shower phase space in matching and merging lead to kinks at the hard scale.

In Fig. 7.11 the MC@NLO-like[¶] (red line) and the NLO merged contribution with NLO corrections to the first emission $H(0^*, 1^*, 2)$ (teal line) are added to the distributions shown in Fig. 7.10. The MC@NLO-like contribution approach the LO merged sample before the $H(0^*, 1)$. This behavior is dictated by the profile scales [70] introduced in **Matchbox** to ensure a smooth continuation between shower region and hard tail. The rise of the MC@NLO-like distribution compared to the LO merged sample is due to the scale choice above the hard scale, see discussion for the transverse momentum of the Z boson in Sec. 7.3.1.2. Here, the MC@NLO-like matching continues to use the hard scale of the process, namely the Higgs mass. The merged sample is using the scale given in Eq. (4.31), which is in this region larger than the Higgs mass.

The $H(0^*, 1^*, 2)$ contribution does not show the 'kink' at the shower starting scale, it further continues with roughly the same differential K -factor ~ 2 with respect to the LO merged contribution. Above the merging scale at 20 GeV the $H(0^*, 1^*, 2)$ receives its NLO corrections solely from the corrections to the first emission. The NLO corrections to the seed process are vetoed by the shower to emit only below the merging scale. The rather smooth continuation compared to the MC@NLO-like contribution at the merging scale $\rho = p_T^H = 20 \text{ GeV}$ ^{||} is therefore not expected from the merging procedure. The large correction to the Born process has the possibility for the $H(0^*, 1)$ sample to emit into the full shower phase space^{**}. The

[¶]The MC@NLO-like distribution is produced by **Matchbox**, which provides two kinds of matching schemes. The shown is close to the MC@NLO approach.

^{||}The transverse momentum of the Higgs and the merging scale coincide for the first emission.

^{**}This only holds for the NLO related contributions which are clustered to Born-like kinematics, see Sec. 5.1.

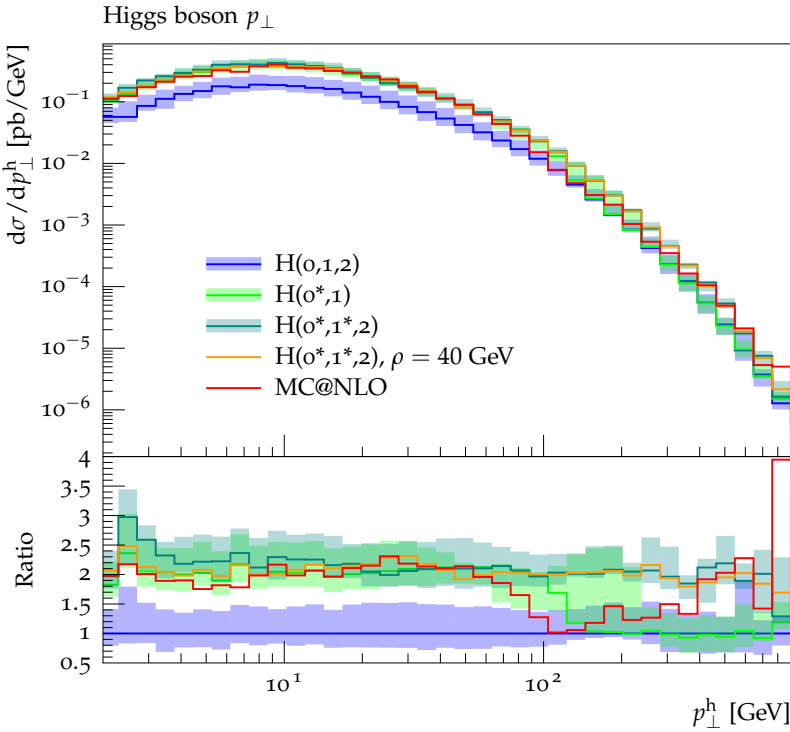


Figure 7.11.: Higgs p_{\perp}^h as in Fig. 7.10. On the left hand side the distributions for a merged cross section with NLO corrections to the first emission $H(0^*, 1^*, 2)$ and the MC@NLO(-like) matching are added to the distributions of Fig. 7.10. While the MC@NLO follows the merged sample with NLO corrections to the seed process, the distribution continues for the $H(0^*, 1^*, 2)$ sample without dropping at the transition of the shower phase space to the high p_T region. The merging scale is $\rho = 20$ GeV. The orange line shows the distribution with an enhanced merging scale $\rho = 40$ GeV.

unitarization contribution of the second NLO correction in $H(0^*, 1^*, 2)$ are also clustered to the kinematic configurations of the seed Born phase space. These suppress the corrections to the seed process. The orange distribution in Fig. 7.11 with an enhanced merging scale shows the same behaviour.

At the shower starting scale^{††} the $H(0^*, 1^*, 2)$ sample change from ordered to unordered configurations like the LO merged sample $H(0, 1)$ or $H(0, 1, 2)$. Since the scale change at the hard scale is smooth in Eq. (4.31), also the distribution has no discontinuities at the shower starting scale. Different scale choices would lead to $\mathcal{O}(\alpha_s^2)$ effects counted from the first emission $pp \rightarrow Hj$, since the $\mathcal{O}(\alpha_s)$ is compensated by the NLO correction to the $pp \rightarrow Hj$ process.

7.3.4. Jet Production at LHC

In Fig. D.1 the results are shown for the transverse momenta of the second and third hardest jets, in 7 TeV proton proton collisions. While we see a similar behaviour in the hard tail of the third jet as reported for the CKKW-L and ULOPS results [22], we also see an unphysical negative differential cross section for large transverse momenta $p_{\perp}(\text{jet}2) \approx 400$ GeV of the

^{††}Technically also below the hard scale, if the emission is not within the shower phase space given by the z-bounds of [57].

second jet. If the shower starting scale is changed to the absolute sum of all transverse momenta of the jets H_T , the distribution remains positive.

Negative configurations in the unitarized LO merging appear in the clustered configurations of the higher multiplicity. These configurations ϕ are clustered, in this approach, to the underlying Born configuration $\tilde{\phi}_i$ with the weights according to the ratio of the CS dipole P_i in the parton shower approximation divided by their Born contribution B_i , see Sec. 4.5. The weight is set to zero if the additional emission configuration ϕ is not reachable from the shower emission of the dipole i in the restricted phase space of $\tilde{\phi}_i$. The starting scale of this emission is evaluated for the underlying Born configuration $\tilde{\phi}_i$. This prefers the underlying Born configurations with large transverse momenta, if the shower starting scale is the transverse momentum of the hardest jet and other underlying configurations cannot be reached by their individual phase spaces. The clustering algorithm also prefers Born configuration with larger transverse momenta for the starting scale H_T , but the phase space is still larger for the underlying Born configurations.

In this approach the aim is to provide a process independent merging, without using information on the hard process, other than the scale choice for the shower starting scale. In processes where the scale of the seed process is given by an electroweak system, the clustering algorithm and the reweighting provides reasonable results, also compared to data. In the physical picture, where the parton shower is used to evolve the scales to lower values by resolving/producing additional collinear and soft emissions, the hard scale used in the PDF should coincide with the hardest possible emission of the shower. The restrictions derived from this on the shower phase space used in the dipole shower of `Herwig++` [57] are respected in the clustering algorithm. With the usage of the H_T definition, the distributions remain positive, but the finding that the differential cross section with respect to the transverse momentum of the second jet is negative for large values open questions, which will be part of future work.

CHAPTER 8

Summary and Outlook

In this thesis a formalism was constructed to consistently include multiple NLO corrections to parton shower simulations. Based on the basic ideas of matching fixed order corrections to resummed expressions, it contributes to the efforts of increasing the accuracy of parton shower simulations. Thereby neither the parton shower algorithm nor the NLO correction lose their precision.

Ch. 4 reviewed the methods used to merge multiple LO calculations and showed how to construct an algorithm that is able to preserve the inclusive LO cross section without introducing uncontrolled $\mathcal{O}(\alpha_s)$ corrections. In addition it was shown that dividing the phase space of overlapping shower emissions, can lead to regions for which the shower produces less emissions as it would, without including the matrix elements. These regions of phase space are not described by matrix elements. It was discussed that the unitarized expressions, which are produced in order to preserve the LO cross section, can be used to fill the regions with emissions from the unsuppressed lower multiplicity. Controlled addition of contributions not described by the shower phase space leads to α_s -corrections that are able to describe high energetic emissions.

In the first part of Ch. 5 the inclusion of NLO corrections to the production process without additional emissions were described as a complement of the MC@NLO approach. The expansion in the coupling constant led to expressions that are needed to include NLO corrections without double counting of similar contributions. Below the merging scale the approach is similar to the MC@NLO expressions. The merging scale dependence is reduced by subtracting shower expansions from the real emission corrections. The next part of Ch. 5 was used to include an additional NLO correction above the merging scale of the first additional parton emissions. The expansion of the shower history led to expressions that act as a counterpart to large logarithms expected in the NLO correction. In the third part of Ch. 5 the algorithm was extended to an arbitrary number of NLO corrections. Here the basic ideas of subtracting the expanded expressions remain the same. The shower history is extended together with the NLO corrections and needs to be expanded, as for the inclusion of the second NLO corrections.

In the last part the parameters to vary the scales of showering and hard process were included to the NLO merging expressions.

We showed with three independent methods that the Sudakov reweighting as a keystone of merging algorithms works and reported on the implementation of interfaces to external amplitude providers. Within this work three automatized interfaces to external amplitude providers (GoSam, MadGraph and OpenLoops) have been implemented into the Matchbox framework. The interface to MadGraph together with the ColorFull package provides the possibility to calculate tree level amplitudes in the large- N_C limit, which is necessary for consistent NLO matching.

In Ch. 7 numerical results are shown and known improvements are included consistently. The NLO corrections to the first additional emission from a $q\bar{q}$ pair, calculated in the $\overline{\text{MS}}$ -scheme shows a large K -factor. The unitarization procedure for the NLO corrections that preserves the NLO cross section showed a kink at the merging scale, originating from finite corrections. It was explained, by referring on knowledge from the early 90s, that this is expected. It was shown, that changing to the MC-scheme by changing the value of α_s spoils the description of data. Understanding the change consistently as an $\mathcal{O}(\alpha_s)$ correction, restores the good description of LEP data. Including NLO corrections to up to four jet final states shows discrepancies to data corrected to parton level but agrees well with uncorrected data.

We discussed the changes produced by including multiple NLO corrections to Drell-Yan processes and saw that data are well described. The inclusion of the MC-scheme related expressions also improved the behaviour for Z boson production at the LHC. The MC@NLO approach and the merging with one NLO correction agreed well. For W^\pm boson production we showed the interplay of different stages of the event simulation and it is seen that the NLO merged result improves the description of data with respect to pure parton shower, LO merged and NLO matched results. As expected the kink seen in MC@NLO in Higgs production via gluon fusion disappears with the inclusion of the second NLO. The smooth transition seen at the merging scale was less expected, since the large virtual corrections from the first NLO corrections are vetoed above the merging scale. The unitarization of the second NLO corrections suppresses the first corrections. For the multi dipole processes of pure dijet production we see non-physical differential cross sections, which will be discussed in future work.

In future work a retuning of non-perturbative parameters used in event simulations will be taken into account. Uncertainty studies by variations of the included parameters will provide reasonable uncertainty estimations. The effects of merging multiple NLO corrections in the approach provided in this thesis will lead to improved simulations of signal and background processes at present and future colliders. In order to test the limitations of the SM and to improve the searches for new physics beyond the SM, higher precision is required to understand nature.

APPENDIX A

Clustering the real emissions kinematics

In Eq. (5.11), (5.12) and (5.13) we add contributions which have different structure in the measurement functions u_i but can be produced with Monte Carlo techniques. The algorithm has the following structure:

1. Produce a phase space point for the real emission kinematic.
2. Decide with adjustable but fixed weights $w'_D/(w'_D+w'_R)$ and $w'_R/(w'_D+w'_R)$ if the integral of Eq. (5.12) (with dipole contributions above $\tilde{\mu}$) or the other two (with real emission contributions) should be performed. Multiply the event weight with $(w'_D+w'_R)/w'_C$, where C is the chosen one.
3. If the dipole contributions should be used:
 - a) Check if all scales are above the cutoff $\tilde{\mu}$. If at least one of the scales is below the merging scale ρ . If not discard the point *.
 - b) Choose one of the dipoles flat. Multiply the event weight with the number of dipoles.
 - c) Check if the tilde kinematics of the chosen dipole respects the cuts on the process. If not discard the point.
 - d) Check if the real emission phase space point is inside the reachable phase space for the shower from the chosen tilde kinematic. If the phase space point is reachable, multiply the event weight with $(P_i - D_i)$, if not, calculate only the dipole expression. P_i is the shower approximation of the dipole [70], see Sec. 4.5.
4. If the real emission contributions should be used:
 - a) If all scales are above the merging scale, we are calculating expression (5.11).

*It is then part with the real emission contributions.

- i. Perform the clustering used in LO merging. If no clustering is possible within the subleading shower phase spaces, the point was already added to the LO merging without unitarization. Do not calculate the real emission weight.
 - ii. Choose one dipole flat multiply the dipole weight with the number of dipoles, stored in the tilde kinematic of the dipole. The shower starting scale is calculated for the tilde kinematics.
 - iii. If the real emission phase space point is reachable, the w_i are not all zero. We already chose the underlying phase space point according to the density $w_i / \sum w_j$ in step i. If the flat chosen dipole of step ii is the same as the LO clustered underlying Born process multiply the real emission contribution with the number of dipoles, else do not calculate the real emission. This will produce the density in a Monte Carlo fashioned way. Return the real emission contribution with the multiplied dipole from the previous step.
- b) If at least one of the scales is below the merging scale, we are calculating Eq. (5.13)
- i. Calculate the real emission contribution.
 - ii. Subtract the shower approximation of each dipole if the scale is above the cutoff $\tilde{\mu}$.
 - iii. Subtract the dipoles for which the scale is below the cutoff $\tilde{\mu}$.
 - iv. Store the real emission in the real emission kinematics if none of the scales is below the cutoff, else store the contribution flat in one of the underlying kinematics.
 - v. Choose the starting scale of the shower according to the lowest scale if not clustered, else it is defined by the underlying kinematic.

APPENDIX B

Algorithm to produce NLO corrections

Algorithm for Eq. (5.44):

$$u_1 \left(-B_1(q_0) \sum_i \frac{w_i}{\sum_j w_j} \partial_{\alpha_s}^1 \Delta_1^{0,i} \theta_{PS}^1 + \bar{V}_1 + IPK_1 \right) \prod_i \theta(k_{T,2}^i > \rho) + \text{clustered}$$

1. Produce the kinematics for a phase space point u_1 .
2. Check if all scales associated with the dipoles are above the merging scale. If not discard the event.
3. Perform a clustering and calculate the history weight as for the LO merging.
4. Decide with probability 1/2 if event is clustered or not. Multiply event weight with 2. Later store the event in the u_1 configuration if the event is labelled not clustered or in the underlying kinematic determined in step 3. If no underlying process was found for the later, discard event.
5. Calculate the virtual and IPK contributions with the scale of the seed process given by the step before. This must not be the $n = 0$ configuration in the case of unordered histories.
6. For the given history calculate the expansions of the history weights, with the algorithm outlined below.

Algorithm for the α_s -expansion of the history weight $\partial_{\alpha_s}^1 \Delta_M^{0,i}$:

1. For each history step add

$$\frac{\alpha_s(q_0^2)}{2\pi} \beta_0 \log \left(\frac{q_k^2}{q_0^2} \right). \quad (\text{B.1})$$

where q_0 is the scale of the seed process, where the history started and q_k^2 is the k 'th history step of the chosen history i from the LO clustering description, with $k \in \{1, \dots, M\}$.

2. If the splitting is associated with a PDF ratio for one of the initial states, calculate the expression proportional to α_s of Eq. (5.33) for this PDF ratio. This can be done by reusing the same expression needed for the P operator in the CS subtraction formalism, without the colour correlations and divided by the PDF of the underlying process. The integration is done by Monte Carlo techniques in the **Matchbox** framework. For the merging we decided to produce multiple z values for the numerical integration in order to get a averaged, more stable result.
3. Integrate for each history step and each dipole configuration which was used to determine the Sudakov suppression of the LO merging the exponent of the Sudakov suppression with fixed scales q_i in α_s and PDF with the phase space boundaries determined for the scale q_i . This produces the correct α_s expansion of the final and initial state Sudakov form factors. Since we implemented the Sudakov factors for the LO merging in a way that we integrate the exponential, we can reuse the routines which were used there by keeping the scales fixed without exponentiation. With this procedure we achieve the correct α_s expansion including phase space boundaries. The multiplication in the LO merging suppression translates into a sum in the α_s expansion.

Algorithm for Eqs. (5.45) - (5.48):

In order to produce the correct weights for the real emission weights, containing the shower approximations, the algorithm for the first real emission outlined in (A) can be reused. The changes which do not effect the first NLO real emission:

1. The cut Θ on the real emission given in Eq. (5.42) needs to be respected.
2. Once a underlying Born process is determined, perform a history reweighting as for the LO merging for the chosen underlying Born process.
3. Assure that for all subtraction dipoles and shower approximations that are calculated the scales of their underlying processes are above the merging scale. The shower approximations must be reachable from any of their underlying processes by shower emissions.

APPENDIX C

Phase Space Boundaries and Variable Definitions

In this appendix the basic variable definitions and phase space boundaries are given, which have been used in the version of the `Herwig++` dipole shower [80]. They changed from [57] to the current Version of `Herwig++`.

The notation is hereby:

- FF, FI, IF, II: e.g. IF = initial state emitter , final state spectator
- p_i, p_j, p_k : Real (emitter,emission,spectator) momentum
- $q_{\tilde{i}j}, q_{\tilde{k}}$: Born (emitter,spectator) momentum
- x_{em}, x_{spe} : Born (emitter,spectator) momentum fraction
- $p_{T,\text{hard}}$: Hard scale of the Born phase space point. For next emissions it is the last splitting scale of the dipole chain. The dipole chain contains all colour connected dipoles.
- p_T^{\max} : Restriction on the maximum transverse momentum.

Dip.	Subtraction Var.	Tilde Kinematic	Usefull Relations, $r = p_T^2/s$	Inverted Kinematic
	u, v, x, z	$p_i, p_j, p_k \rightarrow q_{\tilde{i}j}q_{\tilde{k}}$		$q_{\tilde{i}j}q_{\tilde{k}} \rightarrow p_i, p_j, p_k,$ $k_T^2 = -p_T^2, k_T q_{\tilde{i}j} = k_T q_{\tilde{k}} = 0$
FF	$y = \frac{p_i p_j}{p_i p_j + p_k p_j + p_i p_k}$ $z = \frac{p_i p_k}{p_i p_k + p_j p_k}$ $s = 2q_{\tilde{i}j}q_{\tilde{k}}$	$q_{\tilde{i}j} = p_i + p_j - \frac{y}{1-y}p_k$ $q_{\tilde{k}} = \frac{p_k}{1-y}$	$y = \frac{r}{z(1-z)}$ $p_T^2 = yz(1-z)s$	$p_i = zq_{\tilde{i}j} + y(1-z)q_{\tilde{k}} + k_T$ $p_j = (1-z)q_{\tilde{i}j} + zyq_{\tilde{k}} - k_T$ $p_k = (1-y)q_{\tilde{k}}$
FI	$x = \frac{-p_j p_i + p_j p_k + p_i p_k}{p_i p_k + p_j p_k}$ $z = \frac{p_i p_k}{p_i p_k + p_j p_k}$ $s = 2q_{\tilde{i}j}q_{\tilde{k}}$	$q_{\tilde{i}j} = p_i + p_j - (1-x)p_k$ $q_{\tilde{k}} = xp_k$	$x = \frac{1}{1 + \frac{r}{z(1-z)}}$ $p_T^2 = z(1-z)\frac{1-x}{x}s$	$p_i = zq_{\tilde{i}j} + (1-z)\frac{1-x}{x}q_{\tilde{k}} + k_T$ $p_j = (1-z)q_{\tilde{i}j} + z\frac{1-x}{x}q_{\tilde{k}} - k_T$ $p_k = \frac{1}{x}q_{\tilde{k}}$
IF	$x = \frac{-p_j p_k + p_i p_k + p_i p_j}{p_i p_j + p_i p_k}$ $u = p_i p_j / (p_i p_j + p_i p_k)$ $s = 2q_{\tilde{i}j}q_{\tilde{k}}$	$q_{\tilde{i}j} = xp_i$ $q_{\tilde{k}} = p_k + p_j - (1-x)p_i$	$\rho = 1 - \frac{4rz(1-z)}{(1-z+r)^2}$ $x = \frac{1}{2}\frac{1-z+r}{r}(1 - \sqrt{\rho})$ $u = \frac{1}{2}\frac{1-z+r}{1-z}(1 - \sqrt{\rho})$ $p_T^2 = u(1-u)\frac{1-x}{x}s$ $z = 1 - (1-x)(1-u)$	$p_i = \frac{1}{x}q_{\tilde{i}j}$ $p_j = (1-x)\frac{1-u}{x}q_{\tilde{i}j} + uq_{\tilde{k}} + k_T$ $p_k = \frac{(1-x)u}{x}q_{\tilde{i}j} + (1-u)q_{\tilde{k}} - kt$
II	$x = \frac{p_i p_k - p_i p_j - p_k p_j}{p_i p_k}$ $v = \frac{p_i p_j}{p_i p_k}$ $s = 2q_{\tilde{i}j}q_{\tilde{k}}$	$q_{\tilde{i}j} = xp_i$ $K = p_i + p_k - p_j$ $\tilde{K} = xp_i + p_k$	$x = \frac{z(1-z)}{1-z+r}$ $v = \frac{rz}{1-z+r}$ $p_T^2 = v\frac{1-x-v}{x}s$ $z = x + v$	$p_i = (1/x)q_{\tilde{i}j}$ $p_j = ((1-x-v)/x)q_{\tilde{i}j} + vq_{\tilde{k}} + k_T$ $K = p_i + p_k - p_j$ $\tilde{K} = q_{\tilde{i}j} + q_{\tilde{k}}$
	p_T^{max}	z -bounds, $\kappa = p_T^2/p_{T,hard}^2$		
FF	$\frac{\sqrt{s}}{2}$	$\frac{1}{2}(1 \pm (1-\kappa))$		
FI	$\sqrt{\frac{s(1-x_{sp})}{4x_{sp}}}$	$\frac{1}{2}(1 \pm (1-\kappa))$		
IF	$\sqrt{\frac{s(1-x_{em})}{4x_{em}}}$	$\frac{1}{2}(1 + x_{em} \pm (1 - x_{em})(1 - \kappa))$		
II	$(1 - x_{em}x_{spe})\frac{\sqrt{s}}{2\sqrt{x_{em}x_{spe}}}$	$\frac{1}{2}(1 + x_{em}x_{spe} \pm (1 - x_{em}x_{spe})(1 - \kappa))$		

Table C.1.: Variables and kinematics for CS subtraction [41] and showering as they are implemented in the current version of `Herwig++`, they slightly differ [80] from [57]. The notation is given in Sec. C.

APPENDIX D

Simulation Results

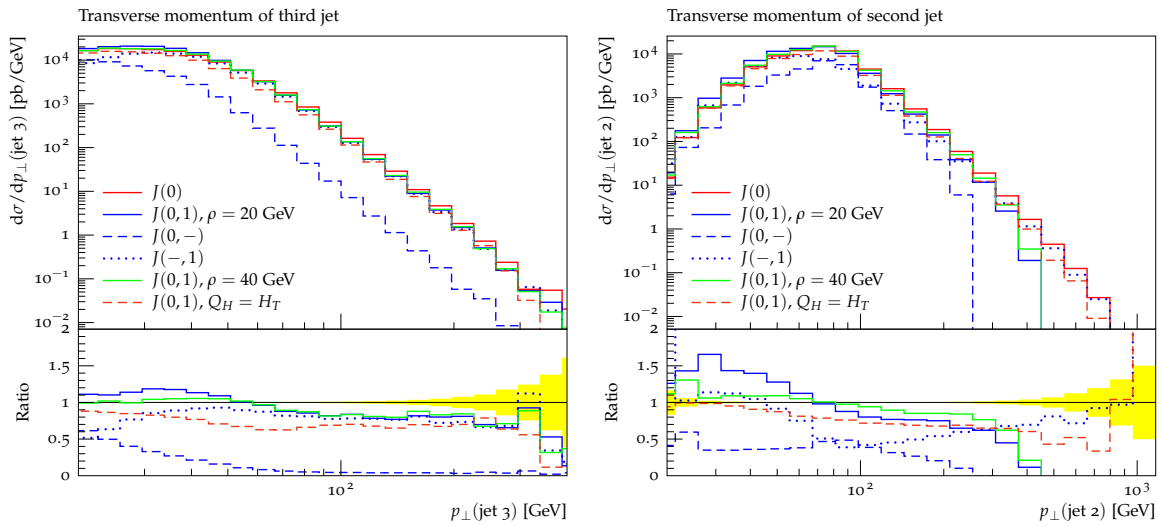


Figure D.1.: Pure dijet QCD events for proton proton collision with collider energy of 7 TeV. A minimal transverse momentum cut on the hardest jet $p_T = 80$ GeV is required for the generation before showering. The merging scales are $\rho = 20$ GeV and $\rho = 40$ GeV. The shower starting scale is the transverse momentum of the hardest jet. Left: The differential cross section for the transverse momentum of the third hardest jet is plotted for LO with parton shower emissions $J(0)$ and LO merging with one additional emission $J(0,1)$. The distribution is splitted into the dashed $J(0,-)$, containing the multiplicity with pure dijet configuration and the clustered contribution with three partons in the final state. Right: The differential cross section for the transverse momentum of the second hardest jet $p_{\perp}(\text{jet}2)$. The distribution with a shower starting $Q_H = H_T$ is added and discussed in the text.

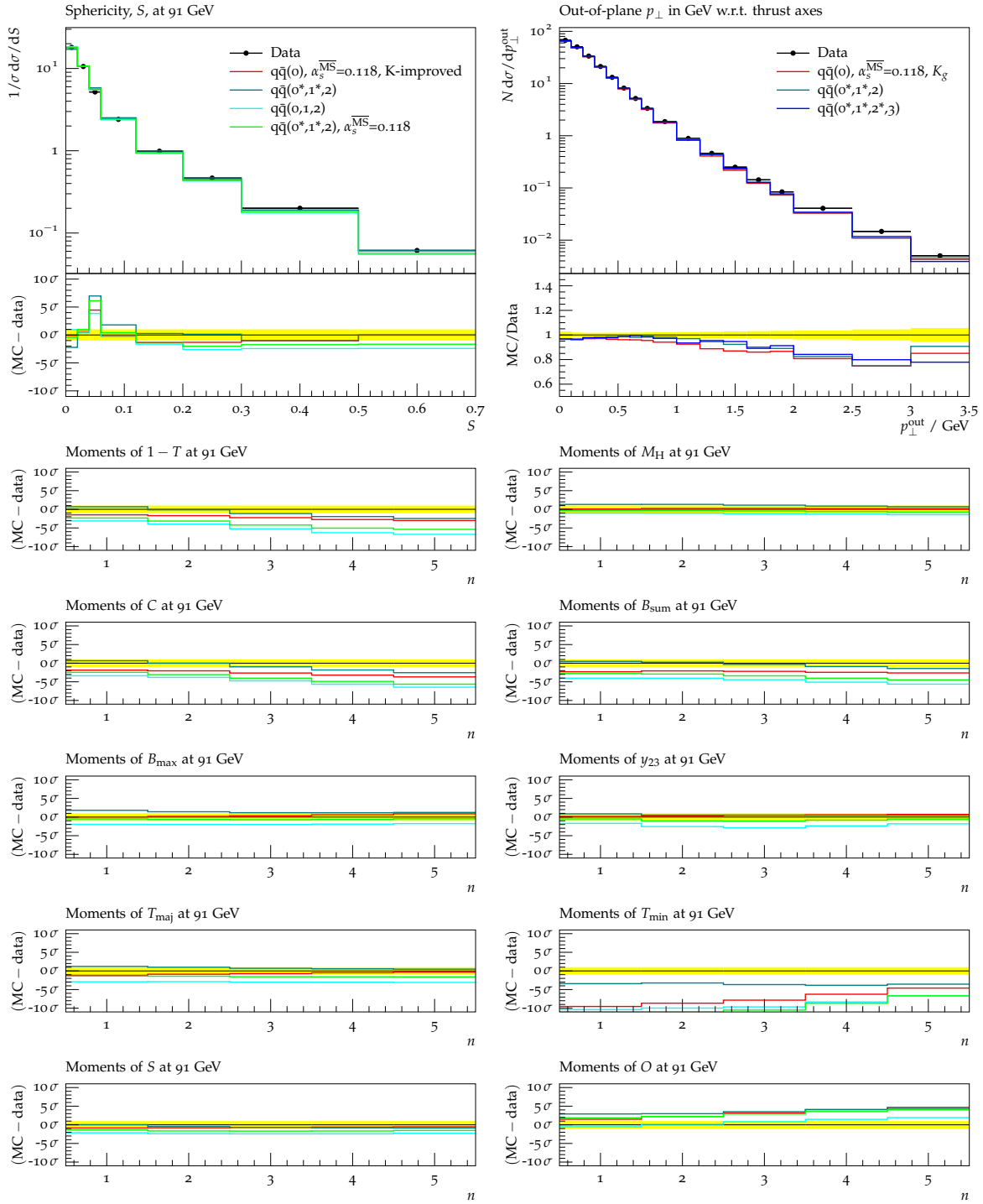


Figure D.2.: An overall good agreement between OPAL data [120] and simulation can be found. The ratio plots in the colour code of the upper left show the moments of several observables as described in [120] and the references therein. We chose to give the ratios as difference in terms of standard deviations to provide a better comparison to the original publication. The upper right plot is one of the observables, which is further improved by including the NLO merging, we use a different colour coding to distinguish the plot as it is a different experimental analysis in this comparison. The DELPHI analysis is described in [98]. It is one of the observables less well predicted, also in the original publication. The third NLO correction has no huge impact on the description of the data.

Bibliography

- [1] **ATLAS** Collaboration, G. Aad *et. al.*, “Observation of a new particle in the search for the Standard Model Higgs boson with the ATLAS detector at the LHC,” *Phys. Lett. B* **716** (2012) 1–29, [hep-ex/1207.7214](#).
- [2] **CMS** Collaboration, S. Chatrchyan *et. al.*, “Observation of a new boson at a mass of 125 GeV with the CMS experiment at the LHC,” *Phys. Lett. B* **716** (2012) 30–61, [hep-ex/1207.7235](#).
- [3] M. Bähr and others, “**Herwig++** Physics and Manual,” *Eur. Phys. J. C* **58** (2008) 639–707, [hep-ph/0803.0883](#).
- [4] T. Sjöstrand, S. Mrenna, and P. Skands, “A Brief Introduction to PYTHIA 8.1,” *Comput. Phys. Commun.* **178** (2008) 852–867, [hep-ph/0710.3820](#).
- [5] T. Gleisberg, S. Höche, *et. al.*, “Event generation with **SHERPA** 1.1,” *JHEP* **02** (2009) 007, [0811.4622](#).
- [6] S. Frixione and B. R. Webber, “Matching NLO QCD computations and parton shower simulations,” *JHEP* **06** (2002) 029, [hep-ph/0204244](#).
- [7] S. Frixione, F. Stoeckli, P. Torrielli, and B. R. Webber, “NLO QCD corrections in **Herwig++** with MC@NLO,” *JHEP* **1101** (2011) 053, [hep-ph/1010.0568](#).
- [8] P. Torrielli and S. Frixione, “Matching NLO QCD computations with PYTHIA using MC@NLO,” *JHEP* **04** (2010) 110, [1002.4293](#).
- [9] S. Plätzer and S. Gieseke, “Dipole Showers and Automated NLO Matching in **Herwig++**,” *Eur.Phys.J. C* **72** (2012) 2187, [hep-ph/1109.6256](#).
- [10] J. Alwall, R. Frederix, *et. al.*, “The automated computation of tree-level and next-to-leading order differential cross sections, and their matching to parton shower simulations,” *JHEP* **07** (2014) 079, [hep-ph/1405.0301](#).
- [11] P. Nason, “A new method for combining NLO QCD with shower Monte Carlo algorithms,” *JHEP* **11** (2004) 040, [hep-ph/0409146](#).

- [12] S. Frixione, P. Nason, and C. Oleari, “Matching NLO QCD computations with Parton Shower simulations: the POWHEG method,” *JHEP* **11** (2007) 070, [hep-ph/0709.2092](#).
- [13] S. Alioli, P. Nason, C. Oleari, and E. Re, “A general framework for implementing NLO calculations in shower Monte Carlo programs: the POWHEG BOX,” *JHEP* **06** (2010) 043, [1002.2581](#).
- [14] S. Höche, F. Krauss, M. Schönher, and F. Siegert, “Automating the POWHEG method in **Sherpa**,” *JHEP* **1104** (2011) 024, [hep-ph/1008.5399](#).
- [15] S. Catani, F. Krauss, R. Kuhn, and B. R. Webber, “QCD Matrix Elements + Parton Showers,” *JHEP* **11** (2001) 063, [hep-ph/0109231](#).
- [16] L. Lönnblad, “Correcting the colour-dipole cascade model with fixed order matrix elements,” *JHEP* **05** (2002) 046, [hep-ph/0112284](#).
- [17] M. L. Mangano, M. Moretti, and R. Pittau, “Multijet matrix elements and shower evolution in hadronic collisions: $Wb\bar{b} + n$ jets as a case study,” *Nucl. Phys.* **B632** (2002) 343–362, [hep-ph/0108069](#).
- [18] N. Lavesson and L. Lönnblad, “Merging parton showers and matrix elements – back to basics,” *JHEP* **04** (2008) 085, [hep-ph/0712.2966](#).
- [19] K. Hamilton, P. Richardson, and J. Tully, “A Modified CKKW matrix element merging approach to angular-ordered parton showers,” *JHEP* **11** (2009) 038, [0905.3072](#).
- [20] S. Höche, F. Krauss, M. Schönher, and F. Siegert, “NLO matrix elements and truncated showers,” *JHEP* **08** (2011) 123, [1009.1127](#).
- [21] L. Lönnblad and S. Prestel, “Matching Tree-Level Matrix Elements with Interleaved Showers,” *JHEP* **1203** (2012) 019, [hep-ph/1109.4829](#).
- [22] L. Lönnblad and S. Prestel, “Unitarising Matrix Element + Parton Shower merging,” *JHEP* **02** (2013) 094, [1211.4827](#).
- [23] K. Hamilton and P. Nason, “Improving NLO-parton shower matched simulations with higher order matrix elements,” *JHEP* **1006** (2010) 039, [hep-ph/1004.1764](#).
- [24] N. Lavesson and L. Lönnblad, “Extending CKKW-merging to One-Loop Matrix Elements,” *JHEP* **12** (2008) 070, [hep-ph/0811.2912](#).
- [25] T. Gehrmann, S. Höche, F. Krauss, M. Schönher, and F. Siegert, “NLO QCD matrix elements + parton showers in $e^+e^- \rightarrow$ hadrons,” [hep-ph/1207.5031](#).
- [26] S. Höche, F. Krauss, M. Schönher, and F. Siegert, “QCD matrix elements + parton showers: The NLO case,” *JHEP* **04** (2013) 027, [1207.5030](#).
- [27] R. Frederix and S. Frixione, “Merging meets matching in MC@NLO,” *JHEP* **12** (2012) 061, [1209.6215](#).
- [28] S. Alioli, C. W. Bauer, C. J. Berggren, A. Hornig, F. J. Tackmann, C. K. Vermilion, J. R. Walsh, and S. Zuberi, “Combining Higher-Order Resummation with Multiple NLO Calculations and Parton Showers in GENEVA,” *JHEP* **09** (2013) 120, [1211.7049](#).

- [29] L. Lönnblad and S. Prestel, “Merging Multi-leg NLO Matrix Elements with Parton Showers,” *JHEP* **03** (2013) 166, [1211.7278](#).
- [30] S. Plätzer, “Controlling inclusive cross sections in parton shower + matrix element merging,” *JHEP* **08** (2013) 114, [1211.5467](#).
- [31] K. Hamilton, P. Nason, E. Re, and G. Zanderighi, “NNLOPS simulation of Higgs boson production,” *JHEP* **10** (2013) 222, [1309.0017](#).
- [32] A. Karlberg, E. Re, and G. Zanderighi, “NNLOPS accurate Drell-Yan production,” *JHEP* **09** (2014) 134, [1407.2940](#).
- [33] K. Hamilton, P. Nason, and G. Zanderighi, “Finite quark-mass effects in the NNLOPS POWHEG+MiNLO Higgs generator,” *JHEP* **05** (2015) 140, [1501.04637](#).
- [34] S. Höche, Y. Li, and S. Prestel, “Higgs-boson production through gluon fusion at NNLO QCD with parton showers,” *Phys. Rev.* **D90** (2014), no. 5 054011, [1407.3773](#).
- [35] S. Höche, Y. Li, and S. Prestel, “Drell-Yan lepton pair production at NNLO QCD with parton showers,” *Phys. Rev.* **D91** (2015), no. 7 074015, [hep-ph/1405.3607](#).
- [36] S. Alioli, C. W. Bauer, C. Berggren, F. J. Tackmann, and J. R. Walsh, “Drell-Yan Production at NNLL’+NNLO Matched to Parton Showers,” [1508.01475](#).
- [37] P. W. Higgs, “Broken Symmetries and the Masses of Gauge Bosons,” *Phys. Rev. Lett.* **13** (1964) 508–509.
- [38] T.-P. Cheng and L.-F. Li, “Gauge theory of elementary particle physics,” *Oxford University Press*. (1988).
- [39] M. E. Peskin and D. V. Schroeder, “An introduction to quantum field theory,” *Westview Pr.* (2006).
- [40] J. C. Collins, “Foundations of Perturbative QCD,” *Cambridge Monographs on Particle Physics, Nuclear Physics and Cosmology* (2011).
- [41] S. Catani and M. Seymour, “A General algorithm for calculating jet cross-sections in NLO QCD,” *Nucl.Phys.* **B485** (1997) 291–419, [hep-ph/9605323](#).
- [42] R. K. Ellis, W. J. Stirling and B. R. Webber, “QCD and Collider Physics,” *Camb. Monogr. Part. Phys. Nucl. Phys. Cosmol.* **8** (1996).
- [43] A. Grozin, “Lectures on QED and QCD,” [hep-ph/0508242](#).
- [44] T. Kinoshita, “Mass singularities of Feynman amplitudes,” *J.Math.Phys.* **3** (1962) 650–677.
- [45] G. Dissertori, I. G. Knowles, and M. Schmelling, “Quantum chromodynamics : high energy experiments and theory,” *Westview Pr.* (2003).
- [46] S. Dittmaier, S. Kallweit, and P. Uwer, “NLO QCD corrections to $pp/p\bar{p} \rightarrow WW + \text{jet} + X$ including leptonic W-boson decays,” *Nucl. Phys.* **B826** (2010) 18–70, [hep-ph/0908.4124](#).

- [47] **Particle Data Group** Collaboration, K. Nakamura *et. al.*, “Review of particle physics,” *J.Phys.G* **G37** (2010) 075021.
- [48] K. G. Chetyrkin, B. A. Kniehl, and M. Steinhauser, “Decoupling relations to $\mathcal{O}(\alpha_s^3)$ and their connection to low-energy theorems,” *Nucl. Phys.* **B510** (1998) 61–87, [hep-ph/9708255](#).
- [49] T. Lee and M. Nauenberg, “Degenerate Systems and Mass Singularities,” *Phys.Rev.* **133** (1964) B1549–B1562.
- [50] G. Altarelli and G. Parisi, “Asymptotic Freedom in Parton Language,” *Nucl.Phys.* **B126** (1977) 298.
- [51] S. Catani and M. Seymour, “The Dipole formalism for the calculation of QCD jet cross-sections at next-to-leading order,” *Phys.Lett.* **B378** (1996) 287–301, [hep-ph/9602277](#).
- [52] S. Catani, S. Dittmaier, M. H. Seymour, and Z. Trocsanyi, “The dipole formalism for next-to-leading order QCD calculations with massive partons,” *Nucl. Phys.* **B627** (2002) 189–265, [hep-ph/0201036](#).
- [53] S. Frixione, Z. Kunszt, and A. Signer, “Three jet cross-sections to next-to-leading order,” *Nucl. Phys.* **B467** (1996) 399–442, [hep-ph/9512328](#).
- [54] D. A. Kosower, “Antenna factorization of gauge theory amplitudes,” *Phys. Rev.* **D57** (1998) 5410–5416, [hep-ph/9710213](#).
- [55] A. Gehrmann-De Ridder and M. Ritzmann, “NLO Antenna Subtraction with Massive Fermions,” *JHEP* **07** (2009) 041, [hep-ph/0904.3297](#).
- [56] G. Marchesini and B.R. Webber, “Simulation of QCD Jets Including Soft Gluon Interference,” *Nucl. Phys.* **B238** (1984) 1.
- [57] S. Plätzer and S. Gieseke, “Coherent Parton Showers with Local Recoils,” *JHEP* **01** (2011) 024, [hep-ph/0909.5593](#).
- [58] Z. Nagy, “Next-to-leading order calculation of three jet observables in hadron hadron collision,” *Phys. Rev.* **D68** (2003) 094002, [hep-ph/0307268](#).
- [59] G. Kramer and B. Lampe, “Two Jet Cross-Section in $e^+ e^-$ Annihilation,” *Z. Phys.* **C34** (1987) 497.
- [60] S. Weinzierl, “Jet algorithms in electron-positron annihilation: Perturbative higher order predictions,” *Eur. Phys. J.* **C71** (2011) 1565, [1011.6247](#). [Erratum: *Eur. Phys. J.* C71,1717(2011)].
- [61] W. J. Stirling, “Hard QCD working group: Theory summary,” *J. Phys.* **G17** (1991) 1567–1574.
- [62] S. Catani, Y. L. Dokshitzer, M. Olsson, G. Turnock, and B. R. Webber, “New clustering algorithm for multi - jet cross-sections in $e^+ e^-$ annihilation,” *Phys. Lett.* **B269** (1991) 432–438.

- [63] S. D. Ellis and D. E. Soper, “Successive combination jet algorithm for hadron collisions,” *Phys. Rev.* **D48** (1993) 3160–3166, [hep-ph/9305266](#).
- [64] M. Cacciari, G. P. Salam, and G. Soyez, “The Anti- k_T jet clustering algorithm,” *JHEP* **04** (2008) 063, [hep-ph/0802.1189](#).
- [65] A. V. Smilga, “Next-to-leading Logarithms in the High-Energy Asymptotics of the Quark Form-Factor and the Jet Cross-Section,” *Nucl. Phys.* **B161** (1979) 449–468.
- [66] T. Sjöstrand, “A Model for Initial State Parton Showers,” *Phys. Lett.* **B157** (1985) 321.
- [67] T. Sjöstrand, S. Mrenna, and P. Skands, “PYTHIA 6.4 Physics and Manual,” *JHEP* **05** (2006) 026, [hep-ph/0603175](#).
- [68] B. R. Webber, “A QCD Model for Jet Fragmentation Including Soft Gluon Interference,” *Nucl. Phys.* **B238** (1984) 492.
- [69] S. Schumann and F. Krauss, “A Parton shower algorithm based on Catani-Seymour dipole factorisation,” *JHEP* **03** (2008) 038, [hep-ph/0709.1027](#).
- [70] S. Plätzer *et. al.*, “Precision LHC Event Generation with **Herwig++**,” *in preparation* (2015).
- [71] L. Magnea and G. F. Sterman, “Analytic continuation of the Sudakov form-factor in QCD,” *Phys. Rev.* **D42** (1990) 4222–4227.
- [72] V. Ahrens, T. Becher, M. Neubert, and L. L. Yang, “Origin of the Large Perturbative Corrections to Higgs Production at Hadron Colliders,” *Phys. Rev.* **D79** (2009) 033013, [hep-ph/0808.3008](#).
- [73] O. Latunde-Dada, S. Gieseke, and B. Webber, “A positive-weight next-to-leading-order Monte Carlo for $e^+ e^-$ annihilation to hadrons,” *JHEP* **02** (2007) 051, [hep-ph/0612281](#).
- [74] K. Hamilton, P. Richardson, and J. Tully, “A Positive-Weight Next-to-Leading Order Monte Carlo Simulation for Higgs Boson Production,” *JHEP* **04** (2009) 116, [hep-ph/0903.4345](#).
- [75] S. Alioli, P. Nason, C. Oleari, and E. Re, “NLO Higgs boson production via gluon fusion matched with shower in POWHEG,” *JHEP* **04** (2009) 002, [hep-ph/0812.0578](#).
- [76] F. Krauss, “Matrix elements and parton showers in hadronic interactions,” *JHEP* **08** (2002) 015, [hep-ph/0205283](#).
- [77] K. Hamilton, P. Nason, and G. Zanderighi, “MINLO: Multi-Scale Improved NLO,” *JHEP* **1210** (2012) 155, [hep-ph/1206.3572](#).
- [78] M. Rubin, G. P. Salam, and S. Sapeta, “Giant QCD K -factors beyond NLO,” *JHEP* **1009** (2010) 084, [hep-ph/1006.2144](#).
- [79] F. Maltoni, K. Paul, T. Stelzer, and S. Willenbrock, “Color flow decomposition of QCD amplitudes,” *Phys. Rev.* **D67** (2003) 014026, [hep-ph/0209271](#).
- [80] S. Plätzer, “Private communication.”

- [81] J. Bellm *et. al.*, “Herwig++ 2.7 Release Note,” [1310.6877](#).
- [82] G. P. Lepage, “Vegas: An Adaptive Multidimensional Integration Program,” .
- [83] K. Arnold *et. al.*, “VBFNLO: A Parton level Monte Carlo for processes with electroweak bosons,” *Comput. Phys. Commun.* **180** (2009) 1661–1670, [0811.4559](#).
- [84] N. P. Hartland and E. R. Nocera, “A **Mathematica** interface to NNPDFs,” [hep-ph/1209.2585](#).
- [85] Z. Bern, L. J. Dixon, *et. al.*, “The **BlackHat** Library for One-Loop Amplitudes,” *J. Phys. Conf. Ser.* **523** (2014) 012051, [hep-ph/1310.2808](#).
- [86] H. van Deurzen *et. al.*, “Automated one-loop calculations with **GoSam** 2.0,” *PoS LL2014* (2014) 021, [hep-ph/1407.0922](#).
- [87] F. Cacioli, P. Maierhöfer, and S. Pozzorini, “Scattering Amplitudes with **Open Loops**,” *Phys. Rev. Lett.* **108** (2012) 111601, [hep-ph/1111.5206](#).
- [88] T. Stelzer and W. F. Long, “Automatic generation of tree level helicity amplitudes,” *Comput. Phys. Commun.* **81** (1994) 357–371, [hep-ph/9401258](#).
- [89] F. Krauss, R. Kuhn, and G. Soff, “AMEGIC++ 1.0: A Matrix element generator in C++,” *JHEP* **02** (2002) 044, [hep-ph/0109036](#).
- [90] M. Sjodahl, “**ColorFull** – a C++ library for calculations in SU(Nc) color space,” *Eur. Phys. J. C* **75** (2015), no. 5 236, [1412.3967](#).
- [91] H. Murayama, I. Watanabe, and K. Hagiwara, “HELAS: HELicity amplitude subroutines for Feynman diagram evaluations.”
- [92] S. Badger, B. Biedermann, P. Uwer, and V. Yundin, “Computation of multi-leg amplitudes with **NJet**,” *J. Phys. Conf. Ser.* **523** (2014) 012057, [hep-ph/1312.7140](#).
- [93] K. Arnold, J. Bellm, *et. al.*, “VBFNLO: A parton level Monte Carlo for processes with electroweak bosons – Manual for Version 2.5.0,” [hep-ph/1107.4038](#).
- [94] S. Alioli *et. al.*, “Update of the Binoth Les Houches Accord for a standard interface between Monte Carlo tools and one-loop programs,” *Comput. Phys. Commun.* **185** (2014) 560–571, [hep-ph/1308.3462](#).
- [95] T. Binoth, F. Boudjema, G. Dissertori, A. Lazopoulos, A. Denner, *et. al.*, “A Proposal for a standard interface between Monte Carlo tools and one-loop programs,” *Comput. Phys. Commun.* **181** (2010) 1612–1622, [hep-ph/1001.1307](#).
- [96] J. M. Campbell and R. Ellis, “MCFM for the Tevatron and the LHC,” *Nucl. Phys. Proc. Suppl.* **205-206** (2010) 10–15, [hep-ph/1007.3492](#).
- [97] A. Buckley *et. al.*, “Rivet user manual,” [hep-ph/1003.0694](#).
- [98] **DELPHI** Collaboration, P. Abreu *et. al.*, “Tuning and test of fragmentation models based on identified particles and precision event shape data,” *Z. Phys. C* **73** (1996) 11–60.

- [99] **JADE** Collaboration, P. Pfeifenschneider *et. al.*, “QCD analyses and determinations of α_s in $e^+ e^-$ annihilation at energies between 35 GeV and 189 GeV,” *Eur. Phys. J. C* **17** (2000) 19–51, [hep-ex/0001055](#).
- [100] **Particle Data Group** Collaboration, K. A. Olive *et. al.*, “Review of Particle Physics,” *Chin. Phys. C* **38** (2014) 090001.
- [101] P. Skands, S. Carrazza, and J. Rojo, “Tuning PYTHIA 8.1: the Monash 2013 Tune,” *Eur. Phys. J. C* **74** (2014), no. 8 3024, [hep-ph/1404.5630](#).
- [102] S. Catani, B. R. Webber, and G. Marchesini, “QCD coherent branching and semiinclusive processes at large x ,” *Nucl. Phys. B* **349** (1991) 635–654.
- [103] **OPAL** Collaboration, G. Abbiendi *et. al.*, “A Simultaneous measurement of the QCD color factors and the strong coupling,” *Eur. Phys. J. C* **20** (2001) 601–615, [hep-ex/0101044](#).
- [104] H. Hoeth, “Messung der Vierjet-Winkelverteilungen und Bestimmung der QCD-Farbfaktoren mit Hilfe des **Apacic++**-Generators,” *Diploma Thesis (in German)*, Bergische Universität Wuppertal (2003).
- [105] A. Buckley, J. Butterworth, Lönnblad, D. Grellscheid, H. Hoeth, J. Monk, H. Schulz, and F. Siegert, “Rivet user manual,” *Comput. Phys. Commun.* **184** (2013) 2803–2819, [1003.0694](#).
- [106] **NNPDF** Collaboration, R. D. Ball *et. al.*, “Parton distributions for the LHC Run II,” *JHEP* **04** (2015) 040, [hep-ph/1410.8849](#).
- [107] A. Buckley, J. Ferrando, S. Lloyd, K. Nordström, B. Page, M. Rüfenacht, M. Schönherr, and G. Watt, “LHAPDF6: parton density access in the LHC precision era,” *Eur. Phys. J. C* **75** (2015), no. 3 132, [1412.7420](#).
- [108] **ATLAS** Collaboration, G. Aad *et. al.*, “Measurement of the Z/γ^* boson transverse momentum distribution in pp collisions at $\sqrt{s} = 7$ TeV with the ATLAS detector,” *JHEP* **09** (2014) 145, [1406.3660](#).
- [109] G. Miu and T. Sjöstrand, “ W production in an improved parton shower approach,” *Phys. Lett. B* **449** (1999) 313–320, [hep-ph/9812455](#).
- [110] N. Cabibbo, “Unitary Symmetry and Leptonic Decays,” *Phys. Rev. Lett.* **10** (1963) 531–533.
- [111] M. Kobayashi and T. Maskawa, “CP Violation in the Renormalizable Theory of Weak Interaction,” *Prog. Theor. Phys.* **49** (1973) 652–657.
- [112] **ATLAS** Collaboration, G. Aad *et. al.*, “Measurement of k_T splitting scales in $W \rightarrow l\nu$ events at $\sqrt{s} = 7$ TeV with the ATLAS detector,” *Eur. Phys. J. C* **73** (2013), no. 5 2432, [hep-ex/1302.1415](#).
- [113] **ATLAS** Collaboration, G. Aad *et. al.*, “Study of jets produced in association with a W boson in pp collisions at $\sqrt{s} = 7$ TeV with the ATLAS detector,” *Phys. Rev. D* **85** (2012) 092002, [hep-ex/1201.1276](#).

- [114] S. Catani, Y. L. Dokshitzer, M. H. Seymour, and B. R. Webber, “Longitudinally invariant K_t clustering algorithms for hadron hadron collisions,” *Nucl. Phys.* **B406** (1993) 187–224.
- [115] J. R. Christiansen and T. Sjöstrand, “Weak Gauge Boson Radiation in Parton Showers,” *JHEP* **04** (2014) 115, [hep-ph/1401.5238](#).
- [116] S. Dawson, “Radiative corrections to Higgs boson production,” *Nucl. Phys.* **B359** (1991) 283–300.
- [117] A. Djouadi, M. Spira, and P. M. Zerwas, “Production of Higgs bosons in proton colliders: QCD corrections,” *Phys. Lett.* **B264** (1991) 440–446.
- [118] R. V. Harlander and W. B. Kilgore, “Next-to-next-to-leading order Higgs production at hadron colliders,” *Phys. Rev. Lett.* **88** (2002) 201801, [hep-ph/0201206](#).
- [119] B. A. Kniehl and M. Spira, “Low-energy theorems in Higgs physics,” *Z. Phys.* **C69** (1995) 77–88, [hep-ph/9505225](#).
- [120] **OPAL** Collaboration, G. Abbiendi *et. al.*, “Measurement of event shape distributions and moments in $e^+e^- \rightarrow$ hadrons at 91 GeV - 209 GeV and a determination of α_s ,” *Eur. Phys. J.* **C40** (2005) 287–316, [hep-ex/0503051](#).

Acknowledgment

First of all, I want to thank PD Dr. Stefan Gieseke for giving me the opportunity to work on this interesting topic and in the collaboration of Herwig++. He always had an open door, which allowed me to ask the questions I had and to profit from his profound knowledge on particle physics and Monte Carlo techniques. I appreciate that he gave me the possibility to present my work at conferences and visit summer schools in Pittsburgh and Maria Laarch.

I thank Prof. Dr. Dieter Zeppenfeld for agreeing to be the second reviewer of this thesis.

I am very grateful to Simon Plätzer for the collaboration on this and other shower related topics. The many fruitful discussions and his hospitality are gratefully acknowledged.

For the collaboration on the amplitude interfaces I want to thank Nicolas Greiner, Philipp Maierhöfer, Olivier Mattelaer, Michael Rauch and Christian Reuschle.

For the proofreading of this thesis, I want to thank Andreas Maier, Simon Plätzer, Michael Rauch, Robin Roth, Richard Ruiz, Peter Schichtel and Alexander Wlotzka.

I want to thank the current and former members of the ITP, especially the colleagues Bastian Feigl, Christian Hangst, Genesis Perez and Kathrin Walz in my office, for the great atmosphere at the institute.

Großer Dank gebührt Bastian Feigl, Robin Roth und Christian Röhr für die Zusammenarbeit bei der Administration der Computeranlage des ITP. Ich habe viel von ihnen gelernt.

The financial support by “Karlsruhe School of Elementary Particle and Astroparticle Physics: Science and Technology (KSETA)” as well as MCnet is greatly acknowledged.

Ein ganz besonderer Dank gilt meiner Familie und meiner Freundin Eva Scharnagl, ohne deren große Unterstützung der Abschluss dieser Arbeit nicht möglich gewesen wäre.